Università degli Studi di Padova

Dipartimento di Fisica e Astronomia
“Galileo Galilei”

Corso di Laurea Magistrale in Fisica

Tesi di Laurea Magistrale

The Dynamical Environment of the Cometary Nucleus 67P/Churyumov-Gerasimenko

Relatore:
Prof. Francesco Marzari
Controrelatore:
Prof. Gabriele Cremonese

Laureando:
Roberto Casotto

Anno Accademico 2014/2015

Acknowledgments

Firstly, I would like to express my sincere gratitude to my father Stefano for the continuous support, for his patience, motivation, and immense knowledge. His guidance helped me in all the time of research and writing of this thesis.

My sincere thanks goes also to my advisor Dr. Marzari, for his insightful comments and encouragement, but also for the hard questions which pushed me to widen my research from various perspectives.

Thanks also to Dr. Robert Werner, for the permission to use his code POLYGRAV, without which this research work would not have been possible, to Prof. Ryan Russell, for his precious help and advice, to Prof. Roberto Ragazzoni, for making it possible to create a 3D print of 67P's nucleus, and to Marco Dima, who crafted the 3D model and provided graphics support. Thanks also to Nicola Baresi for the help and advice on this research.

I am greatful to my mother, my grandparents and my brothers, who were always there for me when I was in need.

I take this opportunity to express my gratitude to all my friends at the Scuola Galileiana. In particular to Riccardo and Andrea for their help and insightful discussions on this work.

Last, but not least, I want to thank my girlfriend Ilenia, who stood by me even in troubled times, reminding me that I have what it takes to make it.

Contents

Chapter 1

Rosetta's Misson to Comet 67P/Churyumov-Gerasimenko

1.1 The Rosetta Mission

Rosetta is an ESA mission that was launched on 2 March 2004, after a delay due to an unrelated launch failure of a European Arianne Rocket in late 2002. The original target, comet 46P/Wirtanen, could no longer be reached. The target was thus changed to comet 67P/Churyumov-Gerasimenko (hereinafter abbreviated to 67P). Comet 67P has a 6.5 year elliptical orbit that takes it from Earth's to Jupiter's orbit.

The mission's primary goals were in the first place to rendezvous with the comet and accompany it into the interior of the Solar System, observe the comet's nucleus and once at close range deploy the Philae lander, measure the increase on cometary activity during perihelion, and observe the changes associated with the change in season as the comet leaves the inner Solar System, when a different pole will be exposed to the Sun. Close mapping of the comet has provided compehensive understanding of the characteristics of the comet, its composition and environment, both by studying the nucleus itself remotely and by measuring the properties of the gas, dust, and plasma in the coma surrounding it.

The scientific goals of the Rosetta mission are to create a portrait of the comet's nucleus, that is its shape and dynamical properties, take a complete inventory of the comet's chemical, mineralogical, and isotopic composition, detail the comet's physical properties, show how the coma emerges from the surface of the nucleus and develops different layers of activity as it grows in the solar wind. An important goal would be to find the comet's origin, that is, when and where it has formed, and the relationship between its constituent materials and those found in the solar wind.

Before reaching 67P, Rosetta travelled 10 years inside the Solar System, performing four fly-bys that allowed the spacecraft to approach the comet, the first with Earth in March, 2005, the second with Mars in February, 2007, and the last two with Earth in November, 2007, and in November, 2009. After a fly-by with asteroid Lutetia, the spacecraft entered deep space hibernation on June, 2011, for 2.5 years. The trajectory of Rosetta is schematically represented in Figure 1.1. After awaking from hibernation in January, 2014, a rendezvous was performed by a series of critical breaking maneuvers between May and August 2014 starting from a distance of 2 million kilometers, which reduced the speed of the comet relative to the target down to walking pace at a distance of 100 km from the comet.

Rosetta carries many scientific packages. Those relevant for this research are OSIRIS (Optical, Spectroscopic, and Infrared Remote Imaging System Camera), a dual camera imaging system

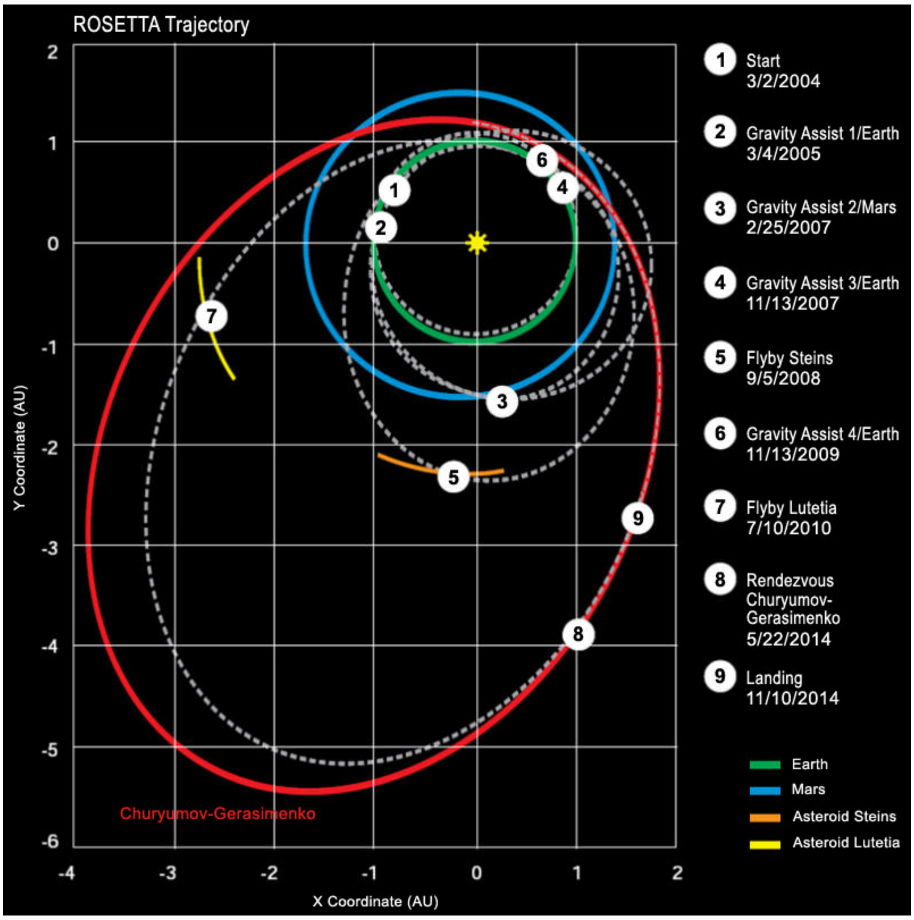

Figure 1.1. Timeline of Rosetta's voyage inside the Solar System to rendezvous with comet 67P. Picture taken from ESA website.

consisting of a narrow angle (NAC) and a wide angle (WAC) camera; CONSERT (COmet Nucleus Sounding Experiment by Radio wave Transmission), for studying the internal structure of the comet with the lander Philae; GIADA (Grain Impact Analyzer and Dust Accumulator), measuring the number, mass, momentum and velocity distribution of the dust grains in the near-comet environment; and MIDAS (Micro-Imaging Dust Analysis System), for studying the dust environment of the comet. OSIRIS is the science package that allowed the recontruction of the shape of the cometary nucleus, which is extensively used in this work to compute the gravitational fields produced by the comet.

Once the comet was reached, a series of triangular paths around the comet (Figure 1.2) allowed the spacecraft to get to a distance of up to 20 km above the nucleus of the comet.

It has been found (Vincent et al., 2015) that pits appearing in the comet's surface are not produced by impacts of external material onto the surface. It may be that they are the result of explosive mechanisms, and that in any case they are active, and probably created by sinkholes process, possibly accompanied by outbursts. An example of outburst is pictured in Figure 1.4.

As already mentioned, the CONSERT scientific package inside Rosetta and Philae was used to investigate the internal structure of the nucleus of the comet. The measures obtained with CONSERT demonstrated that the upper part of the head of 67P is fairly homogeneous on a spatial scale of tens of meters (Kofman et al., 2015). This results are fundamental for our research, since we will make the strong assumption that the whole volume of the comet has homogeneous mass density in oreder to calculate the external gravitational fields.

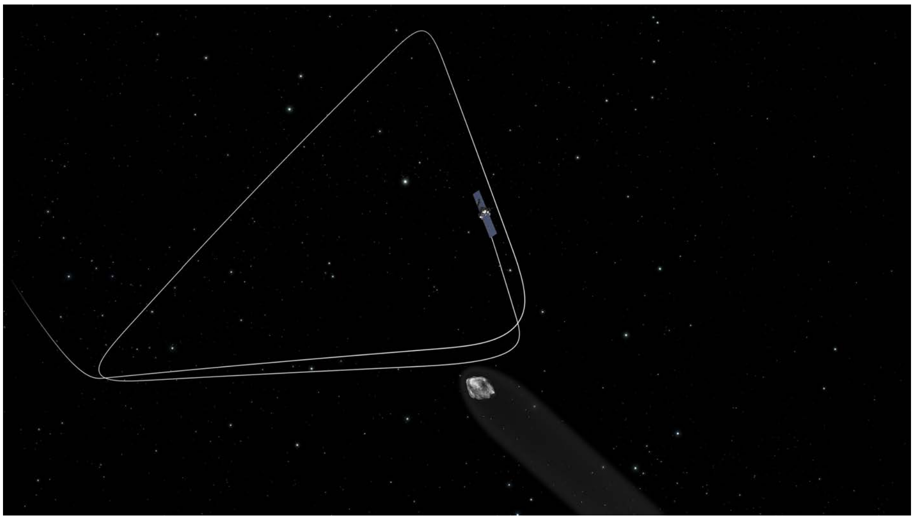

Figure 1.2. Schematic representation of the triangular trajectories followed by Rosetta around 67P. Picture taken from ESA website.

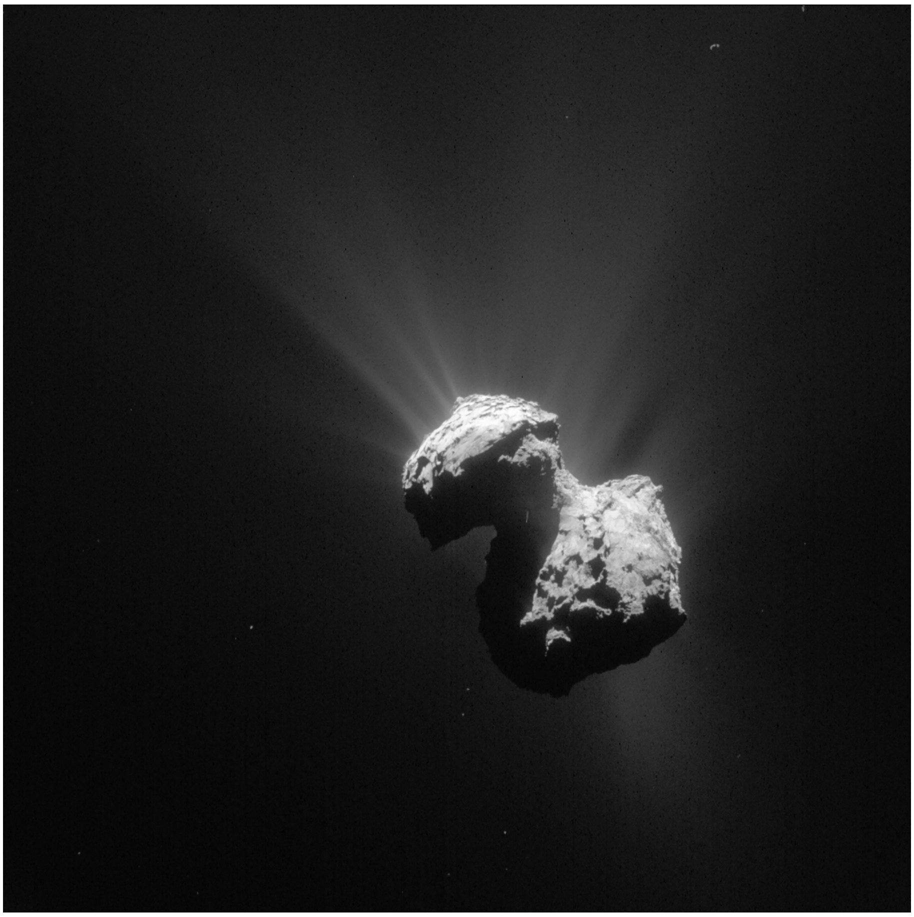

Figure 1.3. Rosetta activity on July 7, 2015, one month before perihelion. Picture taken from ESA website.

Figure 1.4. Outburst. The three pictures have been taken at $\sim$ 20 minutes intervals. Picture from ESA website.

The combined data from GIADA, OSIRIS, MIRO (Microwave Intrument for the Rosetta Orbiter), and ROSINA (Rosetta Orbiter Spectromenter for Ion and Neutral Analysis) showed that the dust to gas mass ratio in on average 4 ± 2 over the sunlit nucleus surface (Rotundi et al., 2015). A cloud of larger grains also encircles the nucleus in bound orbits from the previous perihelion.

The rotational state of 67P is along the principal axis of inerta of the body, and no complex rotation has been detected. Measurements constrain any motion of the spin axis to $< 0.3°$over $\sim$ 55 days (Sierks et al., 2015). The rotation is prograde with a spin axis at RA $= 69.3°\pm0.1°$, Dec $= 64.1°\pm0.1°$, and a period $T = 12.4043 \pm 0.0007$ hours.

As for the origin of the comet, three-dimensional impact simulations using realistic constitutive properties showed results similar to the morphology of the nucleus of 67P (Jutzi and Asphaug, 2015). From these results the hypotesis that the nucleus formed by collisional coagulation either out of cometesimal accreting in the early solar system or out of comparable-sized debris clumps paired in the aftermath of major collisions.

1.2 Dynamical Characterization of 67P – A Research Outline

This work aims to study the dynamical environment of 67P. This research is fundamental for two reasons. The first is to find periodic orbits for future space missions near highly irregular bodies to economically park the spacecraft. The second is the understanding and explanation of the dynamics of ejecta, or even the dynamics of capture of dust particles of various sizes. In particular, it is of great interest to assess the presence of stable regions in which the ejecta might accumulate, which would explain the observation (Rotundi et al., 2015). During the second half of the '90s, many papers were published on the dynamics around cometary nuclei, e.g. Scheeres et al. (1998). However, no one ever thought that we would find such an irregular body generating a gravitational field for which efficient computational tools are still missing.

The next three Chapters will discuss new and old ways to model the gravitational field. To compute the gravitational field at an external point to the body, a polyhedral mesh that best approximates the surface of the body will be used, as seen in Figure 1.5. Three methods will be described in the next Chapters. In particular, Chapter 2 will be devoted to describing the Werner method, which is the most computationally intensive, since every vertex, face and edge contributes to the computation of the gravitational potential in each point in space. However, this is the method that was used to integrate all orbits during this research, since it is the only mathod that can compute the gravitational field in any point outside the volume of the cometary nucleus.

In Chapter 3 the representation of the potential through the use of inertial functions and inertial integrals, the computation of the inertial functions and of the inertial integrals through the use of a polyhedron, will be described. Although the expansion in inertial integrals is well

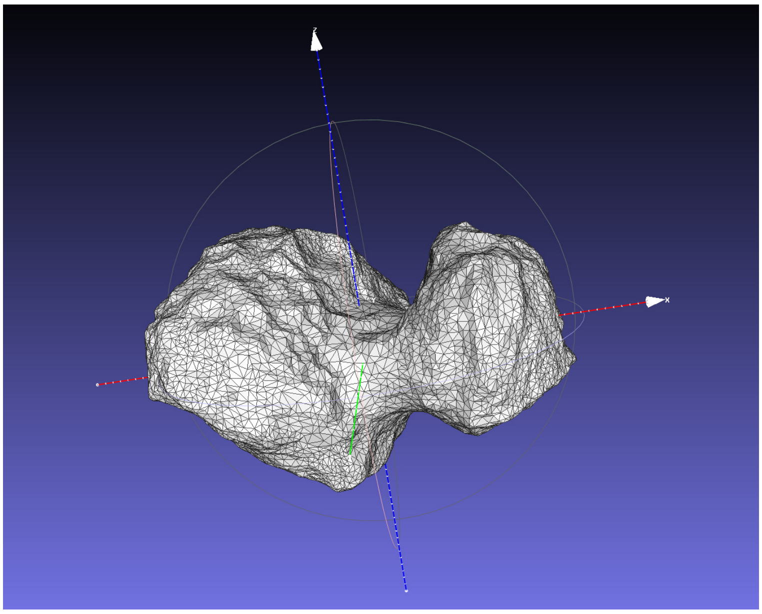

Figure 1.5. The surface of 67P shown as a polyhedron formed by a triangular surface mesh.

known in the literature, the expansion of the potential through the use of inertial functions is completely new, and was developed during this research.

In Chapter 4 the representation of the potential through the use of Spherical Harmonics will be treated. Even though this method is not new, a unifying approach has been undertaken to link the external and internal expansion of the potential.

The interest for the representation of the potential, especially inside a sphere not containing any part of the extended body, is due to the fact that a new, efficient way of computing the potential near the surface of an irregularly shaped body is required for the integration of orbits near the surface of such body. This is, in fact, the case for 67P.

The methods for computing the potential described in Chapters 3 and 4 are expected to be less computationally demanding than the Werner method described in Chapter 2, since the largest computational effort of these two methods is confined to the preprocessing stage, which consists in computing the *inertial functions*, the *inertial integrals*, and the *Stoke's coefficients* around an expansion point.

Chapter 5 contains the theoretical concepts needed to integrate the equations of motion around the comet and to converge to periodic orbits for initial conditions close to an almost periodic orbit. The results of the application of these methods will be shown in Chapter 6, where the resulting periodic orbits will be displayed and discussed.

Chapter 7 describes, instead, a possible way of designing artificial periodic orbits around the body. The reason for this part of the research was the desire to find a periodic orbit that passed deep inside the valley of 67P. Since no natural periodic orbits passing near the valley were found, the addition of an active force, namely, the thrusters of the spacecraft, was implemented in the equations of motion. The computation of the thrust acceleration profile and the required ΔV needed to perform the designed acrobatics with the Rosetta spacecraft is the main point of this last Chapter.

Chapter 2

The Gravitational Potential - 1
Werner's Method

2.1 Introduction

Newton's Law of Universal Gravitation states that two point masses m_1 and m_2 attract each other along the line joining them with a force of magnitude F directly proportional to the product of their masses and inversely proportional to their mutual distance d, i.e., F is given as

$$F = G\frac{m_1 m_2}{d^2}, \tag{2.1}$$

where G is the constant of universal gravitation. Introducing the position vectors $\mathbf{r}_1$ of mass m_1 located at point P_1 and $\mathbf{r}_2$ of mass m_2 at P_2, as well as the vector $\mathbf{r} = \mathbf{r}_2 - \mathbf{r}_1$ pointing from P_1 to P_2, the force $\mathbf{F}$ with which m_1 acts on m_2 is given by the vector

$$\mathbf{F} = -G\frac{m_1 m_2}{r^3}\mathbf{r}, \tag{2.2}$$

where $r = |\mathbf{r}| = d$. Viceversa, the force that m_2 exerts on m_1 is $-\mathbf{F}$.

The extension of Newton's law of gravitation to extended bodies makes use of the principle of superposition of forces and can be stated as follows. Notice that the interest here is only for the region external to the body, i.e., the space where a particle can orbit the extended body. Therefore it will not be necessary to use distributions in the following treatment, nor will it be necessary to use the full power of the Helmoltz Theorem, since the gravitational potential is fully described by a scalar function.

Given a finite, bounded, continuous volumic mass distribution σ as a function of position $\mathbf{r}$, the gravitational force on a unit point mass ($m = 1$) located at the field point P located *outside the body* at $\mathbf{r}$ is given by the three-dimensional integral

$$\mathbf{g}(\mathbf{r}) = -G\iiint\limits_V \sigma(\boldsymbol{\rho})\,\frac{\mathbf{r}-\boldsymbol{\rho}}{|\mathbf{r}-\boldsymbol{\rho}|^3}dV, \tag{2.3}$$

where dV is a volume differential and the integration is extended over the finite volume V enclosing the entire mass distribution of the extended body. In practice, the position vector $\boldsymbol{\rho}$ and the volume differential dV are associated with a source point Q of the extended body. In the future, we will usually adopt the Greek letter $\boldsymbol{\rho}$ and its components (ξ, η, ζ) to indicate the source point Q.

Since it is well-known that the gravitational force is conservative, which is ensured by the fact that the force field[1] $\mathbf{g}$ is irrotational, i.e., $\nabla \times \mathbf{g} \equiv \mathbf{0}$, the gravitational field can be obtained as the gradient of a *potential function* U,

$$\mathbf{g}\left(\mathbf{r}\right) = \nabla U, \tag{2.4}$$

where the ∇ operator indicates the gradient with respect to the standard position variable $\mathbf{r}$, i.e., $\nabla = \nabla_{\mathbf{r}} = \partial/\partial\mathbf{r}$. The potential function, or more simply the *potential,* can be expressed as

$$U\left(\mathbf{r}\right) = G \iiint\limits_{V} \frac{\sigma(\boldsymbol{\rho})}{|\mathbf{r}-\boldsymbol{\rho}|}\, dV. \tag{2.5}$$

If the density is well-behaved, the integral (2.5) converges for all points P outside the mass distribution Kellogg (1929) and if the volume's boundary is stationary differentiation can be moved inside the integration sign so that using (2.5) in (2.4) yields (2.3). Notice that the potential function as used here is the negative of the potential energy. This is the convention adopted in Celestial Mechanics and Geodesy.

The gravitational potential satisfies numerous theorems. Among these we recall that, under the assumptions stated above, the potential and its first derivatives vanish at infinity (Sternberg and Smith, 1946) and that at external points the potential is a continuous and arbitrarily often differentiable function of position (Sigl, 1985, p. 72). Also, since *the gradient operates only on the field coordinates*, it follows that

$$\nabla \cdot \mathbf{g}\left(\mathbf{r}\right) = 0, \tag{2.6}$$

which shows that the external gravitational field is a solenoidal field. Substitution of the potential from (2.4) then leads to Laplace's equation

$$\nabla^2 U\left(\mathbf{r}\right) = 0, \tag{2.7}$$

which implies that *the external potential is a harmonic function.* Therefore the potential U of interest for the present study[2] is composed of *homogenous functions* satisfying Laplace's equation.

The fundamental problem to solve in order to carry out the integration of the equations of motion of a particle orbiting an extended mass is to have a means to compute the gravitational field $\mathbf{g}\left(\mathbf{r}\right)$ of the body. This is indeed a multifacet problem, and the present study will be limited to some restrictive assumptions. In the case of the Rosetta mission to 67P only the shape and the total mass of the cometary nucleus are available from in situ measurements. Therefore, lacking other substantial information or measurements, the density of 67P must be assumed to be homogeneous. Even under these simple assumptions the computation of the gravitational field (2.3) can be carried out in several different ways. The starting point common to all is that the shape of the body is known as a series of surface points (vertices, or nodes) linked in a three-dimensional mesh with a number of edges. This amounts to approximating the real shape of the body as a polyhedron. The gravitational field can be computed directly, or it can be obtained by computing the gradient of the potential (2.5). The integrals appearing in (2.3) and (2.5) can be computed in essentially two ways, i.e., either in a finite formulation, or by means of series expansions. The first approach goes back to Betti (1879) and the recent track of specialized studies by (Werner, 1994; Petrovic, 1996; Werner and Scheeres, 1997; Tsoulis, 2012; **?**). The second approach can be differentiated as to whether inertial integrals or Stokes coefficients

---

[1] We will indifferently refer to $\mathbf{g}\left(\mathbf{r}\right)$ as an acceleration field of a force field, which we implicitly assume *per unit mass.*

[2] More in general, both the divergence (Gauss's Theorem) and the Laplacian (Poisson's Equation) of the gravitational field are proportional to the local mass density.

are used. More precisely, Stokes coefficients can be found not only for expansions in Spherical Harmonics, but also for other basis functions, depending on the geometry of the body. The rest of this chapter is concerned with the introduction of the finite model of the gravitational field through the method of Werner. The next two chapters will be devoted to the expansion of the potential in terms of inertial integrals and in spherical harmonics, respectively.

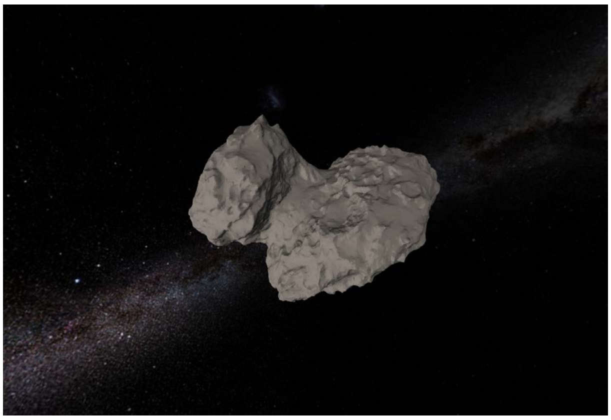

Figure 2.1. Comet 67P/Churyumov-Gerasimenko (ESA rendering)

2.2 Werner's method

Since the nucleus is so irregular, a numerical approach was used to calculate the potential in whatever position outside the nucleus using Werner's algorithm (Werner, 1994; Werner and Scheeres, 1997). We will now briefly outline a derivation of the algorithm and give its final formulation.

We assume from now on that the density σ of the body—in our specific case the nucleus of comet 67P— is constant throughout the volume, so that it can be factored out of the integration. The combined application of Gauss's divergence theorem and Greeen's theorem will enable us to easily calculate the volume integral in (2.5). We first use the particular case of Stokes theorem, known as Gauss Integral theorem, which asserts that the volume integral of the divergence of a vector field $\mathbf{w}$ is equal to the flux of the field through the surface bounding the volume, or

$$\iiint_V (\nabla \cdot \mathbf{w})\, dV = \iint_S \mathbf{w} \cdot d\boldsymbol{\sigma},$$

Application of this theorem to the definition of the potential (2.5) makes use of the fact that $\frac{1}{2}\nabla \cdot \mathbf{r} = 1/r$ to write that

$$2U = \iint_S \mathbf{r} \cdot d\mathbf{s} = \sum_{f\in\mathcal{F}} \iint_f \mathbf{r} \cdot d\boldsymbol{\sigma}_f, \tag{2.8}$$

where we have introduced the fact that the body is modeled as a polyhedron with a certain number of planar, polygonal faces consitituting the set $\mathcal{F}$. Here $d\boldsymbol{\sigma}_f = \hat{\mathbf{n}}_f\, d\sigma_f$ is the differential vectorial surface element aligned with the outer surface unit normal $\hat{\mathbf{n}}_f$. The algoritm thus decomposes the surface integral into the sum of integrals over each face f from the set $\mathcal{F}$. For convenience, a right-handed Cartesian "face" coordinate system is established for each face, with basis unit vectors $\mathbf{i}, \mathbf{j}, \mathbf{k}$, where $\mathbf{i}$ and $\mathbf{j}$ lie parallel to the face plane and $\mathbf{k}$ is aligned with the face's outward unit normal $\hat{\mathbf{n}}_f$. All the face's points, described by a vector $\boldsymbol{\rho}$, or coordinates (ξ, η, ζ), share the same coordinate along $\mathbf{k}$, denoted by ζ_f. The field point P in this reference system has coordinates (x, y, z) and is denoted by the vector $\mathbf{r}$. It is convenient for the derivation to use coordinates relative to P, so we define the components of the vector difference $\boldsymbol{\rho} - \mathbf{r}$ as

$$\begin{aligned} \Delta x &= \xi - x, \\ \Delta y &= \eta - y, \\ \Delta z &= \zeta_f - z. \end{aligned}$$

This implies that $\hat{\mathbf{r}} = \mathbf{i}\frac{\Delta x}{r} + \mathbf{j}\frac{\Delta y}{r} + \mathbf{k}\frac{\Delta z}{r}$, $r^2 = \Delta x^2 + \Delta y^2 + \Delta z^2$, and $d\sigma_f = d\xi d\eta = d(\Delta x)d(\Delta y)$. Substituting $\hat{\mathbf{r}}$ and $d\sigma_f$ in (2.8) and using Green's theorem yields for the contribution of a single face f the potential U_f given by

$$2U_f = \Delta z \oint \frac{1}{r} \left(\Delta x \, d\Delta y - \Delta y \, d\Delta x\right) - \omega_f \, \Delta z, \tag{2.9}$$

where the integral is taken along the perimeter of the face and ω_f is the signed solid angle subtended by the face f when viewed from the field point. It is important to remark that so far no restrictions have been put on the boundary of the face: the former formula is valid for any planar face. Considering now a face with n straight edges, we denote by $P_1, P_{2,} \ldots P_n$ its vertices, described by coordinates $(\Delta x_i, \Delta y_i, \Delta z_i)$ relative to the field pont P. Let r_i denote the distance between P and vertex P_i, and r_{ij} be the distance between vertices P_i and P_j. This allows the computation of the line integral in (2.9), which can be expressed, after appropriate manipulation, as

$$\oint \left(\frac{\Delta x}{r} d\Delta y - \frac{\Delta y}{r} d\Delta x\right) = \sum_{i=1}^{n} \frac{\Delta x_i \Delta y_{i+1} - \Delta x_{i+1} \Delta y_i}{r_{i,i+1}} \log\left(\frac{r_i + r_{i+1} + r_{i,i+1}}{r_i + r_{i+1} - r_{i,i+1}}\right), \tag{2.10}$$

where all indices are taken modulo n and the summation extends over all edges of a face. As for the solid angle ω_f appearing in second term on the RHS of (2.9), we only report the result for a triangular face f of vertices P_i, P_j, P_k and position vecotrs $\mathbf{r}_i, \mathbf{r}_j$ and $\mathbf{r}_k$ as

$$\omega_f = 2 \arctan \frac{\mathbf{r}_i \cdot \mathbf{r}_j \times \mathbf{r}_k}{r_i r_j r_k + r_i \left(\mathbf{r}_j \cdot \mathbf{r}_k\right) + r_j \left(\mathbf{r}_k \cdot \mathbf{r}_i\right) + r_k \left(\mathbf{r}_i \cdot \mathbf{r}_j\right)}. \tag{2.11}$$

The potential U_f of a single face of the homogeneous polyhedron can thus be computed as the sum of terms involving log functions and inverse trig functions. Summing the contributions from all faces and all edges of the polyhedron leads to the total potential U at the field point P. The success of the method rests on the fact that the volume integration over the simplices, defined by the prisms having the faces as bases and vertex at some fixed common origin, can effectively be reduced to integration over the faces only, since the surface integrations over the sides sharing the origin as one vertex are pairwise equal and opposite (due to the direction of the integration path which is always taken counterclockwise) and thus contributing nil.

The expression for the potential can now be used to derive the acceleration ∇U and the gravity gradient, or Hessian, $\nabla\nabla U$. The formulation proposed in (Werner and Scheeres, 1997), including a variant for the expression of the potential is as follows

$$U = \frac{1}{2} G\sigma \sum_{e \in \mathcal{E}} \left(\mathbf{r}_e^T \mathsf{E}_e \mathbf{r}_e\right) L_e - \frac{1}{2} G\sigma \sum_{f \in \mathcal{F}} \left(\mathbf{r}_f^T \mathsf{F}_f \mathbf{r}_f\right) \omega_f, \tag{2.12}$$

$$\nabla U = -G\sigma \sum_{e \in \mathcal{E}} \mathsf{E}_e \mathbf{r}_e \, L_e + G\sigma \sum_{f \in \mathcal{F}} \mathsf{F}_f \, \mathbf{r}_f \, \omega_f, \tag{2.13}$$

$$\nabla\nabla U = G\sigma \sum_{e \in \mathcal{E}} \mathsf{E}_e \, L_e - G\sigma \sum_{f \in \mathcal{F}} \mathsf{F}_f \, \omega_f, \tag{2.14}$$

where $\mathbf{r}_e$ is the vector pointing from the field point P to any point on the straight line containing the edge e, $\mathbf{r}_f$ a similar vector to any point on the plane containing face f , while (with the superscript T indicating transposition (of the algebraic vector!)) $\mathsf{E}_e = \hat{\mathbf{n}}_{f_1}\hat{\mathbf{n}}_e^{f_1T} + \hat{\mathbf{n}}_{f_2}\hat{\mathbf{n}}_e^{f_2T}$ and $\mathsf{F}_e = \hat{\mathbf{n}}_f\hat{\mathbf{n}}_f^T$ are each a square matrix of order 3, so that the terms in parentheses in equation (2.12) for the potential are quadratic forms. Note that $\hat{\mathbf{n}}_e^f$ is a unit vector normal to edge e lying on the plane of face f to which the edge belongs (thus also normal to $\hat{\mathbf{n}}_f$).

As a check on numerical computations it may be useful to compute the Laplacian from the formula

$$\nabla^2 U = -G\sigma \sum_{f\in\mathcal{F}} \omega_f. \tag{2.15}$$

The Laplacian is equal to the trace of the Hessian (2.14), which in free space is null.

2.3 Petrovich's and Tsoulis's Refinements of Werner's Method

An algorithm for the computation of the potential and its first two gradients in the case of a homogeneous polyhedral body was introduced by Petrovic (1996) independently of Werner (1994). The method uses the same strategy of reduction of the volume integral to surface integrals and finally to line integrals using, however, subsequent applications of the divergence theorem. The notable difference with respect to Werner's method is the identification of singularities in the process. For completeness, we will review the Petrovich method and discuss the singularities and corrective actions to take when they present themselves following **?**.

The derivation of the Petrovic algorithm for the computation of the potential U, its gradient ∇U and Hessian $\nabla\nabla U$ starts by noting that

$$U = G\sigma \iiint\limits_V \frac{1}{\Delta} dV, \tag{2.16a}$$

$$\frac{\partial U}{\partial \mathbf{r}} = G\sigma \iiint\limits_V \frac{\partial}{\partial \mathbf{r}}\left(\frac{1}{\Delta}\right) dV, \tag{2.16b}$$

$$\frac{\partial^2 U}{\partial \mathbf{r}^2} = G\sigma \iiint\limits_V \frac{\partial^2}{\partial \mathbf{r}^2}\left(\frac{1}{\Delta}\right) dV, \tag{2.16c}$$

can be transformed to surface integrals by application of the divergence theorem to yield, accounting for the polyhedral nature of the body of constant density σ and using the same notation as before,

$$U = \frac{1}{2} G\sigma \sum_{f\in\mathcal{F}} \sigma_f h_f \iint\limits_{\Sigma_f} \frac{1}{\Delta} dS, \tag{2.17a}$$

$$\partial_i U = G\sigma \sum_{f\in\mathcal{F}} (\hat{\mathbf{n}}_f \cdot \hat{\mathbf{e}}_i) \iint\limits_{\Sigma_f} \frac{1}{\Delta} dS, \qquad i = 1,2,3, \tag{2.17b}$$

$$\partial_{ij} U = G\sigma \sum_{f\in\mathcal{F}} (\hat{\mathbf{n}}_f \cdot \hat{\mathbf{e}}_i) \iint\limits_{\Sigma_f} \frac{\partial}{\partial x_j}\left(\frac{1}{\Delta}\right) dS, \qquad i,j = 1,2,3, \tag{2.17c}$$

where $\hat{\mathbf{n}}_f$ is the outward pointing normal to face f, $\hat{\mathbf{e}}_i$ $(i = 1,2,3)$ is an orthonormal basis centered at the field point P, Σ_f is the integration domain relative to face f, and Δ is the distance between the P and the integration element. σ_f is -1 or $+1$, respectively, depending on whether P is on the positive or negative half-space of face f, where positive and negative is decided by the direction of the outward normal $\hat{\mathbf{n}}_f$.

The ten independent components of the potential and its gradients—recall that the gravity gradient is a symmetrical matrix—clearly reduce to the computation of only two types of integrals, namely $\mathcal{A}_f$ and $\mathcal{B}_{fj}$, defined by

$$\mathcal{A}_f = \iint\limits_{\Sigma_f} \frac{1}{\Delta} dS \tag{2.18a}$$

$$\mathcal{B}_{fj} = \iint\limits_{\Sigma_f} \frac{\partial}{\partial x_j} \left(\frac{1}{\Delta} \right) dS \tag{2.18b}$$

? shows that these can be reduced to line integrals and reformulated as

$$\mathcal{A}_f = \sum_{q=1}^{m} \sigma_{fq} h_{pq} \int\limits_{e_{fq}} \frac{1}{\Delta} ds + h_p^2 \sum_{q=1}^{m} \sigma_{fq} h_{pq} \int\limits_{e_{fq}} \frac{1}{d^2 \Delta} ds, \tag{2.19a}$$

$$\mathcal{B}_{fj} = \sum_{q=1}^{m} \left(\hat{\mathbf{n}}_{fq} \cdot \hat{\mathbf{e}}_j \right) \int\limits_{e_{fq}} \frac{1}{\Delta} ds + \sigma_f h_f \left(\hat{\mathbf{n}}_f \cdot \hat{\mathbf{e}}_j \right) \sum_{q=1}^{m} \sigma_{fq} h_{fq} \int\limits_{e_{fq}} \frac{1}{d^2 \Delta} ds, \tag{2.19b}$$

where d is the distance between the projection P' of the point P on the face's plane and the integration element, h_f is the positive distance of P from the face's plane, $\hat{\mathbf{n}}_f$ is the outward pointing unit normal of face f, σ_f is -1 when the outward pointing surface normal $\hat{\mathbf{n}}_p$ of face Σ_f points to the half space containing the point P and $+1$ when it points to the other half, h_{fq} is the positive distance of the projection of point P onto the line containing the edge e_{pq} of face Σ_f,while $\hat{\mathbf{n}}_{pq}$ is the unit normal of edge e_{fq} pointing outward with respect to the face Σ_f, and finally σ_{fq} equals -1 when $\hat{\mathbf{n}}_{pq}$ points to the half plane containing the point P' and $+1$ if it points to the other half space. If point P' falls inside one of the polygonal faces, however, the application of Gauss's theorem is not permissible. According to Gauss's theorem, in fact, the vector field appearing in the formula must have continuous derivatives inside the integration area. It is obvious how the d^2 at the denominator in both formulas (2.19a) and (2.19b) is such a singular point in the case point P' is contained in the face. The solution to this singularity is well known in potential field theory. One divides the area of integration in two parts: a small circle containing point P' in its interior, and the rest of Σ_f. One obtains that the corrections to the final formula are $-\vartheta h_f$ for $\mathcal{A}_f$, and $-\vartheta \cos\left(\hat{\mathbf{n}}_f, \hat{\mathbf{e}}_j\right) \sigma_f$, where ϑ represents the angle of a circle centered on point P' contained inside the face Σ_f. For example, if point P' is contained in the interior of Σ_f, then $\vartheta = 2\pi$, while if it belongs to an edge $\vartheta = \pi$, and finally if it belongs to a vertex, ϑ is going to be equal to the interior angle of that vertex. After integrating $\mathcal{A}_f$ and $\mathcal{B}_{fj}$, and correcting the cases in which P' belongs to the face considered, one obtains the final formulae

$$U = \frac{1}{2} G\sigma \sum_{f \in \mathcal{F}} \sigma_f h_f \left[\sum_{q=1}^{m} \sigma_{fq} h_{fq} \mathrm{LN}_{fq} + h_f \sum_{q=1}^{m} \sigma_{fq} \mathrm{AN}_{fq} + \Gamma_{\mathcal{A}_f} \right], \tag{2.20a}$$

$$U_i = G\sigma \sum_{f \in \mathcal{F}} \left(\hat{\mathbf{n}}_f \cdot \hat{\mathbf{e}}_i \right) \left[\sum_{q=1}^{m} \sigma_{fq} h_{fq} \mathrm{LN}_{fq} + h_f \sum_{q=1}^{m} \sigma_{fq} \mathrm{AN}_{fq} + \Gamma_{\mathcal{A}_f} \right], \quad (i = 1, 2, 3),$$

$$U_{ij} = G\sigma \sum_{f \in \mathcal{F}} \left(\hat{\mathbf{n}}_f \cdot \hat{\mathbf{e}}_i \right) \left[\sum_{q=1}^{m} \left(\hat{\mathbf{n}}_{fq} \cdot \mathbf{e}_j \right) \mathrm{LN}_{fq} + \left(\hat{\mathbf{n}}_f \cdot \hat{\mathbf{e}}_j \right) \sigma_f \sum_{q=1}^{m} \sigma_{fq} \mathrm{AN}_{fq} + \Gamma_{\mathcal{B}_{fj}} \right], \quad (i, j = 1, 2, 3),$$

where $\Gamma_{\mathcal{A}_f}$ and $\Gamma_{\mathcal{B}_{fj}}$ represent the corrections to be applied to the possible singular cases considered,

$$\mathrm{LN}_{fq} = \log \frac{s_{2fq} + l_{2fq}}{s_{1fq} + l_{1fq}} \tag{2.21}$$

and

$$\mathrm{AN}_{pq} = \arctan\left(\frac{h_f s_{2fq}}{h_{fq} l_{2fq}}\right) - \arctan\left(\frac{h_f s_{1fq}}{h_{fq} l_{1fq}}\right). \tag{2.22}$$

Computationally it is more efficient to combine the two arc tangents into a single one as

$$\mathrm{AN}_{pq} = \arctan \frac{h_{fq} h_f \left(l_{1fq} s_{2fq} - s_{1fq} l_{2fq}\right)}{h_{fq}^2 l_{1fq} l_{2fq} + h_f^2 s_{1fq} s_{2fq}}. \tag{2.23}$$

with l_{1fq} and l_{2fq} the distances between P and the two endpoints of edge e_{fq} and with s_{1fq} and s_{2fq} the distances between the endpoints of edge e_{pq} and the projection of P' onto the edge line, P'', as shown in Figure (2.2).

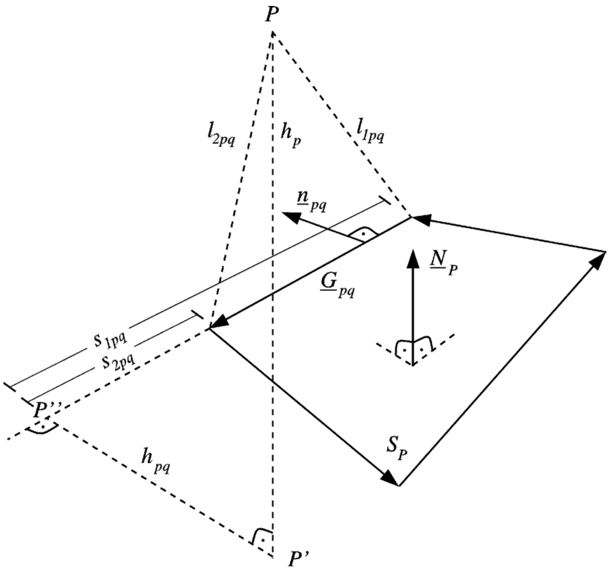

Figure 2.2. Geometric configuration of the field point P with respect to a quadrangular face. (From Petrovic and Tsoulis (2001), with the caveat that $G_{pq} \equiv e_{fq}$, and in general $p \equiv f$ in the subscripts.)

Chapter 3

The Gravitational Potential - 2
Expansion in Inertial Functions

3.1 Introduction

The finite formulation of the potential and the gravitational field presented in the previous chapter has the advantage of providing the correct values at any field point outside or on the surface of a polyhedral body of constant density. The downside is that this model is very intensive computationally, especially in view of the fact that an accurate description of an extended body requires on the order of millions of vertices. Some alternative computational approaches are therefore desirable and can be found in terms of series expansions. Other approaches, most notably in terms of finite elements (Colombi et al., 2008; Russell and Arora, 2012), have also been explored, but with somewhat inconclusive benefits to be reported. In this chapter we will try to carry out a program first delineated by MacMillan (1930) for field points far from the body and consisting of a series expansion in terms of *inertial integrals*.

Here, we will carry out MacMillan's program to the full extent for an extended body described by a polyhedral approximation. We will do so both for the case of distant points and for field points very near the surface of the body by introducing a generalization of the concept of inertial integrals to *inertial functions*. We start with some simple series expansion for a single point mass and then extend it to the cases of practical interest.

3.2 Expansion of $1/\Delta$ in Cartesian coordinates

Consider the points P and Q, whose coordinates are given with respect to a set of orthogonal axes $O[xyz]$ centered at O. Let $\mathbf{r}_P = (x_P, y_P, z_P)^T$ be the position vector of P and $\mathbf{r}_Q = (x_Q, y_Q, z_Q)^T$ the position vector of Q. The Euclidean distance Δ between P and Q is the function

$$\Delta\left(\mathbf{r}_Q;\mathbf{r}_P\right) = [(\mathbf{r}_P - \mathbf{r}_Q)^2]^{1/2} = [(x_P - x_Q)^2 + (y_P - y_Q)^2 + (z - z_Q)^2]^{1/2} \tag{3.1}$$

where the notation adopted for the functional dependence implies that this is to be considered a function of Q, P being considered to be fixed. In the following, for the sake of brevity, the dependence on the parameter $(\mathbf{r}_P)$ may be omitted.

We are interested in the inverse distance Δ^{-1} and would like to express it as a series expansion in the coordinates of the field point P. To address the general case, let us introduce a center of

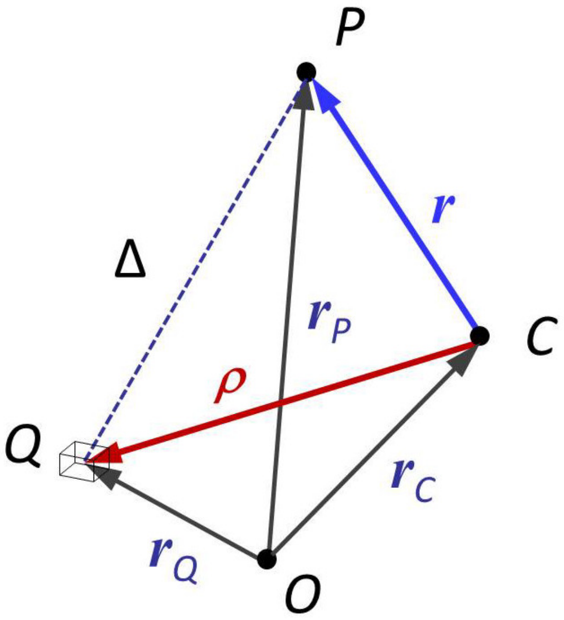

Figure 3.1. General configuration for the expansion abpout point C of the inverse distance $1/\Delta$ between point P and point Q.

expansion at a point C not coincident with either P or Q (see Figure 3.1). Then, with

$$\mathbf{r} = \mathbf{r}_P - \mathbf{r}_C, \tag{3.2}$$

$$\boldsymbol{\rho} = \mathbf{r}_Q - \mathbf{r}_C, \tag{3.3}$$

and $\mathbf{r}_C = (x_C, y_C, z_C)^T$ the distance becomes

$$\Delta\left(\mathbf{r};\boldsymbol{\rho}\right) = [(\mathbf{r}-\boldsymbol{\rho})^2]^{1/2}, \tag{3.4}$$

where the components of the vectors $\mathbf{r}$ and $\boldsymbol{\rho}$,

$$\mathbf{r} = (x, y, z)^T, \tag{3.5}$$

$$\boldsymbol{\rho} = (\xi, \eta, \zeta)^T, \tag{3.6}$$

are

$$x = x_P - x_C, \quad y = y_P - y_C, \quad z = z_P - z_C, \tag{3.7}$$

$$\xi = x_Q - x_C, \quad \eta = y_Q - y_C, \quad \zeta = z_Q - z_C. \tag{3.8}$$

The inverse distance expressed in coordinates referred to the reference system centered at C is now

$$\Delta^{-1}\left(\mathbf{r};\boldsymbol{\rho}\right) = \frac{1}{[(\mathbf{r}-\boldsymbol{\rho})^2]^{1/2}} = \frac{1}{\sqrt{(x-\xi)^2 + (y-\eta)^2 + (z-\zeta)^2}}. \tag{3.9}$$

The purpose is now to expand the inverse distance $1/\Delta$ in a series about C in the coordinates x, y, z of P. From the physical point of view this is relevant in terms of potential theory if a point mass is located at Q and P is the field point. If the reverse were true it would make sense to expand about C using the coordinates ξ, η, ζ of the point Q. However, here we are only interested in the formal aspects of the expansion and any switch of variables will be performed, if necessary, at the appropriate time.

To carry out the expansion let us first rewrite the inverse distance in the form

$$\Delta^{-1}(\mathbf{r};\boldsymbol{\rho}) = \frac{1}{\left(r^2 - 2\mathbf{r}\cdot\boldsymbol{\rho} + \rho^2\right)^{1/2}} \tag{3.10}$$

as an intermediate step toward realizing that it can be put in a form which can be expanded as a geometric series. To do so only requires that the larger of r and ρ be collected outside the square root to yield either

$$\Delta^{-1}(\mathbf{r};\boldsymbol{\rho}) = \frac{1}{r}\left[1 - 2\frac{\rho}{r}\left(\hat{\mathbf{r}}\cdot\hat{\boldsymbol{\rho}}\right) + \left(\frac{\rho}{r}\right)^2\right]^{-1/2}, \qquad \left(\frac{\rho}{r} < 1\right) \tag{3.11}$$

where, as noted, $\rho/r < 1$, or

$$\Delta^{-1}(\mathbf{r};\boldsymbol{\rho}) = \frac{1}{\rho}\left[1 - 2\frac{r}{\rho}\left(\hat{\mathbf{r}}\cdot\hat{\boldsymbol{\rho}}\right) + \left(\frac{r}{\rho}\right)^2\right]^{-1/2}, \qquad \left(\frac{r}{\rho} < 1\right) \tag{3.12}$$

where now $r/\rho < 1$, where the unit vectors $\hat{\mathbf{r}} = \mathbf{r}/r$ and $\hat{\boldsymbol{\rho}} = \boldsymbol{\rho}/\rho$ have been introduced. If now we define the new variables h as

$$h \in \left\{\frac{\rho}{r}, \frac{r}{\rho}\right\} \tag{3.13}$$

and D as the denominator of h, the two forms can be combined into the single form

$$D\Delta^{-}1\left(\mathbf{r};\boldsymbol{\rho}\right) = \left[1 - 2h\left(\hat{\mathbf{r}}\cdot\hat{\boldsymbol{\rho}}\right) + h^2\right]^{-1/2}. \tag{3.14}$$

The convergence properties of this function need to be investigated. The classical analysis of Hobson (1931) is repeated here for convenience, but with a slight twist and a final critique.

Note first that the dot product $\mu = \hat{\mathbf{r}}\cdot\hat{\boldsymbol{\rho}}$ is the cosine of the angle formed by the radii vectores from the center of the expansion C to the points P and Q so that $|\mu| \leq 1$. Thus we need to study the convergence of the series expansion of the function

$$f(h;\mu) = \left[1 - 2\mu h + h^2\right]^{-1/2}, \tag{3.15}$$

where the parameter μ satisfies the constraint just mentioned, i.e., $|\mu| \leq 1$. Let us first rewrite $f(h;\mu)$ as the product

$$f(h;\mu) = \left(\mu + \sqrt{\mu^2-1} - h\right)^{-1/2}\left(\mu - \sqrt{\mu^2-1} - h\right)^{-1/2}. \tag{3.16}$$

It is permissible to view the variable h and the parameter μ as complex quantities. If we now consider that the critical points of the function $f(h;\mu)$ are $h = \mu \pm \sqrt{\mu^2-1}$, the function $f(h;\mu)$ can be expanded in powers of h as long as $|h|$—the radius of convergence—is either less than the smaller h_m of the two quantities $|\mu \pm \sqrt{\mu^2-1}|$, or larger than the greater. As we will see shortly, the region comprised between these two values is of no interest for our analysis. In the first case convergence is assured over a circle centered at C (where $h = 0$) and whose radius is the smaller of $|\mu \pm \sqrt{\mu^2-1}|$, with the proviso that the function being represented is that which has value $+1$ at C. In the second case convergence is guaranteed over the region external to the circle of radius equal to the larger h_M of $|\mu \pm \sqrt{\mu^2-1}|$. Recalling at this point that μ is real and in the interval $[-1,+1]$, it follows that the radius of convergence for the first case is $|h| < 1$, while for the second case it is $|h| > 1$. In fact,

$$\frac{1}{\mu \pm \sqrt{\mu^2-1}} = \mu \mp \sqrt{\mu^2-1} \tag{3.17}$$

and this implies that at the extrema of the interval for μ we have the trivial identity $h_m = h_M = 1$. The form of the expansion is the typical Laurent series

$$f\,(h;\mu) = \sum_{n=-\infty}^{\infty} c_n h^n. \tag{3.18}$$

In the first case considered here this series reduces to the regular part of the Laurent expansion, i.e., to the Taylor series

$$f\,(h;\mu) = \sum_{n=0}^{\infty} c_n h^n, \qquad (|h| < 1) \tag{3.19}$$

since there are no singularities within the unit circle. In the second case the Leurent expansion is limited to the polar, or principal part

$$f\,(h;\mu) = \sum_{n=1}^{\infty} c_{-n} h^{-n}, \qquad (|h| > 1) \tag{3.20}$$

since a singularity exists within the circle $|h| < 1$ and the regular part of the series is identically null due to the fact that it cannot converge in this region. Note that the singularity, due to the nature of the function is an essential singularity, which causes the expansion to be effectively infinite, since it corresponds to, so to speak, a polar singularity of infinte order.

If now we redefine the variable h as

$$h = \min\left(\frac{\rho}{r}, \frac{r}{\rho}\right), \tag{3.21}$$

the Taylor series expansion (3.19) can be written explicitly in terms of the variables and parameters of our problem as

$$\Delta^{-1}\left(\mathbf{r};\boldsymbol{\rho}\right) = \frac{1}{r}\sum_{n=0}^{\infty} c_n \left(\frac{\rho}{r}\right)^n, \qquad \left(\frac{\rho}{r} < 1\right). \tag{3.22}$$

For reasons that will become apparent later, we will refer to this case as the *Brillouin configuration,* as depicted in Figure 3.2. The polar expansion (3.20) can instead be written as

$$\Delta^{-1}\left(\mathbf{r};\boldsymbol{\rho}\right) = \frac{1}{\rho}\sum_{n=0}^{\infty} c_{n+1} \left(\frac{r}{\rho}\right)^{n+1}, \qquad \left(\frac{r}{\rho} < 1\right), \tag{3.23}$$

and we will refer to this as the *Hotine configuration,* as depicted in Figure 3.3. Notice that the circles of convergence are identical and the regions inside and outside the circle are exactly related by the complex transformazion $z \to z^{-1}$. Furthermore, the series of the Hotine case reveals itself as a quasi-Taylor series in the expansion variable r/ρ. By quasi-Taylor we mean the absence of the zeroth-order term, i.e., the lack of c_0 term—a fundamental difference, as we will see from the physical point of view, from the Brillouin case. Also note that from the physical point of view the radius of convergence of the series is the distance of the (nearest) point mass from the center of expansion.

The critique to the analysis carrried out above focuses on the complexification of the real function expressing the inverse distance. The results obtained are certainly correct, since they are in line with a different type of analysis which is usually carried out when expanding in terms of Legendre polynomials. However, the fact that we have made use of the Laurent expansion and used it to derive two different expansions corresponding to its Taylor and polar parts, rests on the fact that the complexification has been introduced at the level of the function $f\,(h;\mu)$. If complexification is done at an earlier stage, i.e., at the level of $\Delta^{-1}(\mathbf{r};\boldsymbol{\rho})$, identifying the vectors $\mathbf{r}$ and $\boldsymbol{\rho}$ with complex variables, then the modulus function appears—and that is well known not to be an analytic function, which implies that we cannot invoke the Laurent expansion at that very early stage. This critique is supported by the remark made by S. Sternberg that there is no relation between the Newtonian potential and the theory of functions of a complex variable as it exists, for instance, in the case of the logarithmic potential (Sternberg and Smith, 1946, p. 167), which is the analog of the Newtonian potential in two dimensions (MacMillan, 1930).

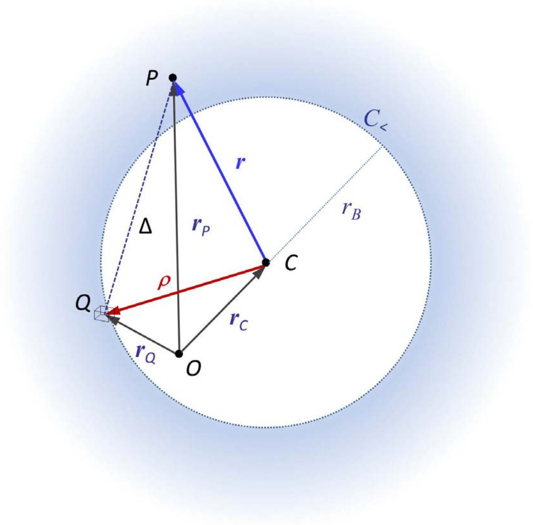

Figure 3.2. General *Brillouin configuration* for the expansion about point C of the inverse distance $1/\Delta$ between point P and point Q. The shaded area is the infinte region of convergence when the expansion is in the coordinates of P.

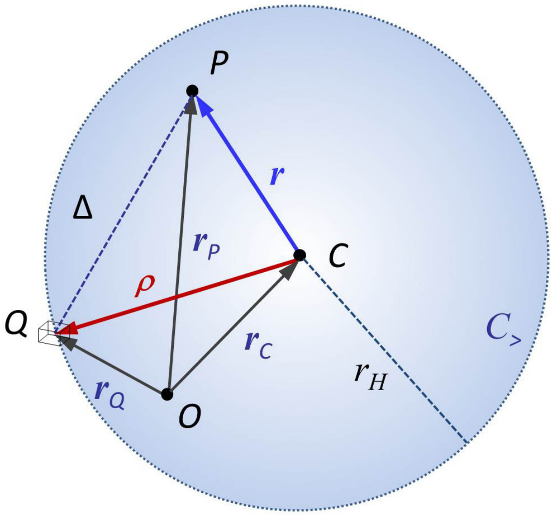

Figure 3.3. General *Hotine configuration* for the expansion about point C of the inverse distance $1/\Delta$ between point P and point Q. The shaded area is the region of convergence when the expansion is in the coordinates of P.

It is instructive at this point to observe that the nature of the expansions of the inverse distance only depend on the center of expansion C, not the location of the origin of the reference system used to describe the geometrical configuration. Taken note of this, we might as well move the origin to coincide with the center of expansion, as shown in 3.4 and Figure 3.5.

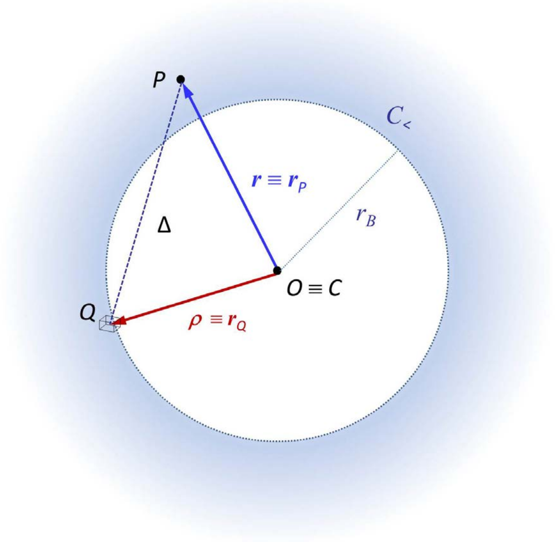

Figure 3.4. General *Pure Brillouin configuration.*

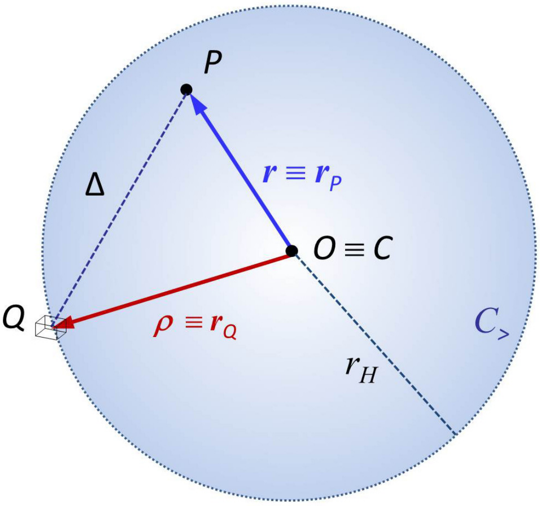

Figure 3.5. General *Pure Hotine configuration.*

Some insight can be earned about the nature of the coefficients of these expansions by writing a more explicit form of the series themselves. Let us first consider the Taylor series (3.22) of the Brillouin configuration. A close look at this equation reveals that formally it is also a Taylor series in the variable ρ, precisely because the expansion was generated for the variable ρ/r. The reason to look at this expansion from this point of view is that from now on we shall be interested in the potential of an extended body, or mass distribution (see Figure 3.6). Therefore, by referring back to the definition (2.5) of the potential function U, it is seen that the volume integration is carried out over the variables of the mass element, which in the current analysis are the components ξ, η, ζ of the vector $\boldsymbol{\rho}$. The Taylor series expansion we are interested in is then

$$\Delta^{-1}(Q) = \Delta^{-1}(C) + \left.\frac{\partial \Delta^{-1}}{\partial \boldsymbol{\rho}}\right|_C \boldsymbol{\rho} + \frac{1}{2!}\boldsymbol{\rho}^T \left.\frac{\partial^2 \Delta^{-1}}{\partial \boldsymbol{\rho}^2}\right|_C \boldsymbol{\rho} + \dots \tag{3.24}$$

In order to write the explicit expansion for the higher order terms, it will be expedient to

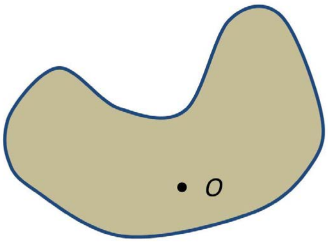

Figure 3.6. Mass distribution of an extended body and the location of the origin O of the coordinate system used to describe it.

make use of multiindex notation. Then, with $\boldsymbol{\alpha} = (\alpha_1, \alpha_2, \alpha_3)$ a multiindex of degree[1] 3, with

$$|\boldsymbol{n}| = n = i + j + k, \qquad \boldsymbol{n}! = i!j!k! \tag{3.25}$$

and

$$\boldsymbol{\rho}^{\boldsymbol{n}} = \xi^i \eta^j \zeta^k \tag{3.26}$$

as well as

$$\nabla_{\boldsymbol{\rho}}^{\boldsymbol{n}} = \partial_{\boldsymbol{\rho}}^{\boldsymbol{n}} = \partial_\xi^i \partial_\eta^j \partial_\zeta^k = \frac{\partial^n}{\partial \xi^i \partial \eta^j \partial \zeta^k}. \tag{3.27}$$

For the multivariable Taylor expansion we will also need the operator

$$\boldsymbol{\rho} \cdot \nabla_{\boldsymbol{\rho}} = \xi \frac{\partial}{\partial \xi} + \eta \frac{\partial}{\partial \eta} + \zeta \frac{\partial}{\partial \zeta} \tag{3.28}$$

so that

$$(\boldsymbol{\rho} \cdot \nabla_{\boldsymbol{\rho}})^{\boldsymbol{n}} = \sum_{|\boldsymbol{n}|=n} \frac{n!}{\boldsymbol{n}!} \boldsymbol{\rho}^{\boldsymbol{n}} \partial_{\boldsymbol{\rho}}^{\boldsymbol{n}} = \sum_{\substack{i,j,k \geq 0 \\ i+j+k=n}} \frac{n!}{i!j!k!} \xi^i \eta^j \zeta^k \frac{\partial^n}{\partial \xi^i \partial \eta^j \partial \zeta^k}. \tag{3.29}$$

Then the multivariable Taylor—effectively a MacLaurin series since it is computed at the origin—expansion can be compactly written as

$$\Delta^{-1}(\boldsymbol{\rho}) = \sum_n \frac{1}{n!} (\boldsymbol{\rho} \cdot \nabla_{\boldsymbol{\rho}})^{\boldsymbol{n}} \left. \Delta^{-1} \right|_{\boldsymbol{\rho}=\mathbf{0}}. \tag{3.30}$$

In our case this becomes

$$\Delta^{-1}(\boldsymbol{\rho}) = \sum_n \sum_{\substack{i,j,k \geq 0 \\ i+j+k=n}} \frac{1}{i!j!k!} \xi^i \eta^j \zeta^k \left(\frac{\partial^{i+j+k} \Delta^{-1}}{\partial \xi^i \partial \eta^j \partial \zeta^k} \right)_{\boldsymbol{\rho}=\mathbf{0}}. \tag{3.31}$$

Due to the special form of the inverse distance function, use can be made of the relationship

$$\frac{\partial}{\partial \boldsymbol{\rho}} = -\frac{\partial}{\partial \mathbf{r}} \tag{3.32}$$

between the gradients with respect to the positions of the two points in question. If this relationship is exploited in the expansion (3.31) we find the simpler expression

$$\boxed{\Delta^{-1}(\boldsymbol{\rho}) = \sum_n \sum_{\substack{i,j,k \geq 0 \\ i+j+k=n}} \frac{(-1)^i + j + k}{i!j!k!} \frac{\partial^i + j + kr^{-1}}{\partial x^i \partial y^j \partial z^k} \xi^i \eta^j \zeta^k} \tag{3.33}$$

---

[1] The usual term adopted for multiindex is actually *order*, but *degree* will be used here in keeping with the standard terminology adopted in dealing with expansions of the potential.

This series clearly consists of terms which are homogeneous polyomials of degree n in the variables ξ, η, ζ. The coefficients are functions of the variables x, y, z which are themselves homogeneous and, in fact, harmonic functions. This is easily proved by considering that the derivative of any order of the fundamental solid harmonic function $r^{-1} = \left(x^2 + y^2 + z^2\right)^{-1/2}$ with respect to $x, y,$ and z satisfies Laplace's equation.

Due to the symmetry between the coordinates of P and those of Q, the expansion (3.33) can be immediately written in the symmetric form

$$\boxed{\Delta^{-1}\left(\mathbf{r}\right) = \sum_{n} \sum_{\substack{i,j,k \geq 0 \\ i+j+k=n}} \frac{(-1)^i + j + k}{i!j!k!} \frac{\partial^i + j + k\rho^-1}{\partial\xi^i \partial\eta^j \partial\zeta^k} \, x^i y^j z^k} \tag{3.34}$$

These expansion formulae can now be applied to the case where P is the field point and Q is the source, i.e., the location of an attracting mass.

3.3 The MacMillan Brillouin sphere expansion

After studying some general features of the expansion of the inverse distance $1/\Delta$ between a source point Q and a field point P, we are now ready for the application to the development of the formulation of the potential of an extended body. The case of the Brillouin configuration will be addressed first. This consists in developing a formulation for points P which are farther from the center of expansion—now taken to coincide with the origin O with respect to which the body itself is described—than any elementary mass making up the body. This amounts to points external to the *Brillouin sphere*, or the sphere of minimum volume and centered at the center of expansion, containing the entire body as shown in Figure 3.7.

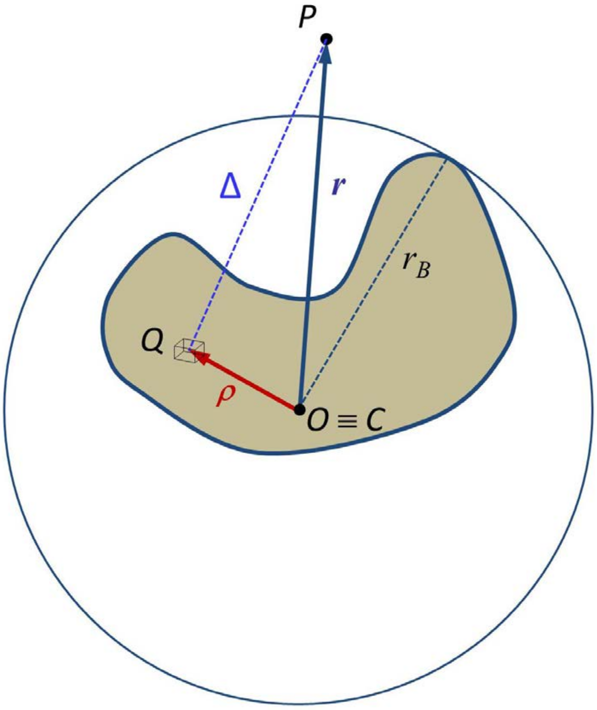

Figure 3.7. Configuration for the Brillouin expansion. The Brillouin sphere with radius r_B is shown centered at $O \equiv C$ containing the entire body.

The formulation of the potential will now be carried out by more elementary means than implied by the formulation of the Taylor series just given. That would unnecessarily require more sophisticated tools, like for instance Faà di Bruno operators (Murdock, 1983; Krantz and Parks, 2002).

Let us go back and reconsider the expression (3.9) of the inverse distance. Rewrite it according to the case of (3.11) as

$$\frac{1}{|\mathbf{r}-\boldsymbol{\rho}|}=\frac{1}{|\mathbf{r}|}\frac{1}{\sqrt{1-2\dfrac{\mathbf{r}\cdot\boldsymbol{\rho}}{\mathbf{r}\cdot\mathbf{r}}+\dfrac{\boldsymbol{\rho}\cdot\boldsymbol{\rho}}{\mathbf{r}\cdot\mathbf{r}}}},\qquad |\boldsymbol{\rho}|<|\mathbf{r}|\,. \tag{3.35}$$

Now apply the binomial expansion

$$(1+\alpha)^{-1/2}=\sum_{k=0}^{\infty}\binom{-1/2}{k}\alpha^{k}, \tag{3.36}$$

irrespective of the fact that the condition $(\boldsymbol{\rho}\cdot\boldsymbol{\rho})/r^2-2(\mathbf{r}\cdot\rho)/r^2<1$ may not be satisfied (this will be justified later), to yield

$$\frac{1}{|\mathbf{r}-\boldsymbol{\rho}|}=\frac{1}{r}\sum_{n=0}^{\infty}\binom{-1/2}{n}\left(-2\frac{\mathbf{r}\cdot\boldsymbol{\rho}}{\mathbf{r}\cdot\mathbf{r}}+\frac{\boldsymbol{\rho}\cdot\boldsymbol{\rho}}{\mathbf{r}\cdot\mathbf{r}}\right)^{n} \tag{3.37}$$

and develop the power so that

$$\frac{1}{|\mathbf{r}-\boldsymbol{\rho}|}=\sum_{n=0}^{\infty}\binom{-1/2}{n}\frac{1}{r^{2n+1}}\sum_{m=0}^{n}(-1)^{m}\,2^{m}\binom{n}{m}(\mathbf{r}\cdot\boldsymbol{\rho})^{m}(\boldsymbol{\rho}\cdot\boldsymbol{\rho})^{n-m} \tag{3.38}$$

Replacing the scalar products in terms of coordinates then

$$\frac{1}{|\mathbf{r}-\boldsymbol{\rho}|}=\sum_{n=0}^{\infty}\binom{-1/2}{n}\frac{1}{r^{2n+1}}\sum_{m=0}^{n}(-1)^{m}\,2^{m}\binom{n}{m}(x\xi+y\eta+z\zeta)^{m}\left(\xi^2+\eta^2+\zeta^2\right)^{n-m}. \tag{3.39}$$

At this point we use the expansion of the power of a trinomial,

$$(a+b+c)^{n}=\sum_{i=0}^{n}\sum_{j=0}^{i}\binom{n}{i}\binom{i}{j}a^{n-i}b^{i-j}c^{j}, \tag{3.40}$$

to get

$$\begin{aligned}\frac{1}{|\mathbf{r}-\boldsymbol{\rho}|}=\sum_{n=0}^{\infty}\binom{-1/2}{n}\frac{1}{r^{2n+1}}\sum_{m=0}^{n}(-1)^{m}\,2^{m}\binom{n}{m}\sum_{i=0}^{m}\sum_{j=0}^{i}\sum_{k=0}^{n-m}\sum_{l=0}^{k}\\ \binom{m}{i}\binom{i}{j}\binom{n-m}{k}\binom{k}{l}x^{m-i}y^{i-j}z^{j}\left[\xi^{2n-m-i-2k}\eta^{i-j+2k-2l}\zeta^{j+2l}\right]\end{aligned} \tag{3.41}$$

Note that the monomials

$$P_m^{ij}(x,y,z)=x^{m-i}y^{i-j}z^{j} \tag{3.42}$$

are homogeneous of degree m, since $P_m^{ij}(\alpha x,\alpha y,\alpha z)=\alpha^{m}P_m^{ij}(x,y,z)\,.$ In the expression of the inverse distance these monomials span from degree 0 to degree n.

Likewise, the monomials

$$Q_{2n-m}^{ijkl}\left(\xi,\eta,\zeta\right)=\xi^{2n-m-i-2k}\eta^{i-j+2k-2l}\zeta^{j+2l} \tag{3.43}$$

are homogeneous of degree $2n-m$ and span from degree n to degree $2n$. Now, since $0\leq n\leq N$, the span of the degree of these monomials is effectively from 0 to $2N$. The number N_Q of Q_{2n-m}^{ijkl} monomials that appear in the summation is $N_Q=(2N+1)\left(4N^2+16N+33\right)/6$, so $N_Q\sim N^3$.

The expansion (3.41) can now be inserted in the formula of the potential (2.5)

$$U\left(\mathbf{r}\right)=G\iiint\limits_V\frac{\sigma\left(\boldsymbol{\rho}\right)}{\left|\mathbf{r}-\boldsymbol{\rho}\right|}\,d\xi\,d\eta\,d\zeta. \tag{3.44}$$

We get

$$\begin{aligned}U\left(\mathbf{r}\right)=G\iiint\limits_V\sum_{n=0}^{\infty}\binom{-1/2}{n}\frac{1}{r^{2n+1}}\sum_{m=0}^{n}\left(-1\right)^m2^m\binom{n}{m}\\ \sum_{i=0}^{m}\sum_{j=0}^{i}\sum_{k=0}^{n-m}\sum_{l=0}^{k}\binom{m}{i}\binom{i}{j}\binom{n-m}{k}\binom{k}{l}x^{m-i}y^{i-j}z^j\\ \iiint\limits_V\sigma\left(\boldsymbol{\rho}\right)\xi^{2n-m-i-2k}\eta^{i-j+2k-2l}\zeta^{j+2l}\,d\xi\,d\eta\,d\zeta\end{aligned} \tag{3.45}$$

Introducing the *inertial integrals* I_{ijk} (MacMillan (1930)) defined by

$$\boxed{I_ijk=\iiint\limits_V\sigma\left(\boldsymbol{\rho}\right)\,\xi^i\eta^j\zeta^k\,d\xi\,d\eta\,d\zeta} \tag{3.46}$$

the potential can be finally cast in the form

$$\begin{aligned}U\left(\mathbf{r}\right)=G\sum_{n=0}^{\infty}\binom{-1/2}{n}\sum_{m=0}^{n}\left(-1\right)^m2^m\binom{n}{m}\sum_{i=0}^{m}\sum_{j=0}^{i}\sum_{k=0}^{n-m}\sum_{l=0}^{k}\\ \binom{m}{i}\binom{i}{j}\binom{n-m}{k}\binom{k}{l}\left[I_{2n-m-i-2k,i-j+2k-2l,j+2l}\right]\frac{x^{m-i}y^{i-j}z^j}{r^{2n+1}}\end{aligned} \tag{3.47}$$

Introducing the normalized inertial integrals $\bar{I}_{nm}^{ijkl}$ defined as

$$\bar{I}_{nm}^{ijkl}=M^{-1}I_{2n-m-i-2k,i-j+2k-2l,j+2l}, \tag{3.48}$$

the potential can be written more compactly in the form

$$\boxed{U\left(\mathbf{r}\right)=\frac{GM}{r}\sum_{n=0}^{\infty}\sum_{m=0}^{n}\sum_{i=0}^{m}\sum_{j=0}^{i}\sum_{k=0}^{n}-m\sum_{l=0}^{k}C_nm^ijkl\bar{I}_{nm}^{ijkl}\frac{x^{m-i}y^{i-j}z^j}{r^{2n}},} \tag{3.49}$$

where

$$C_{nm}^{ijkl}=\left(-1\right)^m2^m\binom{-1/2}{n}\binom{n}{m}\binom{m}{i}\binom{i}{j}\binom{n-m}{k}\binom{k}{l}. \tag{3.50}$$

The computation of the binomial coefficients so profusely appearing in these development is addressed in Appendix B.

Notice that in the expansion (3.49) the indices k and l do not appear in the expansion variables. Thus, by introducing the *lumped inertial integrals* $\bar{I}^{ij}_{nm}$ as

$$\bar{I}^{ij}_{nm} = \sum_{k=0}^{n-m}\sum_{l=0}^{k}\binom{n-m}{k}\binom{k}{l}\bar{I}^{ijkl}_{nm} \tag{3.51}$$

and the reduced coefficients

$$C^{ij}_{nm} = (-1)^m\, 2^m\binom{-1/2}{n}\binom{n}{m}\binom{m}{i}\binom{i}{j}, \tag{3.52}$$

the potential assumes the simpler form

$$\boxed{U(\mathbf{r}) = \frac{GM}{r}\sum_{n=0}^{\infty}\sum_{m=0}^{n}\sum_{i=0}^{m}\sum_{j=0}^{i}C_n m^i j\bar{I}^{ij}_{nm}\frac{x^{m-i}y^{i-j}z^j}{r^{2n}}} \tag{3.53}$$

3.3.1 The First- and Second-Order Gradients (Gravity and Gravity Gradient)

The first-order gradients can be easily computed from the expression (3.53) of the potential. Since the function to be differentiated is of the form

$$\frac{x^a y^b z^c}{r^d} \tag{3.54}$$

with $a = m - i$, $b = i - j$, $c = j$ and $d = 2n + 1$, it will be easier to provide the first- and second-order partials of this template function. The results for use in computing the acceleration are

$$\frac{\partial}{\partial x}\frac{x^a y^b z^c}{r^d} = \left(a - d\frac{x^2}{r^2}\right)\frac{x^{a-1}y^b z^c}{r^d}, \tag{3.55}$$

$$\frac{\partial}{\partial y}\frac{x^a y^b z^c}{r^d} = \left(b - d\frac{y^2}{r^2}\right)\frac{x^a y^{b-1} z^c}{r^d}, \tag{3.56}$$

$$\frac{\partial}{\partial z}\frac{x^a y^b z^c}{r^d} = \left(c - d\frac{z^2}{r^2}\right)\frac{x^a y^b z^{c-1}}{r^d}, \tag{3.57}$$

while those for the gravity gradients are

$$\frac{\partial^2}{\partial x^2}\frac{x^a y^b z^c}{r^d} = \left[d(2+d)\frac{x^4}{r^4} - d(1+2a)\frac{x^2}{r^2} + a(a-1)\right]\frac{x^{a-2}y^b z^c}{r^d}, \tag{3.58}$$

$$\frac{\partial^2}{\partial y^2}\frac{x^a y^b z^c}{r^d} = \left[d(2+d)\frac{y^4}{r^4} - d(1+2b)\frac{y^2}{r^2} + b(b-1)\right]\frac{x^a y^{b-2} z^c}{r^d}, \tag{3.59}$$

$$\frac{\partial^2}{\partial z^2}\frac{x^a y^b z^c}{r^d} = \left[d(2+d)\frac{z^4}{r^4} - d(1+2c)\frac{z^2}{r^2} + c(c-1)\right]\frac{x^a y^b z^{c-2}}{r^d}, \tag{3.60}$$

for the diagonal elements, and

$$\frac{\partial^2}{\partial y \partial x}\frac{x^a y^b z^c}{r^d} = \left[2d\frac{x^2 y^2}{r^4} + \left(a - d\frac{x^2}{r^2}\right)\left(b - d\frac{y^2}{r^2}\right)\right]\frac{x^{a-1}y^{b-1}z^c}{r^d}, \tag{3.61}$$

$$\frac{\partial^2}{\partial z \partial x}\frac{x^a y^b z^c}{r^d} = \left[2d\frac{x^2 z^2}{r^4} + \left(a - d\frac{x^2}{r^2}\right)\left(c - d\frac{z^2}{r^2}\right)\right]\frac{x^{a-1}y^b z^{c-1}}{r^d}, \tag{3.62}$$

$$\frac{\partial^2}{\partial z \partial y}\frac{x^a y^b z^c}{r^d} = \left[2d\frac{y^2 z^2}{r^4} + \left(b - d\frac{y^2}{r^2}\right)\left(c - d\frac{z^2}{r^2}\right)\right]\frac{x^a y^{b-1} z^{c-1}}{r^d}, \tag{3.63}$$

for the symmetric, off-diagonal terms.

When numerically evaluating the acceleration and the gravity gradient components efficient schemes can be devised due to the many different recurrence formulae that can be exploited in passing to indices one unit higher.

3.3.2 Computation of the Inertial Integrals

The next step toward the numerical evaluation of the potential and its gradients for the Brillouin configuration is to develop an efficient algorithm for the computation of the inertial integrals. Following the approach adopted in the method of Werner we can exploit to the fullest extent the fact that the surface of the body is described as a polyhedron. This will be done in connection with the simplifying assumption that the body be homogeneous, so that the constant density will not enter the computation of the volume integrals. The method introduced here appears to be novel, since no trace of it has been found in the literature.

We first begin by analyzing how many, and which inertial integrals appear in the expansion of the potential when this is limited to a maximum degree N. The integrals are defined by three indices, each of which is a linear combination of the six summation indices in equation (3.47). Given the range of the summation indices and the fact that the monomials $Q_{2n-m}^{ijkl}(\xi, \eta, \zeta)$ defined in (3.43) are homogeneous and span orders from 0 to $2N$, it can be seen that the inertial integrals involved in the expansion are the same that appear in the expression

$$\sum_{m=0}^{2N}\sum_{p=0}^{m}\sum_{q=0}^{p} I_{m-p,p-q,q}, \tag{3.64}$$

where the summation is merely used as a surrogate for the associated loops when writing computer code.

Now then we have to compute the set of integrals

$$V\bar{I}_{m-p,p-q,q} = \iiint\limits_{V} \xi^{m-p}\eta^{p-q}\zeta^{q}\, d\xi\, d\eta\, d\zeta \tag{3.65}$$

for the indices noted above. The strategy is to reduce the volume integral over the polyhedral body to a series of surface integrals over the faces and each of these finally to a number of line integrals along the edges. The tools that allow this transformation are the theorems of Gauss, of Stokes and of Green.

Volume to surface integration

In order to reduce the integral over the volume to an integral of the surface bounding the volume we make use of Gauss's divergence theorem. This theorem states that the flux of a vector field $\mathbf{T}$ over a closed surface is equal to the integral of the divergence of the vector field over the volume contained within the surface. In formal mathematical terms we have that

$$\iiint\limits_{V} \nabla \cdot \mathbf{T}\, d\xi\, d\eta\, d\zeta = \iint\limits_{\Sigma} \mathbf{T} \cdot d\boldsymbol{\sigma}, \tag{3.66}$$

where $d\boldsymbol{\sigma} = d\left(\sigma \hat{\mathbf{n}}\right)$ is the differential vector of the surface element $d\sigma$ in the direction of the outer surface normal $\hat{\mathbf{n}}$.

Applied to the case at hand we first have to solve the partial differential equation

$$\nabla \cdot \mathbf{T} = \frac{\partial T_\xi}{\partial \xi} + \frac{\partial T_\eta}{\partial \eta} + \frac{\partial T_\zeta}{\partial \zeta} = \xi^{m-p}\eta^{p-q}\zeta^{q} \tag{3.67}$$

to determine the vector field $\mathbf{T}$. We can take for simplicity any of the three solutions

$$(A) \quad \mathbf{T} = T_\xi \hat{\boldsymbol{\xi}} = \frac{1}{m-p+1} \xi^{m-p+1} \eta^{p-q} \zeta^q \, (1,0,0)^T \,, \tag{3.68}$$

$$(B) \quad \mathbf{T} = T_\eta \hat{\boldsymbol{\eta}} = \frac{1}{p-q+1} \xi^{m-p} \eta^{p-q+1} \zeta^q \, (0,1,0)^T \,, \tag{3.69}$$

$$(C) \quad \mathbf{T} = T_\zeta \hat{\boldsymbol{\zeta}} = \frac{1}{q+1} \xi^{m-p} \eta^{p-q} \zeta^{q+1} \, (0,0,1)^T \,, \tag{3.70}$$

where the field $\mathbf{T}$ has been chosen to have only one component, each of the three solutions being along one of the coordinate axes. For each of the three cases we have the following application of the divergence theorem

$$\begin{aligned}(A) \quad V\bar{I}_{m-p,p-q,q} &= \sum_{f=1}^{F} \iint_{\Sigma_f} T_\xi \hat{\boldsymbol{\xi}} \cdot d\boldsymbol{\sigma} \\ &= \frac{1}{m-p+1} \sum_{f=1}^{F} \iint_{\Sigma_f} \xi^{m-p+1} \eta^{p-q} \zeta^q \, (1,0,0)^T \cdot d\sigma,\end{aligned} \tag{3.71}$$

$$\begin{aligned}(B) \quad V\bar{I}_{m-p,p-q,q} &= \sum_{f=1}^{F} \iint_{\Sigma_f} T_\eta \hat{\boldsymbol{\eta}} \cdot d\boldsymbol{\sigma} \\ &= \frac{1}{p-q+1} \sum_{f=1}^{F} \iint_{\Sigma_f} \xi^{m-p} \eta^{p-q+1} \zeta^q \, (0,1,0)^T \cdot d\sigma,\end{aligned} \tag{3.72}$$

$$\begin{aligned}(C) \quad V\bar{I}_{m-p,p-q,q} &= \sum_{f=1}^{F} \iint_{\Sigma_f} T_\zeta \hat{\boldsymbol{\zeta}} \cdot d\boldsymbol{\sigma} \\ &= \frac{1}{q+1} \sum_{f=1}^{F} \iint_{\Sigma_f} \xi^{m-p} \eta^{p-q} \zeta^{q+1} \, (0,0,1)^T \cdot d\sigma.\end{aligned} \tag{3.73}$$

Accounting for the polyhedral form of the body volume, the surface integral is taken over the set of F faces, Σ_f indicating the surface of face f. For short we may in the following denote the area of the set of faces simply with the symbol Σ. Note that the surface normal $\hat{\mathbf{n}}$ is constant over each face of the polyhedron, a property which can be exploited to simplify the evaluation of the integrals.

Surface to line integral

To evaluate these surface integrals we now apply Green's theorem in Stokes's form which states that the flux of the curl of a vector field $\mathbf{H}$ through a surface Σ is equal to the circulation of the field along the boundary of the surface. In symbols,

$$\iint_{\Sigma} \nabla \times \mathbf{H} \cdot d\boldsymbol{\sigma} = \int_{\partial\Sigma} \mathbf{H} \cdot d\mathbf{s} \tag{3.74}$$

where $d\mathbf{s}$ is the line element on the countour $\partial\Sigma$ of the surface Σ. Application to the present case, in which $\nabla \times \mathbf{H} = \mathbf{T}$, starts with the solution of the three simple equations

$$(A)\quad \nabla\times\mathbf{H}=T_\xi\hat{\boldsymbol{\xi}}=\frac{1}{m-p+1}\xi^{m-p+1}\eta^{p-q}\zeta^{q}\,(1,0,0)^T\,, \tag{3.75}$$

$$(B)\quad \nabla\times\mathbf{H}=T_\eta\hat{\boldsymbol{\eta}}=\frac{1}{p-q+1}\xi^{m-p}\eta^{p-q+1}\zeta^{q}\,(0,1,0)^T\,, \tag{3.76}$$

$$(C)\quad \nabla\times\mathbf{H}=T_\zeta\hat{\boldsymbol{\zeta}}=\frac{1}{q+1}\xi^{m-p}\eta^{p-q}\zeta^{q+1}\,(0,0,1)^T\,, \tag{3.77}$$

which have been set up corresponding to the three cases being carried through in our analysis. Upon recalling that the components of the curl of the as yet unknown vector field **H** are

$$\nabla\times\mathbf{H}\cdot\hat{\boldsymbol{\xi}}=\frac{\partial H_\zeta}{\partial\eta}-\frac{\partial H_\eta}{\partial\zeta}, \tag{3.78}$$

$$\nabla\times\mathbf{H}\cdot\hat{\boldsymbol{\eta}}=\frac{\partial H_\xi}{\partial\zeta}-\frac{\partial H_\zeta}{\partial\xi}, \tag{3.79}$$

$$\nabla\times\mathbf{H}\cdot\hat{\boldsymbol{\zeta}}=\frac{\partial H_\eta}{\partial\xi}-\frac{\partial H_\xi}{\partial\eta}, \tag{3.80}$$

it follows that the partial differential equations to be solved in the three cases are the following

$$(A)\quad \frac{\partial H_\zeta}{\partial\eta}-\frac{\partial H_\eta}{\partial\zeta}=T_\xi=\frac{1}{m-p+1}\xi^{m-p+1}\eta^{p-q}\zeta^{q}, \tag{3.81}$$

$$(B)\quad \frac{\partial H_\xi}{\partial\zeta}-\frac{\partial H_\zeta}{\partial\xi}=T_\eta=\frac{1}{p-q+1}\xi^{m-p}\eta^{p-q+1}\zeta^{q}, \tag{3.82}$$

$$(C)\quad \frac{\partial H_\eta}{\partial\xi}-\frac{\partial H_\xi}{\partial\eta}=T_\zeta=\frac{1}{q+1}\xi^{m-p}\eta^{p-q}\zeta^{q+1}. \tag{3.83}$$

At this point we use the freedom to set to zero two of the components of **H** in each case. It follows that if we eliminate the component appearing in the second partial on the LHS of the previous equations and the component not appearing at all, we find the simple solutions

$$(A)\quad H_\zeta=\frac{1}{p-q+1}\frac{1}{m-p+1}\xi^{m-p+1}\eta^{p-q+1}\zeta^{q} \tag{3.84}$$

$$(B)\quad H_\xi=\frac{1}{p-q+1}\frac{1}{q+1}\xi^{m-p}\eta^{p-q+1}\zeta^{q+1} \tag{3.85}$$

$$(C)\quad H_\eta=\frac{1}{q+1}\frac{1}{m-p+1}\xi^{m-p+1}\eta^{p-q}\zeta^{q+1} \tag{3.86}$$

We can now write the Green's formula (3.74) in the three different case. If we generically indicate with $\hat{\boldsymbol{\omega}}$ the direction—one of the coordinate axes' unit vectors $\hat{\xi},\hat{\boldsymbol{\eta}}$, or $\hat{\boldsymbol{\zeta}}$—of the only component of the field **H**, i.e., we generically indicate with $H_\omega\,\hat{\boldsymbol{\omega}}$ the solution to the PDE $\nabla\times\mathbf{H}=\mathbf{T}$ exhibited in (3.84), (3.85) and (3.86), Green's formula becomes

$$\iint\limits_{\Sigma}\mathbf{T}\cdot d\boldsymbol{\sigma}=\sum_f\int\limits_{\partial\Sigma_f}H_\omega\,\hat{\boldsymbol{\omega}}\cdot d\mathbf{s}=\sum_f\int\limits_{\partial\Sigma_f}H_\omega\,ds_\omega, \tag{3.87}$$

where we have used the representation $d\,(s_\omega\hat{\boldsymbol{\omega}})$ to indicate the generic line element along a coordinate axis, i.e., any of the three components of $d\mathbf{s}=d(\xi\hat{\boldsymbol{\xi}}+\eta\hat{\boldsymbol{\eta}}+\zeta\hat{\zeta})$.

Applied to each of the three cases under study yields

$$(A) \quad V\bar{I}_{m-p,p-q,q} = \frac{1}{p-q+1}\frac{1}{m-p+1}\sum_f \int\limits_{\partial\Sigma_f} \xi^{m-p+1}\eta^{p-q+1}\zeta^q d\zeta \tag{3.88}$$

$$(B) \quad V\bar{I}_{m-p,p-q,q} = \frac{1}{p-q+1}\frac{1}{q+1}\sum_f \int\limits_{\partial\Sigma_f} \xi^{m-p}\eta^{p-q+1}\zeta^{q+1} d\xi \tag{3.89}$$

$$(C) \quad V\bar{I}_{m-p,p-q,q} = \frac{1}{q+1}\frac{1}{m-p+1}\sum_f \int\limits_{\partial\Sigma_f} \xi^{m-p+1}\eta^{p-q}\zeta^{q+1} d\eta \tag{3.90}$$

The conversion from volume to line integrals is now complete. Any of the three cases can be applied in practice, as long as it is consistently applied to all the edges of the polyhedron. This is because the vector field in each reduction of the dimension of the intergrals must be common to the entire space considered.

One last step is necessary in order to carry out the final integration along the boundary of each face of the polyhedron.

3.3.3 Evaluation of the line integrals

In order to compute the line integrals we need a parametrizaion of the integration path. Given the polyhedral description of the body's surface, every integration path is the perimeter of a triangular face. The fact that all faces are triangles in no way limits the approach that follows, as long as each face is the polygonal face of a polyhedron. Let us assume that the generic segment of the boundary $\partial\Sigma_f^\zeta$ connects the points $P_{fi}\left(\xi_{fi}, \zeta_{fi}\right)$ and $P_{f,i+1}\left(\xi_{f,i+1}, \zeta_{f,i+1}\right)$, $i = 1, 2, 3$ (here the sums are taken modulo 3 since we are assuming the polyhedron to be made of triangular faces). This can be represented as the vector

$$\mathbf{r}_{fi,i+1}(t) = \begin{pmatrix} \xi_{fi}(t) \\ \eta_{fi}(t) \\ \zeta_{fi}(t) \end{pmatrix} = \begin{pmatrix} \xi_{fi}(1-t) + \xi_{f,i+1}\,t \\ \eta_{fi}(1-t) + \eta_{f,i+1}\,t \\ \zeta_{fi}(1-t) + \zeta_{f,i+1}\,t \end{pmatrix}, \qquad 0 \le t \le 1 \tag{3.91}$$

from which we quickly get the expressions for the differentials

$$d\xi = \left(\xi_{f,i+1} - \xi_{fi}\right) dt = \Delta\xi_{fi} dt, \tag{3.92}$$

$$d\eta = \left(\eta_{f,i+1} - \eta_{fi}\right) dt = \Delta\eta_{fi} dt, \tag{3.93}$$

$$d\zeta = \left(\zeta_{f,i+1} - \zeta_{fi}\right) dt = \Delta\zeta_{fi} dt, \tag{3.94}$$

where we have introduced the projections of the edge as the quantities $\Delta\xi_{fi} = \left(\xi_{f,i+1} - \xi_{fi}\right)$, $\Delta\eta_{fi} = \left(\eta_{f,i+1} - \eta_{fi}\right)$ and $\Delta\zeta_{fi} = \left(\zeta_{f,i+1} - \zeta_{fi}\right)$ which are the lengths of the components of the integration path associated with each edge i of face f.

Let us now focus on case (B), where the vector field $\mathbf{H}$ is aligned in the direction $\hat{\boldsymbol{\xi}}$. Then, upon changing to the new integration variable t (3.89) can be rewritten as

$$V\bar{I}_{m-p,p-q,q} = \frac{1}{(p-q+1)(q+1)}\sum_f \sum_{i=1}^{3} \Delta\xi_{fi} \int\limits_0^1 \left[\xi(t)\right]^{m-p} \left[\eta(t)\right]^{p-q+1} \left[\zeta(t)\right]^{q+1} dt$$

The integrand function can be written explicitly through the use of the parameterization (3.91) as

$$\begin{aligned}[\xi(t)]^{m-p}[\eta(t)]^{p-q}[\zeta(t)]^{q+1} = {} & [\xi_{fi}(1-t)+\xi_{f,i+1}\,t]^{m-p} \\ & \times [\eta_{fi}(1-t)+\eta_{f,i+1}\,t]^{p-q+1} \\ & \times [\zeta_{fi}(1-t)+\zeta_{f,i+1}\,t]^{q+1}\,. \end{aligned} \tag{3.95}$$

This can be greatly simplified and made ready for integration through the application of the Bernstein polynomials (Farin, 1997) and their useful properties. Bernstein polynomials and their properties are presented in Appendix C. To illustrate the use of Bernstein polynomials in this contex, consider the espression $[a(1-t)+b\,t]^k$, which is the paradigm for the three factors of the integrand, and expand it using the binomial theorem to yield

$$[a(1-t)+b\,t]^n = a^n\left[(1-t)+\frac{b}{a}\,t\right]^n = a^n\sum_{u=0}^{n}\binom{n}{u}\left(\frac{b}{a}\right)^u t^u(1-t)^{n-u}\,. \tag{3.96}$$

Now recall that the Bernstein polynomial of degree n and order k is defined as

$$B_k^n(\lambda) = \binom{n}{k}\lambda^k(1-\lambda)^{n-k}\,, \tag{3.97}$$

which allows rewriting (3.96) as

$$[a(1-t)+b\,t]^n = a^n\sum_{u=0}^{n}\left(\frac{b}{a}\right)^u B_u^n(t)\ . \tag{3.98}$$

On this basis we can write the three factors in (3.95) as

$$[\xi_{fi}(1-t)+\xi_{f,i+1}\,t]^{m-p} = (\xi_{fi})^{m-p}\sum_{u=0}^{m-p}\left(\frac{\xi_{f,i+1}}{\xi_{fi}}\right)^u B_u^{m-p}(t)\,, \tag{3.99}$$

$$[\eta_{fi}(1-t)+\eta_{f,i+1}\,t]^{p-q+1} = (\eta_{fi})^{p-q}\sum_{v=0}^{p-q}\left(\frac{\eta_{f,i+1}}{\eta_{fi}}\right)^v B_v^{p-q+1}(t)\,, \tag{3.100}$$

$$[\zeta_{fi}(1-t)+\zeta_{f,i+1}\,t]^{q+1} = (\zeta_{fi})^{q+1}\sum_{w=0}^{q+1}\left(\frac{\zeta_{f,i+1}}{\zeta_{fi}}\right)^w B_w^{q+1}(t)\,. \tag{3.101}$$

The multiplication property C.7 of Bernstein polynomials

$$B_i^p(\lambda)\,B_k^q(\lambda)\,B_l^r(\lambda) = \frac{\binom{p}{i}\binom{q}{k}\binom{r}{l}}{\binom{p+q}{i+k}\binom{p+q+r}{i+k+l}}B_{i+k+l}^{p+q+r}(\lambda) \tag{3.102}$$

can now be used to write the integrand as

$$\begin{aligned}[\xi(t)]^{m-p}[\eta(t)]^{p-q+1}[\zeta(t)]^{q+1} = {} & (\xi_{fi})^{m-p}(\eta_{fi})^{p-q+1}(\zeta_{fi})^{q+1} \\ & \sum_{u=0}^{m-p}\sum_{v=0}^{p-q+1}\sum_{w=0}^{q+1}\frac{\binom{m-p}{u}\binom{p-q+1}{v}\binom{q+1}{w}}{\binom{m-q+1}{u+v}\binom{m+2}{u+v+w}} \\ & \left(\frac{\xi_{f,i+1}}{\xi_{fi}}\right)^u\left(\frac{\eta_{f,i+1}}{\eta_{fi}}\right)^v\left(\frac{\zeta_{f,i+1}}{\zeta_{fi}}\right)^w B_{u+v+w}^{m}(\lambda)\,. \end{aligned} \tag{3.103}$$

As a last step now invoke the integration property of the Bernstein polynomial,

$$\int_0^1 B_k^n(\lambda)\, d\lambda = \frac{1}{n+1}, \tag{3.104}$$

to explicitly write the inertial integral as

$$V\bar{I}_{m-p,p-q,q} = \frac{1}{(p-q+1)(q+1)(m+1)} \sum_f \sum_{i=1}^{3} \Delta\xi_{fi} (\xi_{fi})^{m-p} (\eta_{fi})^{p-q+1} (\zeta_{fi})^{q+1} \tag{3.105}$$

$$\sum_{u=0}^{m-p} \sum_{v=0}^{p-q+1} \sum_{w=0}^{q+1} \frac{\binom{m-p}{u}\binom{p-q+1}{v}\binom{q+1}{w}}{\binom{m-q+1}{u+v}\binom{m+2}{u+v+w}} \left(\frac{\xi_{f,i+1}}{\xi_{fi}}\right)^u \left(\frac{\eta_{f,i+1}}{\eta_{fi}}\right)^v \left(\frac{\zeta_{f,i+1}}{\zeta_{fi}}\right)^w \tag{3.106}$$

This is the final expression for the normalized inertial integral using the development of case (B). Cases (A) and (C) can be handled similarly.

3.4 The Hotine sphere expansion

The expansion associated with the Hotine configuration is rather more complicated than that of the Brillouin configuration. A definite advantage, however, is the much simpler form of the gradients, since the expansion variables appear only with positive powers in homogeneous polynomials. The penalty on the other hand is only paid once during the computation of the coefficients of the expansion. As in the Brillouin case, only elementary methods will be used to arrive at the final formulation.

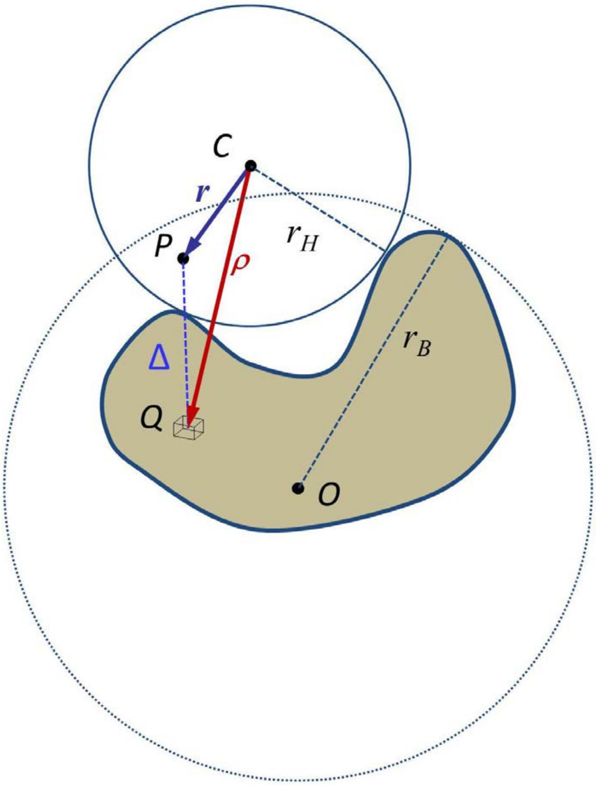

Figure 3.8. Configuration for the Hotine expansion. The Hotine sphere with radius r_H is shown centered at a point C external to the body, the sphere being tangent to the body itself.

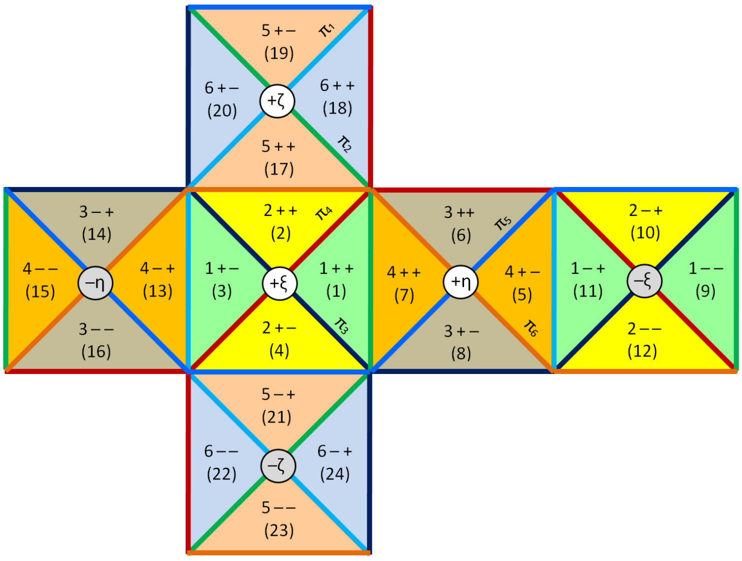

Figure 3.9. The six regions in which 3D space is subdivided to guarantee convergence of the expansion of the inverse distance function. Each of the six regions is further divided into four subregions coded by + and − superscripts. Positive and negative directions of the ξ, η, ζ axes are clearly marked. Numbers in parentheses are the sequential numbering scheme of the resulting 24 subregions. The six region-generating planes passing through the origin are also shown and designated $\pi_1, \pi_2, ..., \pi_6$.

3.4.1 Expansion of the inverse distance

Consider then the inverse distance function in the Hotine form (3.12) and express it in the form

$$\frac{1}{|\mathbf{r}-\boldsymbol{\rho}|} = \frac{1}{|\boldsymbol{\rho}|}\frac{1}{\sqrt{1-2\dfrac{\mathbf{r}\cdot\boldsymbol{\rho}}{\boldsymbol{\rho}\cdot\boldsymbol{\rho}}+\dfrac{\mathbf{r}\cdot\mathbf{r}}{\boldsymbol{\rho}\cdot\boldsymbol{\rho}}}}, \qquad |\mathbf{r}| < |\boldsymbol{\rho}|\,. \tag{3.107}$$

Now expand according to the geometric series and then using the binomial formula to yield

$$\frac{1}{|\mathbf{r}-\boldsymbol{\rho}|} = \sum_{n=0}^{\infty}\binom{-1/2}{n}\frac{1}{\rho^{2n+1}}\sum_{m=0}^{n}(-1)^m\,2^m\binom{n}{m}(\mathbf{r}\cdot\boldsymbol{\rho})^m\,(\mathbf{r}\cdot\mathbf{r})^{n-m}\,. \tag{3.108}$$

Attention in now focuse on the coordinates ξ, η, and ζ of the source point Q, which are the expansion variables, which we readily introduce by writing the previous formula as

$$\frac{1}{|\mathbf{r}-\boldsymbol{\rho}|} = \sum_{n=0}^{\infty}\binom{-1/2}{n}\frac{1}{\rho^{2n+1}}\sum_{m=0}^{n}(-1)^m\,2^m\binom{n}{m}(x\xi+y\eta+z\zeta)^m\,r^{2(n-m)}. \tag{3.109}$$

Therefore we first expand

$$(\mathbf{r}\cdot\boldsymbol{\rho})^m = (x\xi+y\eta+z\zeta)^m = \sum_{i=0}^{m}\sum_{j=0}^{i}\binom{m}{i}\binom{i}{j}(x\xi)^{m-i}\,(y\eta)^{i-j}\,(z\zeta)^j \tag{3.110}$$

and then consider $\rho^{-2n-1} = \left(\xi^2+\eta^2+\zeta^2\right)^{-2n-1}$. This latter function can be expanded using the binomial theorem with special care to ensure convergence of the geometric series involved at the two steps of the process. With a view at conciseness, we will follow a normalizing procedure. Let us then assume that[2]

$$\max\left(\xi^2+\eta^2, \xi^2+\zeta^2, \eta^2+\zeta^2\right) = \xi^2+\eta^2 \tag{3.111}$$

---

[2] Geometrically, this is can be interpreted as choosing the (square of the) largest of the sides of the triangle formes by the tips of the vectors along the coordinate axes which sum to give $\boldsymbol{\rho}$. The degenerate case of equal coordinates is of no consequence in the present analysis.

so that we can write

$$\frac{1}{\rho^{2n+1}} = \frac{1}{\left(\xi^2+\eta^2\right)^{(2n+1)/2}} \frac{1}{\left(1+\dfrac{\zeta^2}{\xi^2+\eta^2}\right)^{(2n+1)/2}} \tag{3.112}$$

and expand the second factor on the right hand side as

$$\frac{1}{\rho^{2n+1}} = \frac{1}{\left(\xi^2+\eta^2\right)^{(2n+1)/2}} \sum_{p=0}^{\infty} \binom{-(2n+1)/2}{p} \left(\frac{\zeta^2}{\xi^2+\eta^2}\right)^p . \tag{3.113}$$

We then need to expand $\left(\xi^2+\eta^2\right)^{(2n-2p+1)/2}$. To ensure convergence we assume, according to the normalization procedure, that[3]

$$\max\left(\xi^2,\eta^2\right) = \xi^2 \tag{3.115}$$

so that

$$\frac{1}{\left(\xi^2+\eta^2\right)^{(2n+2p+1)/2}} = \frac{1}{\xi^{2n+2p+1}} \frac{1}{\left[1+\left(\dfrac{\eta}{\xi}\right)^2\right]^{(2n+2p+1)/2}} \tag{3.116}$$

can be expanded into the convergent series

$$\frac{1}{\left(\xi^2+\eta^2\right)^{(2n+2p+1)/2}} = \frac{1}{\xi^{2n+2p+1}} \sum_{q=0}^{\infty} \binom{-(2n+2p+1)/2}{q} \left(\frac{\eta}{\xi}\right)^{2q} \tag{3.117}$$

Subject to the restrictions (3.111) and (3.115), the final form of the expasnion of ρ^{-2n-1} is then

$$\frac{1}{\rho^{2n+1}} = \sum_{p=0}^{\infty}\sum_{q=0}^{\infty} \binom{-(2n+1)/2}{p} \binom{-(2n+2p+1)/2}{q} \frac{\eta^{2q}\zeta^{2p}}{\xi^{2n+2p+2q+1}}, \tag{3.118}$$

which, for $\xi^2=\eta^2$, simplifies to

$$\frac{1}{\rho^{2n+1}} = \frac{1}{\xi^{2n+1}} \sum_{p=0}^{\infty} \binom{-(2n+1)/2}{p} \frac{1}{[2]^{(2n+2p+1)/2}} \left(\frac{\zeta^2}{\xi^2}\right)^p \tag{3.119}$$

or

$$\frac{1}{\rho^{2n+1}} = \frac{1}{(2\xi)^{(2n+1)/2}} \sum_{p=0}^{\infty} \binom{-(2n+1)/2}{p} \frac{1}{2^p} \left(\frac{\zeta^2}{\xi^2}\right)^p . \tag{3.120}$$

For implementation purposes it can be noted that this case is already included in the general formula (3.118).

The expansion (3.118) can be taken as a template if we can reduce, or "normalize," all positions $\boldsymbol{\rho}$ to satisfy the two constraints (3.111) and (3.115). This is easily done if we separate

---

[3] The case $\xi^2=\eta^2$ deserves some attention. In that case we do not need to expand since we simply have

$$\frac{1}{\left(\xi^2+\eta^2\right)^{(2n+2p+1)/2}} = \frac{1}{2^{2n+2p+1}\xi^{2n+2p+1}} . \tag{3.114}$$

	R$_1$	R$_1$	R$_3$	R$_4$	R$_5$	R$_6$
$\xi_R =$	ξ	ξ	η	η	ζ	ζ
$\eta_R =$	η	ζ	ζ	ξ	ξ	η
$\zeta_R =$	ζ	η	ξ	ζ	η	ξ

Table 3.1. Mapping of the source point coordinates to the standardized naming.

$\mathbb{R}^3$ into the six regions R$_1$, R$_2$, ..., R$_6$ defined by the inequalities

$$\text{R}_1\text{:} \quad \xi^2 \geq \eta^2 \geq \zeta^2, \tag{3.121}$$
$$\text{R}_2\text{:} \quad \xi^2 \geq \zeta^2 \geq \eta^2, \tag{3.122}$$
$$\text{R}_3\text{:} \quad \eta^2 \geq \zeta^2 \geq \xi^2, \tag{3.123}$$
$$\text{R}_4\text{:} \quad \eta^2 \geq \xi^2 \geq \zeta^2, \tag{3.124}$$
$$\text{R}_5\text{:} \quad \zeta^2 \geq \xi^2 \geq \eta^2, \tag{3.125}$$
$$\text{R}_6\text{:} \quad \zeta^2 \geq \eta^2 \geq \xi^2. \tag{3.126}$$

That these are the regions defined by the constraints necessary to ensure convergence of the geometric series in the expansion of ρ^{-2n-1} is easily seen. In the case examined above the assumptions were

$$\xi^2 + \eta^2 = \max\left(\xi^2 + \eta^2, \xi^2 + \zeta^2, \eta^2 + \zeta^2\right) \tag{3.127}$$
$$\xi^2 \geq \eta^2 \tag{3.128}$$

and these are easily seen to be equivalent to the ordering

$$\xi^2 \geq \eta^2 \geq \zeta^2, \tag{3.129}$$

which is precisley the definition of the region R$_1$. The region of space R$_1$ defined by (3.121) is a double, square-based pyramid with vertex at the origin C of the expansion, whose axis is the ξ-axis. The other regions are associated with all other relevant constraints. The coordinates of a point in any of the six regions can be mapped, or normalized, to the the coordinates ξ_R, η_R and ζ_R of the standard case treated above (note that for R$_1$ the mapping is clearly the identity map) according to the scheme shown in Table 3.1.

To keep track of this ragional mapping, let us rewrite the expansion (3.118) in the normalized form

$$\frac{1}{\rho^{2n+1}} = \sum_{p=0}^{\infty}\sum_{q=0}^{\infty} \binom{-(2n+1)/2}{p} \binom{-(2n+2p+1)/2}{q} \frac{1}{\xi_R^{2n+1}} \left(\frac{\zeta_R^2}{\xi_R^2}\right)^p \left(\frac{\eta_R^2}{\xi_R^2}\right)^q. \tag{3.130}$$

We can now combine this expansion (3.130) with the expansion (3.110) into (3.109). Before doing that, however, we need to take care of the fact that not all the coordinates of the source point need to be remapped—those associated with the expansion (3.110) must retain their original identity. However, in order to use a homogeneous set of coordinates, we will find it expedient in the case of the original coordinates to remap their exponents. In fact, we can introduce the indices α, β, and γ as functions of the indices m, i, j that appear in the exponents of the source point original coordinates in equation (3.110) as

$$\alpha = \alpha_R(m,i,j), \qquad \beta = \beta_R(m,i,j), \qquad \gamma = \gamma_R(m,i,j), \tag{3.131}$$

	R_1	R_2	R_3	R_4	R_5	R_6
$\alpha_R =$	$m-i$	$m-i$	$i-j$	$i-j$	j	j
$\beta_R =$	$i-j$	j	j	$m-i$	$m-i$	$i-j$
$\gamma_R =$	j	$i-j$	$m-i$	j	$i-j$	$m-i$

Table 3.2. Mapping of the source point coordinates to the standardized naming

where the explicit form of the functions are given in Table 3.2. Not surprisingly, these functions are identical to the regional coordinate mappings of Table 3.1. Equation (3.110) can now be more appropriately written as

$$(x\xi + y\eta + z\zeta)^m = \sum_{i=0}^{m}\sum_{j=0}^{i} \binom{m}{i}\binom{i}{j} x^{m-i}y^{i-j}z^j \, \xi_R^\alpha \eta_R^\beta \zeta_R^\gamma. \tag{3.132}$$

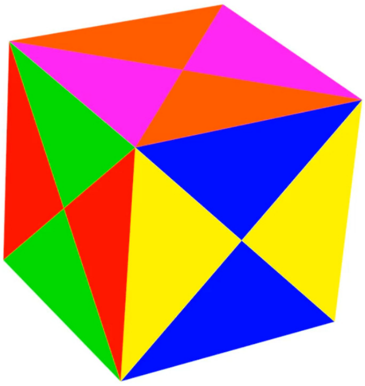

Figure 3.10. The six color-coded regions of $\mathbb{R}^3$for the expansion of the inverse distance in the Hotine configutration. The axes of the reference system centered at the center if the cube exit the cube at the center of the "butterflies." Opposite faces have the same appearance in terms of subregions and their color.

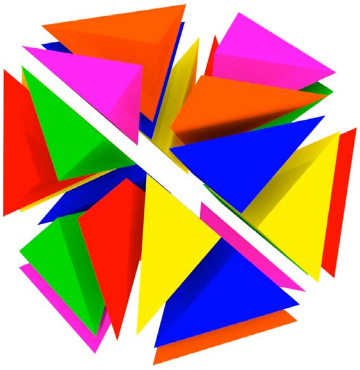

Figure 3.11. Exploded view of the six color-coded regions of $\mathbb{R}^3$ showing the butterfly-pyramid nature of each region.

Substitution of (3.130) and (3.132) into (3.109) finally yields the expansion

$$\frac{1}{|\mathbf{r}-\boldsymbol{\rho}|} = \sum_{n=0}^{\infty}\sum_{m=0}^{n}\sum_{i=0}^{m}\sum_{j=0}^{i} (-2)^m \binom{-1/2}{n}\binom{n}{m}\binom{m}{i}\binom{i}{j} r^{2(n-m)} x^{m-i} y^{i-j} z^j$$
$$\sum_{p=0}^{\infty}\sum_{q=0}^{\infty}\binom{-(2n+1)/2}{p}\binom{-(2n+2p+1)/2}{q}\frac{1}{\xi_R^{2n+1}}\left(\frac{\zeta_R^2}{\xi_R^2}\right)^p\left(\frac{\eta_R^2}{\xi_R^2}\right)^q \xi_R^{\alpha}\eta_R^{\beta}\zeta_R^{\gamma}$$

Defining the numerical coefficients

$$D_{nm}^{ij} = (-2)^m \binom{-1/2}{n}\binom{n}{m}\binom{m}{i}\binom{i}{j}, \tag{3.133}$$

the expansion formula can finally be written concisely as

$$\boxed{\frac{1}{|\mathbf{r}-\boldsymbol{\rho}|} = \sum_{n=0}^{\infty}\sum_{m=0}^{n}\sum_{i=0}^{m}\sum_{j=0}^{i} D_n m^i j\; \tilde{F}_{npq}^{mij}\left(\xi_R,\eta_R,\zeta_R\right) r^2\left(n-m\right) x^{m-i} y^{i-j} z^j,} \tag{3.134}$$

where we have also defined the quatities $\tilde{F}_n^{mij}$ as

$$\tilde{F}_n^{mij}\left(\xi_R,\eta_R,\zeta_R\right) = \sum_{p=0}^{\infty}\sum_{q=0}^{\infty} C_n^{pq}\frac{\eta_R^{\beta+2q}\zeta_R^{\gamma+2p}}{\xi_R^{2n-\alpha+2p+2q+1}} \tag{3.135}$$

with the numerical coefficient C_n^{pq} given by

$$C_n^{pq} = \binom{-(2n+1)/2}{p}\binom{-(2n+2p+1)/2}{q}. \tag{3.136}$$

3.4.2 Formulation of the potential for an extended body

The expansion (3.134) can now be inserted in the formula of the potential (2.5)

$$U\left(\mathbf{r}\right) = G\iiint_V \frac{\sigma\left(\boldsymbol{\rho}\right)}{|\mathbf{r}-\boldsymbol{\rho}|}\,d\xi\,d\eta\,d\zeta \tag{3.137}$$

to get

$$U\left(\mathbf{r}\right) = G\sum_{n=0}^{\infty}\sum_{m=0}^{n}\sum_{i=0}^{m}\sum_{j=0}^{i} D_{nm}^{ij}\; r^{2(n-m)}\, x^{m-i} y^{i-j} z^j$$
$$\iiint_V \sigma\left(\boldsymbol{\rho}\right)\tilde{F}_n^{mij}\left(\xi_R,\eta_R,\zeta_R\right)\,d\xi\,d\eta\,d\zeta \tag{3.138}$$

Introducing the *inertial functions* F_n^{mij} defined by

$$\boxed{F_n^{mij} = \iiint_V \sigma\left(\boldsymbol{\rho}\right)\tilde{F}_n^{mij}\left(\xi_R,\eta_R,\zeta_R\right)\,d\xi_R\,d\eta_R\,d\zeta_R} \tag{3.139}$$

the potential can be finally put into the form

$$\boxed{U\left(\mathbf{r}\right) = G\sum_{n=1}^{\infty}\sum_{m=0}^{n}\sum_{i=0}^{m}\sum_{j=0}^{i} D_{nm}^{ij}\; F_n^{mij}\, r^{2(n-m)}\, x^{m-i} y^{i-j} z^j.} \tag{3.140}$$

Note that the first summation starts with degree $n = 0$, but the term generated is ineffective for the computation of the acceleration and the gravity gradient, since it is constant with respect to the field point coordinates.

3.4.3 The First- and Second-Order Gradients (Gravity and Gravity Gradient)

The first-order gradients can be easily computed from the expression (3.140) of the potential. Since the function to be differentiated is of the form

$$r^d x^a y^b z^c \tag{3.141}$$

with $a = m - i$, $b = i - j$, $c = j$ and $d = 2\,(n - m)$, it will be easier to provide the first- and second-order partials of this template function.

The results for use in computing the acceleration are

$$\frac{\partial}{\partial x}\left(r^d\, x^a y^b z^c\right) = \left(d\, x^2 + a r^2\right) r^{d-2} x^{a-1} y^b z^c, \tag{3.142}$$

$$\frac{\partial}{\partial y}\left(r^d\, x^a y^b z^c\right) = \left(d\, y^2 + b r^2\right) r^{d-2} x^a y^{b-1} z^c, \tag{3.143}$$

$$\frac{\partial}{\partial z}\left(r^d\, x^a y^b z^c\right) = \left(d\, z^2 + c r^2\right) r^{d-2} x^a y^b z^{c-1}. \tag{3.144}$$

while those for the gravity gradients are

$$\frac{\partial^2}{\partial x^2}\left(r^d\, x^a y^b z^c\right) = \left[d\,(d-2)\,\frac{x^4}{r^4} + d\,(\,2a+1)\,\frac{x^2}{r^2} + a\,(a-1)\,\right] r^d x^{a-2} y^b z^c \tag{3.145}$$

$$\frac{\partial^2}{\partial y^2}\left(r^d\, x^a y^b z^c\right) = \left[d\,(d-2)\,\frac{y^4}{r^4} + d\,(2b+1\,)\,\frac{y^2}{r^2} + b\,(b-1)\right] r^d x^a y^{b-2} z^c \tag{3.146}$$

$$\frac{\partial^2}{\partial z^2}\left(r^d\, x^a y^b z^c\right) = \left[d\,(d-2)\,\frac{z^4}{r^4} + d\,(2c+1\,)\,\frac{z^2}{r^2} + c\,(c-1)\right] r^d x^a y^b z^{c-2} \tag{3.147}$$

for the diagonal elements, and

$$\frac{\partial^2}{\partial y \partial x}\left(r^d\, x^a y^b z^c\right) = \left[d\,(d-2)\,\frac{x^2 y^2}{r^4} + bd\frac{x^2}{r^2} + ad\frac{y^2}{r^2} + ab\right] r^d x^{a-1} y^{b-1} z^c \tag{3.148}$$

$$\frac{\partial^2}{\partial z \partial x}\left(r^d\, x^a y^b z^c\right) = \left[d\,(d-2\,)\,\frac{x^2 z^2}{r^4} + cd\frac{x^2}{r^2} + ad\frac{z^2}{r^2} + ac\right] r^d x^{a-1} y^b z^{c-1} \tag{3.149}$$

$$\frac{\partial^2}{\partial z \partial y}\left(r^d\, x^a y^b z^c\right) = \left[d\,(d-2\,)\,\frac{y^2 z^2}{r^4} + cd\frac{y^2}{r^2} + bd\frac{z^2}{r^2} + bc\right] r^d x^a y^{b-1} z^{c-1} \tag{3.150}$$

for the symmetric, off-diagonal terms.

When numerically evaluating the acceleration and the gravity gradient components efficient schemes can be devised due to the many different recurrence formulae that can be exploited in passing to indices one unit higher.

3.4.4 Computation of the Inertial Integrals

The *inertial function* defined in (3.139) can be computed subject to the fundamental assumption of constant mass density and, in view of the analysis of Section 3.4, the integration must be carried out over the six regions $\mathrm{R}_1, \mathrm{R}_2, ..., \mathrm{R}_6$ defined in (3.121) to (3.122). Each of these regions is the union of *four disjoint subregions*, or simplices, as exhibited graphically in the exploded view of Figure 3.11, which shows that each region is made up of four symmetrically placed, pyramidal subregions of the same color. These pyramidal simplices share the same vertex and show pairwise symmetry about it. In some respect their configuration is reminiscent of a butterfly, so we will

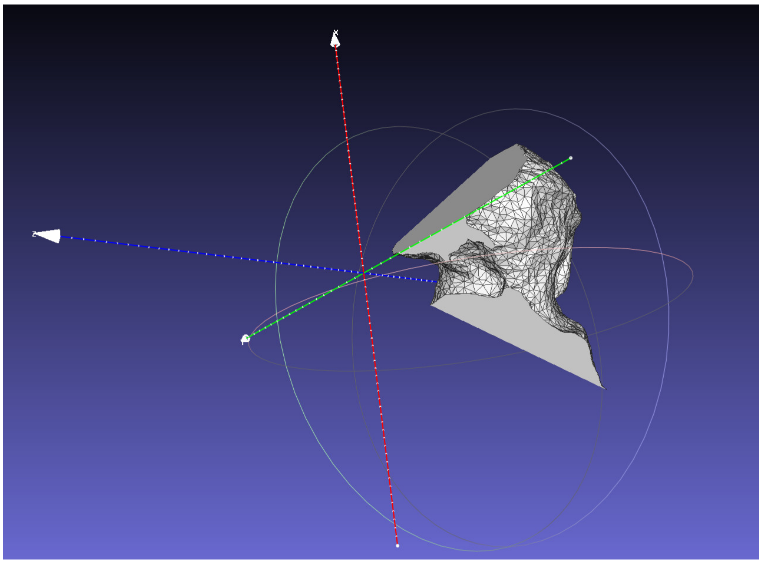

Figure 3.12. Example of one of the subregions in which the body must be separated to ensure convergence of the series expansion inside the HOtine sphere.

	R_k^{++}	R_k^{--}	R_k^{+-}	R_k^{-+}
R_1	$\xi \geq 0, \quad \eta \geq 0$	$\xi \leq 0, \quad \eta \leq 0$	$\xi > 0, \quad \eta < 0$	$\xi < 0, \quad \eta > 0$
R_2	$\xi \geq 0, \quad \zeta \geq 0$	$\xi \leq 0, \quad \zeta \leq 0$	$\xi > 0, \quad \eta < 0$	$\xi < 0, \quad \eta > 0$
R_3	$\eta \geq 0, \quad \zeta \geq 0$	$\eta \leq 0, \quad \zeta \leq 0$	$\eta \geq 0, \quad \zeta < 0$	$\eta < 0, \quad \zeta > 0$
R_4	$\eta \geq 0, \quad \xi \geq 0$	$\eta \leq 0, \quad \xi \leq 0$	$\eta \geq 0, \quad \xi < 0$	$\eta < 0, \quad \xi > 0$
R_5	$\zeta \geq 0, \quad \xi \geq 0$	$\zeta \leq 0, \quad \xi \leq 0$	$\zeta \geq 0, \quad \xi < 0$	$\zeta < 0, \quad \xi > 0$
R_6	$\zeta \geq 0, \quad \eta \geq 0$	$\zeta \leq 0, \quad \eta \leq 0$	$\zeta \geq 0, \quad \eta < 0$	$\zeta < 0, \quad \eta < 0$

Table 3.3. Coordinates restrictions defining the 24 simplices. Column headings show the subregion's code.

refer to each of the six regions as showing a pyramidal-butterfly shape. As a consequence, in order to carry out the 3D integration as indicated in (3.139) to compute the inertial functions, the volume of the body must be divided into 24 disjoint simplices. This is shown in the case of just one subregion for the nucleus of comet 67P in Figure 3.12. The separation of the triangular mesh into 24 submeshes has required intense work. Note, however, that since the center of expansion for the Hotine configuration is external to the body, not all 24 subregions will be generated by the regional subdivision.

The 24 simplices, or subregions into which the fundamental six regions are subdivided have been defined as per Tables 3.3 and 3.4.

A		B		C		D		E		F	
R_{01}	R_1^{++}	R_{05}	R_4^{+-}	R_{09}	R_1^{--}	R_{13}	R_4^{-+}	R_{17}	R_5^{++}	R_{21}	R_5^{-+}
R_{02}	R_2^{++}	R_{06}	R_3^{++}	R_{10}	R_2^{-+}	R_{14}	R_3^{-+}	R_{18}	R_6^{++}	R_{22}	R_6^{--}
R_{03}	R_1^{+-}	R_{07}	R_4^{++}	R_{11}	R_1^{-+}	R_{15}	R_4^{--}	R_{19}	R_5^{+-}	R_{23}	R_5^{--}
R_{04}	R_2^{+-}	R_{08}	R_3^{+-}	R_{12}	R_2^{--}	R_{16}	R_3^{--}	R_{20}	R_6^{+-}	R_{24}	R_6^{-+}

Table 3.4. Association of subregional code with simplex order number, four for each of the faces A, B, C, D, E, F of the cube.

To start let us rewrite equation (3.139) in the form

$$F_n^{mij} = \sigma \sum_{p=0}^{\infty}\sum_{q=0}^{\infty} C_n^{pq} F_{npq}^{mij}, \tag{3.151}$$

where we have isolated the core of the computation through the integral

$$F_{npq}^{mij} = \iiint_V \frac{\eta^{\beta+2q}\zeta^{\gamma+2p}}{\xi^{2n-\alpha+2p+2q+1}}\, d\xi\, d\eta\, d\zeta. \tag{3.152}$$

In view of what has just been said, the actual inertial functions F_n^{mij} of the full body will result from the sum of up to 24 contributions of the form of equation (3.151), where each contribution is associated with the integral (3.152) evaluated over one of the 24 simplices. In order not to overload the notation, while developing a method for the evaluation of the integral (3.152) no explicit reference will be made to the specific simplex to which it applies.

The strategy we will follow is the same as that adopted in the case of the inertial integrals in Section 3.3.2: the volume integral will be reduced to surface integrals, and these in turn to line integrals.

Volume to surface integral

In order to reduce (3.152) from an integral over the volume to an integral of the surface bounding the volume we make use of Gauss's divergence theorem (3.66). In this present case we recall that the volume is the volume of one of the simplices, or subregions in which the body has been subdivided. The vector field $\mathbf{T}$ is obtained as the solution the PDE

$$\nabla \cdot \mathbf{T} = \frac{\partial T_\xi}{\partial \xi} + \frac{\partial T_\eta}{\partial \eta} + \frac{\partial T_\zeta}{\partial \zeta} = \frac{\eta^{\beta+2q}\zeta^{\gamma+2p}}{\xi^{2n-\alpha+2p+2q+1}} \tag{3.153}$$

twhere the right hand side is the integrand appearing in (3.152). We can take for simplicity any of the three solutions

$$(A)\quad \mathbf{T} = T_\xi \hat{\boldsymbol{\xi}} = \frac{1}{-(2n-\alpha+2p+2q)} \frac{\eta^{\beta+2q}\zeta^{\gamma+2p}}{\xi^{2n-\alpha+2p+2q}} (1,0,0)^T, \tag{3.154}$$

$$(B)\quad \mathbf{T} = T_\eta \hat{\boldsymbol{\eta}} = \frac{1}{\beta+2q+1} \frac{\eta^{\beta+2q+1}\zeta^{\gamma+2p}}{\xi^{2n-\alpha+2p+2q+1}} (0,1,0)^T, \tag{3.155}$$

$$(C)\quad \mathbf{T} = T_\zeta \hat{\boldsymbol{\zeta}} = \frac{1}{\gamma+2p+1} \frac{\eta^{\beta+2q}\zeta^{\gamma+2p+1}}{\xi^{2n-\alpha+2p+2q+1}} (0,0,1)^T, \tag{3.156}$$

where the field has been chosen to have only one component, each of the three solutions being along one of the coordinate axes. Note that form (A) has been obtained by integrating w.r.t. ξ, form (B) has been obtained by integrating w.r.t. η, and form (C) has been obtained by integrating w.r.t. ζ. Substitution of the RHS's of (3.154), (3.155) and (3.156) into the divergence theorem formula leads to the equations

$$(A)\quad F_{npq}^{mij} = \frac{1}{-(2n-\alpha+2p+2q)} \sum_f \iint_{\Sigma_f} \frac{\eta^{\beta+2q}\zeta^{\gamma+2p}}{\xi^{2n-\alpha+2p+2q}} \hat{\xi} \cdot d\boldsymbol{\sigma}, \tag{3.157}$$

$$(B)\quad F_{npq}^{mij} = \frac{1}{\beta+2q+1} \sum_f \iint_{\Sigma_f} \frac{\eta^{\beta+2q+1}\zeta^{\gamma+2p}}{\xi^{2n-\alpha+2p+2q+1}} \hat{\boldsymbol{\eta}} \cdot d\boldsymbol{\sigma}, \tag{3.158}$$

$$(C)\quad F_{npq}^{mij} = \frac{1}{\gamma+2p+1} \sum_f \iint_{\Sigma_f} \frac{\eta^{\beta+2q}\zeta^{\gamma+2p+1}}{\xi^{2n-\alpha+2p+2q+1}} \hat{\boldsymbol{\zeta}} \cdot d\boldsymbol{\sigma}. \tag{3.159}$$

The above formulae can now be further simplified through the use of Stokes theorem in Green's form.

Surface to line integral

The next step in the reduction scheme is the application of Stokes' theorem. The preliminary step is to solve the PDE

$$\nabla \times \mathbf{H} = \mathbf{T} \tag{3.160}$$

or, component-wise,

$$\frac{\partial H_\zeta}{\partial \eta} - \frac{\partial H_\eta}{\partial \zeta} = T_\xi, \tag{3.161}$$

$$\frac{\partial H_\xi}{\partial \zeta} - \frac{\partial H_\zeta}{\partial \xi} = T_\eta, \tag{3.162}$$

$$\frac{\partial H_\eta}{\partial \xi} - \frac{\partial H_\xi}{\partial \eta} = T_\zeta. \tag{3.163}$$

In the three case being carried along the vector field **T** only a one component, and this is aligned with a coordinate axis. Therefore we ony need to solve one of the three component equations of equation (3.160). Furthermore, we are also free to zero out one of the two components of the field **H** that appear in the PDE. Thus we always select to kill the component with the negative sign. As a result we find the three solutions

$$(A) \quad H_\zeta = \frac{1}{\beta + 2q + 1} \frac{\eta^{\beta+2q+1} \zeta^{\gamma+2p}}{\xi^{2n-\alpha+2p+2q}}, \tag{3.164}$$

$$(B) \quad H_\xi = \frac{1}{\gamma + 2p + 1} \frac{\eta^{\beta+2q+1} \zeta^{\gamma+2p+1}}{\xi^{2n-\alpha+2p+2q+1}}, \tag{3.165}$$

$$(C) \quad H_\eta = -\frac{1}{2n - \alpha + 2p + 2q} \frac{\eta^{\beta+2q} \zeta^{\gamma+2p+1}}{\xi^{2n-\alpha+2p+2q}}. \tag{3.166}$$

Substitution of these expression in the formula of Stokes' theorem leads to

$$(A) \quad F_{npq}^{mij} = \frac{-1}{(2n - \alpha + 2p + 2q)(\beta + 2q + 1)} \sum_f \sum_{k=1}^{3} \int_{e_k^f} \frac{\eta^{\beta+2q+1} \zeta^{\gamma+2p}}{\xi^{2n-\alpha+2p+2q}} \, d\zeta_{fk} \tag{3.167}$$

$$(B) \quad F_{npq}^{mij} = \frac{1}{(\beta + 2q + 1)(\gamma + 2p + 1)} \sum_f \sum_{k=1}^{3} \int_{e_k^f} \frac{\eta^{\beta+2q+1} \zeta^{\gamma+2p+1}}{\xi^{2n-\alpha+2p+2q+1}} \, d\xi_{fk} \tag{3.168}$$

$$(C) \quad F_{npq}^{mij} = \frac{-1}{(\gamma + 2p + 1)(2n - \alpha + 2p + 2q)} \sum_f \sum_{k=1}^{3} \int_{e_k^f} \frac{\eta^{\beta+2q} \zeta^{\gamma+2p+1}}{\xi^{2n-\alpha+2p+2q}} \, d\eta_{fk} \tag{3.169}$$

3.4.5 Evaluation of the line integrals

The line integrals involved in the expressions (3.167), (3.168) and (3.169) can be evaluated using the same edge parameterization (3.91) that was introduced for the Brillouin case, but written as

$$\mathbf{r}_{fk,k+1}(t)=\begin{pmatrix}\xi_{fk}(t)\\ \eta_{fk}(t)\\ \zeta_{fk}(t)\end{pmatrix}=\begin{pmatrix}\xi_{fk}+(\xi_{f,k+1}-\xi_{fk})\,t\\ \eta_{fk}+(\eta_{f,k+1}-\eta_{fk})\,t\\ \zeta_{fk}+(\zeta_{f,k+1}-\zeta_{fk})\,t\end{pmatrix},\qquad 0\le t\le 1. \tag{3.170}$$

We will focus on the first case, described in equation (3.167), which can be written as

$$F_{npq}^{mij}=\frac{-1}{(2n-\alpha+2p+2q)\,(\beta+2q+1)}\sum_{f}\sum_{k=1}^{3}E_{npq}^{mij}(f,k) \tag{3.171}$$

after introduction of the auxiliary quantity

$$E_{npq}^{mij}(f,k)=\int\limits_{e_k^f}\frac{\eta_{fk}^{\beta+2q+1}\zeta_{fk}^{\gamma+2p}}{\xi_{fk}^{2n-\alpha+2p+2q}}\,d\zeta_{fk} \tag{3.172}$$

which is precisely the integral we need to evaluate. Recall that e_k^f indicates edge k of face f of the polyhedron subregion being examined.

Te keep the notation simple and general, introduce new indices according to[4]

$$u=\beta+2q+1, \tag{3.173}$$
$$v=\gamma+2p, \tag{3.174}$$
$$w=2n-\alpha+2p+2q, \tag{3.175}$$

so that

$$E_{npq}^{mij}(f,k)=\int\limits_{e_k^f}\frac{\eta^{u}(t)\,\zeta^{v}(t)}{\xi^{w}(t)}\,d\zeta_{fk}(t), \tag{3.176}$$

where for brevity's sake we have neglected to write the face and edge indices. Since

$$\xi(t)=\xi_{fk}+\Delta\xi_{fk}\,t \tag{3.177}$$
$$\eta(t)=\eta_{fk}+\Delta\eta_{fk}\,t \tag{3.178}$$
$$\zeta(t)=\zeta_{fk}+\Delta\zeta_{fk}\,t \tag{3.179}$$

it follows that

$$E_{npq}^{mij}(f,k)=\Delta\zeta_{fk}\int\limits_{e_k^f}\frac{(\eta_{fk}+\Delta\eta_{fk}\,t)^{u}\,(\zeta_{fk}+\Delta\zeta_{fk}\,t)^{v}}{(\xi_{fk}+\Delta\xi_{fk}\,t)^{w}}\,dt. \tag{3.180}$$

Now the integrand can be written using the binomial expansion to handle the product at the numerator, but the denominator will be kept unaltered, since the use of Bernstein's polynomial will be of no use in this context since they only apply to finite binomial expansions, not to the infinite binomial series that would ensue from the expansion of the denominator. We then have

$$\begin{aligned}\frac{(\eta_{fk}+\Delta\eta_{fk}\,t)^{u}\,(\zeta_{fk}+\Delta\zeta_{fk}\,t)^{v}}{(\xi_{fk}+\Delta\xi_{fk}\,t)^{w}}&=\eta_{fk}^{u}\zeta_{fk}^{v}\frac{\left(1+\frac{\Delta\eta_{fk}}{\eta_{fk}}t\right)^{u}\left(1+\frac{\Delta\zeta_{fk}}{\zeta_{fk}}t\right)^{v}}{(\xi_{fk}+\Delta\xi_{fk}t)^{w}}\\&=\frac{\eta_{fk}^{u}\zeta_{fk}^{v}}{(\xi_{fk}+\Delta\xi_{fk}t)^{w}}\sum_{k}^{u}\sum_{l}^{v}\binom{u}{k}\binom{v}{l}\left(\frac{\Delta\eta_{fk}}{\eta_{fk}}\right)^{k}\left(\frac{\Delta\zeta_{fk}}{\zeta_{fk}}\right)^{l}t^{k+l}\end{aligned} \tag{3.181}$$

---

[4] Similar definitions can be made for cases (B) and (C), the development that follows remaining unaltered.

$$E_{npq}^{mij}\left(f,k\right)=\sum_{k}^{u}\sum_{l}^{v}\binom{u}{k}\binom{v}{l}\left(\frac{\Delta\eta_{fk}}{\eta_{fk}}\right)^{k}\left(\frac{\Delta\zeta_{fk}}{\zeta_{fk}}\right)^{l}\eta_{fk}^{u}\zeta_{fk}^{v}\Delta\zeta_{fk}\int\limits_{0}^{1}\frac{t^{k+l}}{\left(\xi_{fk}+\Delta\xi_{fk}t\right)^{w}}dt. \qquad (3.182)$$

A search in the tables of integrals of Dwight (1989) shows that

$$\int\frac{x^{m}}{\left(a+bx\right)^{n}}dx=\frac{1}{b^{m+1}}\sum_{s=0}^{m}\binom{m}{s}\left(-a\right)^{s}\frac{\left(a+bx\right)^{m-n-s+1}}{m-n-s+1}, \qquad (3.183)$$

except when $s=m-n+1$, in which case the corresponding term in the summation is

$$\left(-a\right)^{s}\binom{m}{n-1}\log\left|a+bx\right|. \qquad (3.184)$$

Then, with $m\equiv k+l$ and $n\equiv w$,

$$E_{npq}^{mij}\left(f_{k}\right)=\sum_{k}^{u}\sum_{l}^{v}\binom{u}{k}\binom{v}{l}\left(\frac{\Delta\eta_{fk}}{\eta_{fk}}\right)^{k}\left(\frac{\Delta\zeta_{fk}}{\zeta_{fk}}\right)^{l}\eta_{fk}^{u}\zeta_{fk}^{v}\frac{\Delta\zeta_{fk}}{\Delta\xi_{fk}^{k+l+1}} \qquad (3.185)$$

$$\sum_{s=0}^{k+l}\left(-\xi_{fk}\right)^{s}\begin{cases}\binom{k+l}{s}\dfrac{\xi_{fk}^{k+l-w-s+1}}{k+l-w-s+1}\left[\left(1+\dfrac{\Delta\xi_{fk}}{\xi_{fk}}\right)^{k+l-w-s+1}-1\right], & s\neq k+l-w+1\\ \binom{k+l}{w-1}\log\left|1+\dfrac{\Delta\xi_{fk}}{\xi_{fk}}\right|, & s=k+l-w+1\end{cases}$$

The case may occur in which $\Delta\xi_{fk}=0$. Then the integral is much simpler and from

$$\int\limits_{0}^{1}\frac{x^{m}}{a^{n}}dx=\frac{1}{m+1}\left.\frac{x^{m+1}}{a^{n}}\right|_{0}^{1}=\frac{1}{\left(m+1\right)a^{n}} \qquad (3.186)$$

it follows that

$$E_{npq}^{mij}\left(f_{k}\right)=\sum_{k}^{u}\sum_{l}^{v}\binom{u}{k}\binom{v}{l}\left(\frac{\Delta\eta_{fk}}{\eta_{fk}}\right)^{k}\left(\frac{\Delta\zeta_{fk}}{\zeta_{fk}}\right)^{l}\frac{\eta_{fk}^{u}\zeta_{fk}^{v}}{\xi_{fk}^{k+l}}\frac{\Delta\zeta_{fk}}{\left(k+l+1\right)}. \qquad (3.187)$$

Chapter 4

The Gravitational Potential - 3
Expansion in Spherical Harmonics

4.1 Introduction

It has been seen in the previous Chapter that expansions for the external and internal potential can be fully carried out in Cartesian coordinates in terms of inertial integrals and inertial functions. These are methodologies not in common use within the astrodynamical or geophysical communities. It is therefore of interest to apply the methods developed in Chapter 3, i.e., the computation of the volume integrals in the definitions of the inertial integrals and functions, to the case of the more widely used expansions of the potential in Spherical Harmonics. In particular, this Chapter is concerned with the numerical evaluation of the Stokes coefficients associated with both the internal and the external gravitational potential field.

Previous work in this area has been done by Werner (1997) using the integration method of Lien and Kajiya (1984), but is limited to the external potential. Subsequent work, more of a refinement of Werner's pioneering analysis, has been presented by Tsoulis et al. (2009) and Jamet et al. (2010). No study has been found related to the computation of the harmonic coefficients of the spherical harmonic expansion of the internal potential, except for an approximation method introduced in Takahashi and Scheeres (2013) in the evaluation of the volume integrals over the simplices. Other work has also been done by Takahashi and Scheeres (2014) in the way of determining the Stokes coefficients of the internal potential by a process of numerical fitting to a three-dimensional grid of data generated by the polyhedron method of Werner introduced in Chapter 2. Thus, a direct method to evaluate the Stokes coefficients of the internal gravitational field for an extended body modeled as a homogeneous polyhedron is not currently available. The following analysis will fill this gap.

4.2 The Representation of the Gravitational Field in Spherical Harmonics

The expansion of the potential in spherical harmonics is usually separated into the *internal potential* U^i and the *external potential* U^e. The latter expansion is valid *outside* the *Brillouin sphere,* already introduced in the previous Chapter, while the expansion of the internal potential U^i is valid *inside* what we have introduced there as the *Hotine sphere.*

In terms of spherical coordinates, with r indicating the radial distance, ϕ the latitude and λ

the East-longitude, these expansions can be written as

$$U^e(\mathbf{r}) = \frac{GM}{R}\sum_{n=0}^{\infty}\sum_{m=0}^{n}\left(\frac{R}{r}\right)^{n+1}\left[C^e_{nm}\cos(m\lambda) + S^e_{nm}\sin(m\lambda)\right]P_{nm}(\sin\phi) \tag{4.1}$$

and

$$U^i(\mathbf{r}) = \frac{GM}{R}\sum_{n=1}^{\infty}\sum_{m=0}^{n}\left(\frac{r}{R}\right)^{n}\left[C^i_{nm}\cos(m\lambda) + S^i_{nm}\sin(m\lambda)\right]P_{nm}(\sin\phi) \tag{4.2}$$

where GM is the gravitational factor, R a typical length of the extended body which simply acts as a scale factor, $P_{nm}(\sin\phi)$ are the Associated Legendre Functions of degree n and order m defined as $P_{nm}(\mu) = \left(1-\mu^2\right)^{m/2}/\left(2^n n!\right)d^m\left(\mu^2-1\right)^n/d\mu^m$ and the constants C^e_{nm}, S^e_{nm}, C^i_{nm} and S^i_{nm} are known as the Stokes coefficients. Their *fully normalized* expressions in terms of volume integrals over the body are

$$\begin{pmatrix} C^e_{nm} \\ S^e_{nm} \end{pmatrix} = \frac{2-\delta_{0m}}{M}\frac{(n-m)!}{(n+m)!}\iiint_V \sigma(\rho,\phi,\lambda)\left(\frac{\rho}{R}\right)^n \begin{pmatrix} \cos(m\lambda) \\ \sin(m\lambda) \end{pmatrix} P_{nm}(\sin\phi)\, dV \tag{4.3}$$

$$\begin{pmatrix} C^i_{nm} \\ S^i_{nm} \end{pmatrix} = \frac{2-\delta_{0m}}{M}\frac{(n-m)!}{(n+m)!}\iiint_V \sigma(\rho,\phi,\lambda)\left(\frac{R}{\rho}\right)^{n+1} \begin{pmatrix} \cos(m\lambda) \\ \sin(m\lambda) \end{pmatrix} P_{nm}(\sin\phi)\, dV \tag{4.4}$$

where δ_{ij} is the Kronecker delta.

In Space Geodesy, as a scaling device for numerical representation purposes, both the ALF's and the Stokes coefficients are used in their *fully normalized* versions (Heiskanen and Moritz, 1967), denoted with an overbar. The relationships between the unnormalized and the fully normalized quantities are

$$\begin{aligned} \bar{P}_{nm} &= N_{nm}P_{nm}, && (4.5)\\ \bar{C}^k_{nm} &= C^k_{nm}/N_{nm}, && (4.6)\\ \bar{S}^k_{nm} &= S^k_{nm}/N_{nm}, && (4.7) \end{aligned}$$

where the normalization factor N_{nm} is defined

$$N_{nm} = \sqrt{(2-\delta_{0m})(2n+1)\frac{(n-m)!}{(n+m)!}}. \tag{4.8}$$

In order to apply the methods developed in the previous chapter, we need to transform the volume integrals from spherical polar coordinates to Cartesian coordinates. The relationship between the two sets is

$$\xi = \rho\cos\phi\cos\lambda, \tag{4.9}$$

$$\eta = \rho\cos\phi\sin\lambda, \tag{4.10}$$

$$\zeta = \rho\sin\phi, \tag{4.11}$$

where we have used ρ to indicate the distance from the origin to a mass element of the body. Note that the origin of the coordinate system is of course the same for the expansion of the potential as for the definition of the Stokes coefficients. Working under the same hypothesis as before, i.e., under the assumption of constant density, $\sigma(\boldsymbol{\rho})$ can be factored out of the integral sign and the integrand functions (here effectively a two-dimensional vector) can then be defined as the two *regular solid spherical harmonics*

$$\begin{pmatrix} c^e_{nm}(\boldsymbol{\rho}) \\ s^e_{nm}(\boldsymbol{\rho}) \end{pmatrix} = \left(\frac{\rho}{R}\right)^n \begin{pmatrix} \cos(m\lambda) \\ \sin(m\lambda) \end{pmatrix} P_{nm}(\sin\phi) \tag{4.12}$$

for the Brillouin case, and the two *irregular solid spherical harmonics*

$$\begin{pmatrix} c_{nm}^{i}(\boldsymbol{\rho}) \\ s_{nm}^{i}(\boldsymbol{\rho}) \end{pmatrix} = \left(\frac{R}{\rho}\right)^{n+1} \begin{pmatrix} \cos(m\lambda) \\ \sin(m\lambda) \end{pmatrix} P_{nm}(\sin\phi) \tag{4.13}$$

for the Hotine case. These harmonic functions are pairwise related by Kelvin's theorem.

The Stokes coefficients then assume the form

$$\begin{pmatrix} C_{nm}^{e} \\ S_{nm}^{e} \end{pmatrix} = \frac{2-\delta_{0m}}{M}\frac{(n-m)!}{(n+m)!}\sigma \iiint\limits_{V} \begin{pmatrix} c_{nm}^{e}(\boldsymbol{\rho}) \\ s_{nm}^{e}(\boldsymbol{\rho}) \end{pmatrix} dV \tag{4.14}$$

and

$$\begin{pmatrix} C_{nm}^{i} \\ S_{nm}^{i} \end{pmatrix} = \frac{2-\delta_{0m}}{M}\frac{(n-m)!}{(n+m)!}\sigma \iiint\limits_{V} \begin{pmatrix} c_{nm}^{i}(\boldsymbol{\rho}) \\ s_{nm}^{i}(\boldsymbol{\rho}) \end{pmatrix} dV \tag{4.15}$$

The key to the method introduced in this chapter is the transformation of the spherical harmonics $c_{nm}(\phi,\lambda)$ and $s_{nm}(\phi,\lambda)$ from spherical coordinates to Cartesian coordinates. We will consider the transformation of the surface harmonics first.

4.3 Cartesian Formulation of Surface Spherical Harmonics

Expressions in Cartesian coordinates for the surface spherical harmonics are known, although seldom used. A useful reference in this regard is still MacMillan (1930). Here we follow a direct method in a self-consistent manner. In order to isolate the angular dependence of the solid harmonic functions defined in equations (4.12) and (4.13), introduce the *fundamental surface spherical harmonics*

$$\tilde{c}_{nm}(\phi,\lambda) = \cos(m\lambda)\,P_{nm}(\sin\phi)\,, \tag{4.16}$$

$$\tilde{s}_{nm}(\phi,\lambda) = \sin(m\lambda)\,P_{nm}(\sin\phi)\,, \tag{4.17}$$

so that the regular solid harmonics can be rewritten as

$$c_{nm}^{e}(\boldsymbol{\rho}) = \left(\frac{\rho}{R}\right)^{n}\tilde{c}_{nm}(\hat{\boldsymbol{\rho}})\,, \tag{4.18}$$

$$s_{nm}^{e}(\boldsymbol{\rho}) = \left(\frac{\rho}{R}\right)^{n}\tilde{s}_{nm}(\hat{\boldsymbol{\rho}})\,, \tag{4.19}$$

and the irregular solid harmonics as

$$c_{nm}^{i}(\boldsymbol{\rho}) = \left(\frac{R}{\rho}\right)^{n+1}\tilde{c}_{nm}(\hat{\boldsymbol{\rho}})\,, \tag{4.20}$$

$$s_{nm}^{i}(\boldsymbol{\rho}) = \left(\frac{R}{\rho}\right)^{n+1}\tilde{s}_{nm}(\hat{\boldsymbol{\rho}})\,. \tag{4.21}$$

We need to use series expansion for the trigonometric functions and the Associated Legendre Functions appearing in the spherical harmonics (4.16) and (4.17). These are the well-known expansions (Abramowitz and Stegun, 1965) of sines and cosines of multiples of an angle in terms of that angle

$$\cos(m\lambda) = \sum_{k=0}^{\lfloor \frac{m}{2} \rfloor} (-1)^{k}\frac{m!}{(2k)!\,(m-2k)!}\cos^{m-2k}\lambda\sin^{2k}\lambda, \tag{4.22}$$

$$\sin(m\lambda) = \sum_{k=0}^{\lfloor \frac{m-1}{2} \rfloor} (-1)^{k}\frac{m!}{(2k+1)!\,(m-2k-1)!}\cos^{m-2k-1}\lambda\sin^{2k+1}\lambda, \tag{4.23}$$

and a suitable representation of the ALF that will facilitate the conversion, such as

$$P_{nm}(\sin\phi) = \frac{\cos^m\phi}{2^n}\sum_{l=0}^{\left\lfloor\frac{n-m}{2}\right\rfloor}(-1)^l\,\frac{(2n-2l)!}{l!\,(n-l)!\,(n-m-2l)!}\sin^{n-m-2l}\phi. \tag{4.24}$$

Substitution of these expressions into (4.16) and (4.17) yields

$$\tilde{c}_{nm}(\hat{\boldsymbol{\rho}}) = \sum_{k=0}^{\left\lfloor\frac{m}{2}\right\rfloor}\sum_{l=0}^{\left\lfloor\frac{n-m}{2}\right\rfloor}K_{nm}^{c,kl}\,\hat{c}_{nm}^{kl}(\hat{\boldsymbol{\rho}}) \tag{4.25}$$

$$\tilde{s}_{nm}(\hat{\boldsymbol{\rho}}) = \sum_{k=0}^{\left\lfloor\frac{m-1}{2}\right\rfloor}\sum_{l=0}^{\left\lfloor\frac{n-m}{2}\right\rfloor}K_{nm}^{s,kl}\,\hat{s}_{nm}^{kl}(\hat{\boldsymbol{\rho}}) \tag{4.26}$$

where

$$K_{nm}^{c,kl} = (-1)^{k+l}\,\frac{1}{2^n}\,\frac{m!}{(2k)!\,(m-2k)!}\,\frac{(2n-2l)!}{l!\,(n-l)!\,(n-m-2l)!}, \tag{4.27}$$

$$K_{nm}^{s,kl} = (-1)^{k+l}\,\frac{1}{2^n}\,\frac{m!}{(2k+1)!\,(m-2k-1)!}\,\frac{(2n-2l)!}{l!\,(n-l)!\,(n-m-2l)!} \tag{4.28}$$

and

$$\hat{c}_{nm}^{kl}(\phi,\lambda) = \cos^{m-2k}\lambda\sin^{2k}\lambda\cos^m\phi\sin^{n-m-2l}\phi, \tag{4.29}$$

$$\hat{s}_{nm}^{kl}(\phi,\lambda) = \cos^{m-2k-1}\lambda\sin^{2k+1}\lambda\cos^m\phi\sin^{n-m-2l}\phi. \tag{4.30}$$

Now transform equation (4.29) as follows

$$\begin{aligned}
\hat{c}_{nm}^{kl}(\hat{\boldsymbol{\rho}}) &= \cos^{m-2k}\lambda\sin^{2k}\lambda\cos^m\phi\sin^{n-m-2l}\phi \\
&= \left[\cos^m\phi\cos^{m-2k}\lambda\right]\left[\sin^{2k}\lambda\right]\left[\sin^{n-m-2l}\phi\right] \\
&= \left[\cos^{m-2k}\phi\cos^{m-2k}\lambda\right]\left[\cos^{2k}\phi\sin^{2k}\lambda\right]\left[\sin^{n-m-2l}\phi\right] \\
&= \frac{[\rho\cos\phi\cos\lambda]^{m-2k}}{\rho^{m-2k}}\,\frac{[\rho\cos\phi\sin\lambda]^{2k}}{\rho^{2k}}\,\frac{[\rho\sin\phi]^{n-m-2l}}{\rho^{n-m-2l}}
\end{aligned}$$

leading finally to

$$\hat{c}_{nm}^{kl}(\hat{\boldsymbol{\rho}}) = \left(\frac{\xi}{\rho}\right)^{m-2k}\left(\frac{\eta}{\rho}\right)^{2k}\left(\frac{\zeta}{\rho}\right)^{n-m-2l} = \frac{\xi^{m-2k}\eta^{2k}\zeta^{n-m-2l}}{\rho^{n-2l}}. \tag{4.31}$$

A similar transformation of equation (4.30) for $\hat{s}_{nm}^{kl}(\hat{\boldsymbol{\rho}})$ leads to the following expression

$$\hat{s}_{nm}^{kl}(\hat{\boldsymbol{\rho}}) = \left(\frac{\xi}{\rho}\right)^{m-2k-1}\left(\frac{\eta}{\rho}\right)^{2k+1}\left(\frac{\zeta}{\rho}\right)^{n-m-2l} = \frac{\xi^{m-2k-1}\eta^{2k+1}\zeta^{n-m-2l}}{\rho^{n-2l}}. \tag{4.32}$$

The last two equations will now be used during the transformation process of all forms of the Stokes coefficients from spherical to Cartesian coordinates.

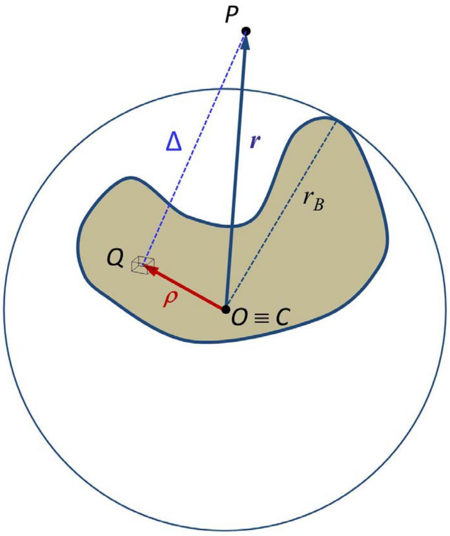

Figure 4.1. Configuration for the Brillouin expansion. The Brillouin sphere with radius r_B is shown centered at $O \equiv C$ containing the entire body.

4.4 The Stokes-Brillouin coefficients for the External Potential

On the basis of the results from the previous Section, the Stokes coefficients of the external potential—which we shall refer to as the *Stokes-Brillouin coefficients*—can now be written as

$$C^e_{nm} = \frac{2-\delta_{0m}}{MR^n}\frac{(n-m)!}{(n+m)!}\sigma \sum_{k=0}^{\lfloor \frac{m}{2} \rfloor} \sum_{l=0}^{\lfloor \frac{n-m}{2} \rfloor} K^{c,kl}_{nm}\, C^{e,kl}_{nm}, \tag{4.33}$$

$$S^e_{nm} = \frac{2-\delta_{0m}}{MR^n}\frac{(n-m)!}{(n+m)!}\sigma \sum_{k=0}^{\lfloor \frac{m-1}{2} \rfloor} \sum_{l=0}^{\lfloor \frac{n-m}{2} \rfloor} K^{s,kl}_{nm}\, S^{e,kl}_{nm}, \tag{4.34}$$

where the coefficients $C^{e,kl}_{nm}$ and $S^{e,kl}_{nm}$ have been defined as

$$C^{e,kl}_{nm} = \iiint\limits_V \rho^{2l} \xi^{m-2k} \eta^{2k} \zeta^{n-m-2l}\, d\xi\, d\eta\, d\zeta, \tag{4.35}$$

$$S^{e,kl}_{nm} = \iiint\limits_V \rho^{2l} \xi^{m-2k-1} \eta^{2k+1} \zeta^{n-m-2l}\, d\xi\, d\eta\, d\zeta. \tag{4.36}$$

The evaluation of these integrals is clearly the crucial point of the method being developed. The first factor of the integrands in (4.35) and (4.36) can be developed as the integer power of a trinomial to yield

$$\rho^{2l} = \left(\xi^2+\eta^2+\zeta^2\right)^l = \sum_{p=0}^{l}\sum_{q=0}^{p} \binom{l}{p}\binom{p}{q} \xi^{2(l-p)}\eta^{2(p-q)}\zeta^{2q}. \tag{4.37}$$

We can then write

$$C^{e,kl}_{nm} = \sum_{p=0}^{l}\sum_{q=0}^{p} K^e_{lpq} \iiint\limits_V \xi^{m-2(k-l+p)}\eta^{2(k+p-q)}\zeta^{n-m-2(l-q)}\, d\xi\, d\eta\, d\zeta, \tag{4.38}$$

and

$$S_{nm}^{e,kl} = \sum_{p=0}^{l}\sum_{q=0}^{p} K_{lpq}^{e} \iiint\limits_{V} \xi^{m-2(k-l+p)-1}\eta^{2(k+p-q)+1}\zeta^{n-m-2(l-q)}\, d\xi\, d\eta\, d\zeta, \tag{4.39}$$

in both of which we have used the numerical coefficients K_{lpq}^{e} defined by

$$K_{lpq}^{e} = \binom{l}{p}\binom{p}{q}. \tag{4.40}$$

A close look at (4.38) and (4.39) reveals that the triple integrals involved are the very same inertial integrals (3.46) developed in the previous Chapter. In fact

$$C_{nm}^{e,kl} = \sum_{p=0}^{l}\sum_{q=0}^{p} K_{lpq}^{e}\, I_{m-2(k-l+p),2(k+p-q),n-m-2(l-q)} \tag{4.41}$$

and

$$S_{nm}^{e,kl} = \sum_{p=0}^{l}\sum_{q=0}^{p} K_{lpq}^{e}\, I_{m-2(k-l+p)-1,2(k+p-q)+1,n-m-2(l-q)}. \tag{4.42}$$

What becomes apparent at this point is that the *Stokes coefficients are* expressed here as finite *linear combinations of the inertial integrals*,—a well-known result in the case of the external potential from (Hotine, 1969)—which has here been found in a constructive manner.

4.5 The Stokes-Hotine coefficients for the Internal Potential

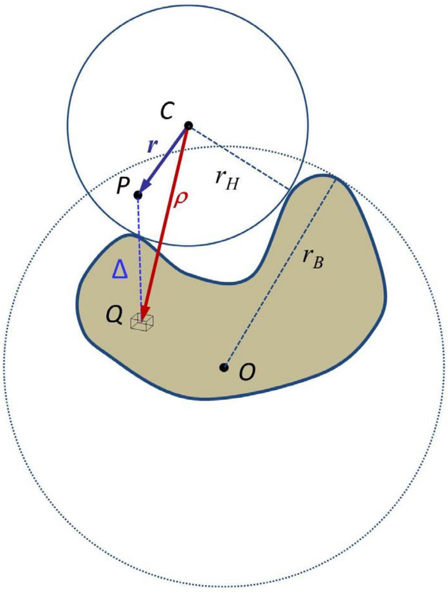

Figure 4.2. Configuration for the Hotine expansion. The Hotine sphere with radius r_H is shown centered at a point C external to the body, the sphere being tangent to the body itself.

On the basis of the results of Section 4.3, the Stokes coefficients (4.15) of the *internal poten-*

tial—which we shall refer to as the *Stokes-Hotine coefficients*—can now be written as

$$C^i_{nm} = (2-\delta_{0m})\,\frac{(n-m)!}{(n+m)!}\frac{R^{n+1}}{M}\sum_{k=0}^{\lfloor\frac{m}{2}\rfloor}\sum_{l=0}^{\lfloor\frac{n-m}{2}\rfloor} K^{c,kl}_{nm}C^{i,kl}_{nm}, \tag{4.43}$$

$$S^i_{nm} = (2-\delta_{0m})\,\frac{(n-m)!}{(n+m)!}\frac{R^{n+1}}{M}\sum_{k=0}^{\lfloor\frac{m-1}{2}\rfloor}\sum_{l=0}^{\lfloor\frac{n-m}{2}\rfloor} K^{s,kl}_{nm}\,S^{i,kl}_{nm}, \tag{4.44}$$

where the coefficients $C^{i,kl}_{nm}$ and $S^{i,kl}_{nm}$ have been defined as

$$C^{i,kl}_{nm} = \sigma\iiint\limits_V \frac{\xi^{m-2k}\eta^{2k}\zeta^{n-m-2l}}{\rho^{2n-2l+1}}dV, \tag{4.45}$$

$$S^{i,kl}_{nm} = \sigma\iiint\limits_V \frac{\xi^{m-2k-1}\eta^{2k+1}\zeta^{n-m-2l}}{\rho^{2n-2l+1}}dV. \tag{4.46}$$

The integrands on the RHS's of these equations are of the same form as already encountered in the previous Chapter when dealing with the inertial functions, except for the fact that the numerator contains three, rather than two factors. In particular, the expansion of the factor $\rho^{-(n-2l+1)}$ can be carried out according the the regional subdivision of $\mathbb{R}^3$ already introduced in Section 3.4.1. The result can be obtained by a direct extension of the expansion (3.130), i.e., by performing the replacement $2n+1 \longrightarrow 2n-2l+1$, as

$$\frac{1}{\rho^{2n-2l+1}} = \sum_{p=0}^{\infty}\sum_{q=0}^{\infty} K^{i,lpq}_n \frac{1}{\xi_R^{2n-2l+1}}\left(\frac{\zeta_R^2}{\xi_R^2}\right)^p\left(\frac{\eta_R^2}{\xi_R^2}\right)^q, \tag{4.47}$$

where we have used the numerical coefficient $K^{i,lpq}_n$ defined by

$$K^{i,lpq}_n = \binom{-(2n-2l+1)/2}{p}\binom{-(2n-2l+2p+1)/2}{q}. \tag{4.48}$$

For the regional mapping associated with the coordinates ξ_R, η_R, ζ_R reference should be made to Table 3.1.

We can now write the coefficients (4.45) and (4.46) in the form

$$C^{i,kl}_{nm} = \sigma\sum_{p=0}^{\infty}\sum_{q=0}^{\infty} K^{i,lpq}_n \iiint\limits_V \frac{1}{\xi_R^{2n-2l+1}}\left(\frac{\zeta_R^2}{\xi_R^2}\right)^p\left(\frac{\eta_R^2}{\xi_R^2}\right)^q \xi^{m-2k}\eta^{2k}\zeta^{n-m-2l}\,d\xi\,d\eta\,d\zeta, \tag{4.49}$$

$$S^{i,kl}_{nm} = \sigma\sum_{p=0}^{\infty}\sum_{q=0}^{\infty} K^{i,lpq}_n \iiint\limits_V \frac{1}{\xi_R^{2n-2l+1}}\left(\frac{\zeta_R^2}{\xi_R^2}\right)^p\left(\frac{\eta_R^2}{\xi_R^2}\right)^q \xi^{m-2k-1}\eta^{2k+1}\zeta^{n-m-2l}\,d\xi\,d\eta\,d\zeta. \tag{4.50}$$

As in Section 3.4.1, in order to use the same set of "regional" coordinates, the exponents of the original coordinates ξ, η, ζ in (4.49) and (4.50) need to be remapped. In the first case (4.49) we introduce the exponents α, β, γ with a C lower index, in the second case (4.50) we use the lower index S. The exponents are explicitly defined respectively in Table 4.1 and Table 4.2. The resulting compact expressions are

$$\boxed{C^{i,kl}_{nm} = \sigma\sum_{p=0}^{\infty}\sum_{q=0}^{\infty} K^{i,lpq}_n \iiint\limits_V \frac{\eta_R^{\beta_C+2q}\zeta_R^{\gamma_C+2p}}{\xi_R^{2n-2l+2p+2q+1-\alpha_C}}\,d\xi\,d\eta\,d\zeta,} \tag{4.51}$$

	R$_1$	R$_2$	R$_3$	R$_4$	R$_5$	R$_6$
$\alpha_C =$	$m-2k$	$m-2k$	$2k$	$2k$	$n-m-2l$	$n-m-2l$
$\beta_C =$	$2k$	$n-m-2l$	$n-m-2l$	$m-2k$	$m-2k$	$2k$
$\gamma_C =$	$n-m-2l$	$2k$	$m-2k$	$n-m-2l$	$2k$	$m-2k$

Table 4.1. Mapping of the exponents of the source point coordinates to the standardized naming (case of the C_{nm} coefficients).

	R$_1$	R$_2$	R$_3$	R$_4$	R$_5$	R$_6$
$\alpha_S =$	$m-2k-1$	$m-2k-1$	$2k+1$	$2k+1$	$n-m-2l$	$n-m-2l$
$\beta_S =$	$2k+1$	$n-m-2l$	$n-m-2l$	$m-2k-1$	$m-2k-1$	$2k+1$
$\gamma_S =$	$n-m-2l$	$2k+1$	$m-2k-1$	$n-m-2l$	$2k+1$	$m-2k-1$

Table 4.2. Mapping of the exponents of the source point coordinates to the standardized naming (case of the S_{nm} coefficients).

and

$$\boxed{S_{nm}^{i,kl} = \sigma\sum_{p=0}^{\infty}\sum_{q=0}^{\infty}K_n^{i,lpq}\iiint_V \frac{\eta_R^{\beta_S+2q}\,\zeta_R^{\gamma_S+2p}}{\xi_R^{2n-2l+2p+2q+1-\alpha_S}}\,d\xi\,d\eta\,d\zeta.} \tag{4.52}$$

As in the case of the Stokes Brillouin coefficients, also in this case we identify in (4.51) and (4.52) the presence of the integrals F_{npq}^{mij} defined in (3.152). In fact, note that in terms of the coefficient C_n^{pq} defined in equation (3.136) we have that

$$K_n^{i,lpq} = C_{n-l}^{pq} \tag{4.53}$$

and both $C_{nm}^{i,kl}$ and $S_{nm}^{i,kl}$ can be related to the *inertial functions* defined in equation (3.151) as

$$C_{nm}^{i,kl} = \sigma\sum_{p=0}^{\infty}\sum_{q=0}^{\infty}C_{n-l}^{pq}\,F_{(n-l)pq}^{mij}\left(R_C\right) = F_{n-l}^{mij}\left(R_C\right) \tag{4.54}$$

and

$$S_{nm}^{i,kl} = \sigma\sum_{p=0}^{\infty}\sum_{q=0}^{\infty}C_{n-l}^{pq}\,F_{(n-l)pq}^{mij}\left(R_S\right) = F_{n-l}^{mij}\left(R_S\right), \tag{4.55}$$

where with the symbols R_C and R_S we have explicitly added the dependence on the exponent mapping of Table 4.1 and Table 4.2, respectively, for the computation of the inertial functions F_{n-l}^{mij} given by equation (3.139) and successive developments found in the previous Chapter.

We conclude by noting that, as in the Stokes Brillouin coefficients, the *Stokes Hotine coefficients* can be expressed as

$$\boxed{C_{nm}^{i} = \left(2-\delta_0 m\right)\frac{(n-m)!}{(n+m)!}\,\frac{R^{n+1}}{M}\sum_{k=0}^{\left\lfloor\frac{m}{2}\right\rfloor}\sum_{l=0}^{\left\lfloor\frac{n-m}{2}\right\rfloor}K_n m^{c,kl}F_{n-l}^{mij}\left(R_C\right),} \tag{4.56}$$

and

$$\boxed{S_{nm}^{i} = \left(2-\delta_0 m\right)\frac{(n-m)!}{(n+m)!}\,\frac{R^{n}+1}{M}\sum_{k=0}^{\left\lfloor\frac{m-1}{2}\right\rfloor}\sum_{l=0}^{\left\lfloor\frac{n-m}{2}\right\rfloor}K_{nm}^{s,kl}\,F_{n-l}^{mij}\left(R_S\right),} \tag{4.57}$$

which shows that they *are finite linear combinations of the inertial functions* derived in the previous Chapter. The fully normalized versions of the Stokes Hotine coefficients can easily be found with the use of the relationships (4.6) and (4.7).

The acceleration and the gravity gradients can easily be computed using very well-known formulae and making efficient use of recurrence relations to compute the Associated Legendre Function, for which reference can be made to Fantino and Casotto (2009) or to Fukushima (2012).

Chapter 5

Orbit Dynamics Near 67P

5.1 Introduction

Characterizing the dynamical space around 67P is of great importance for two reasons. The first is the understanding of the dynamics of natural ejecta, or even the dynamics of capture (or, possibly, recapture) of gas or dust particles of various sizes. In particular, it is of great interest to assess the presence of stable regions in which the ejecta might accumulate, which would explain their observation. The second reason is the desire to measure the system parameters in order to make it possible to fly exploration missions close around the body. Of course this is an iterative process, since flying close means knowing the environmental parameters, but these parameters can only be measured by “sensing,” or probing the dynamics in the near regions. What actually is done in practice is that the parameters are determined progressively as the probe get closer, starting with some very rough assumptions—like a homogeneous mass distribution—while orbiting far away or imaging the body even from Earth and using the shape information as we have done in the previous chapters to generate a gravitational field for it. Then, knowing the system parameters, one can study the dynamical environment and search, for instance, for periodic orbits, possibly of a stable nature, which can be used to safely and economically park a spacecraft while it is performing scientific observations. For these reasons, this Chapter will address the problem of identifying periodic orbits around the nucleus of 67P.

For these reasons, this Chapter will introduce the dynamical equations to study the orbital evolution of a spacecraft and natural particles in the near space of 67P. The various components of the force field will be described and assessed in terms of their relevance for the purposes at hand. The dynamical equations will also include the sensitivity equations, what is known as the state transition matrix, which will also be formulated for the special case in which the integration is carried out in a non-inertial system. This will be a preliminary step to the Section devoted to the introduction of an algorithm for the computation of periodic orbits around the nucleus of 67P. Some general remarks will be made about the conditions of stability of these orbits. As a special case, stationary orbits will also be briefly discussed.

5.2 Force Modeling

To integrate orbits around the nucleus of 67P, we first have to define the forces that act on the orbiter in order to write the equations of motion. In the following, we are going to consider only the accelerations acting on the orbiter, factoring out its mass m_S, considered to be negligible with respect to the mass M_{67P}. The accelerations acting on a satellite can be distinguished in two main categories: the gravitational accelerations and the non-gravitational accelerations.

The relevant gravitational accelerations acting on the orbiter are the acceleration $\mathbf{a}_{67P}$ due to the mass distribution and the third-body acceleration $\mathbf{a}_S$ due to the Sun. We will not consider the perturbations of other planets for simplicity, even though the comet could enter the sphere of influence of one of them—Jupiter in particular,—making its gravitational attraction a major effect. The passage through the asteroid belt could also produce significant perturbations.

The non-gravitational forces acting on the spacecraft are due the acceleration caused by the solar radiation pression $\mathbf{a}_{SP}$, the drag acceleration $\mathbf{a}_D$ due to the gas and dust present around the cometary nucleus and the outgassing in the form of jets near perihelion. If the aim is to find periodic orbits closer than 10 km from the surface of the comet, such that their period is shorter than a few Earth days, we can make the assumption that the reference frame centered at the center of mass of the comet is inertial, thus neglecting its motion around the Sun. In this inertial reference frame, the differential equations of motion are

$$\dot{\mathbf{x}} = \mathbf{a}_{67P} + \mathbf{a}_S + \mathbf{a}_{SP} + \mathbf{a}_D \tag{5.1}$$

which are to be integrated from given initial conditions $\mathbf{x}(t_0) = \mathbf{x}_0$. The different force models at play will now be briefly described.

5.2.1 Third body effects

We can treat the third body forces of external bodies by considering these bodies as point masses. In the reference frame with origin O centered on the center of mass of the dominant body, the third body acceleration $\mathbf{a}_{TB}$ due to the action of N bodies can be expressed as (Danby, 1976; Roy, 2004; Battin, 1989; Vallado, 2001)

$$\mathbf{a}_{TB} = G\sum_{i}^{N} m_i \left(\frac{\mathbf{r}_i - \mathbf{r}}{|\mathbf{r}_i - \mathbf{r}|^3} - \frac{\mathbf{r}_i}{r_i^3} \right), \tag{5.2}$$

where m_i and $\mathbf{r}_i$ are respectively the mass and the position of the i^{th} perturbing body, and $\mathbf{r}$ is the position of the spacecraft. In the present case, the only perturbing body worth considering is the Sun, and thus the formula we need is simply

$$\mathbf{a}_S = Gm_S \left(\frac{\mathbf{r}_S - \mathbf{r}}{|\mathbf{r}_S - \mathbf{r}|^3} - \frac{\mathbf{r}_S}{r_S^3} \right). \tag{5.3}$$

The difference inside the parenthesis can get very small, especially in the present case, where the size of the orbit of the spacecraft around the nucleus is less than 10 km. As formulated in equation (5.3) the difference in parenthesis can be quickly driven to zero by the finite numerical representation on a computing machine—which would cause a possibly fatal loss of significant digits. This *singularity* can be avoided by adopting the *regularized* Encke-Battin formulation (Battin, 1989)

$$\mathbf{a}_S = -\frac{Gm_S}{|\mathbf{r}_S - \mathbf{r}|^3} \left[\mathbf{r} + f\left(q_S\right) \mathbf{r}_S \right], \tag{5.4}$$

where the auxiliary variable q_S and its function $f\left(q_S\right)$ are defined by

$$q_S = \frac{(\mathbf{r} - 2\mathbf{r}_S) \cdot \mathbf{r}}{\mathbf{r}_S \cdot \mathbf{r}_S}, \tag{5.5}$$

$$f\left(q_S\right) = q_S \frac{3 + 3q_S + q_S^2}{1 + \left(1 + q_S\right)^{3/2}}. \tag{5.6}$$

5.2.2 Drag force

The drag force is caused by the interaction of the satellite with the gas and the dust particles that surround the body around which it is orbiting. The drag force

$$\mathbf{F}_D = -\frac{1}{2}\rho V_r^2 S \left(C_D \mathbf{a} - C_L \mathbf{b}\right) \tag{5.7}$$

where ρ is the density of the gas, C_D is the *drag* coefficient, C_L is the *lift* coefficient, S is the cross section area of the satellite, and $\mathbf{V}_r$ is the relative velocity of the satellite with respect to the gas and **a** is its unit vector. The unit vector **b** is the direction in which the lift force acts. However, since the lift forces are in this case negligible with respect to the drag forces, we can safely set $C_L = 0$. It is clear that when approaching perihelion, this contribution will increase because of the higher outgassing activity in the vicinity of the Sun. This will increase the density and velocity of the surrounding gas, effectively increasing the drag force acting on the orbiter. Unfortunately, a density model of the gas surrounding the comet 67P is not yet available. We can just make suppositions on the magnitude of such force. This is also the reason why we did not take into account this contribution when integration the equations of motion. This formula is quadratic in the relative velocity because, when orbiting Earth, the velocity of the satellite are on the order of 10 km/s. In our case, the velocities involved are four orders of magnitudes lower. This means probably means that the best model of the drag force might be the one linear in the relative velocity V_r.

5.2.3 Solar radiation pressure

The solar radiation pressure produces a force acting on the satellite due to the absorption, reflection and scattering of the photons hitting the satellite. It can be described as a momentum flux P on the satellite, and has a value $P_{\text{Earth}} = 9 \cdot 10^{-6}$ N/m^2 at 1 AU and $P_{\text{Mars}} = 4 \cdot 10^{-6}$ N/m^2 at 1.52 AU. The force of the direct solar radiation pressure from the Sun on a spherically symmetric satellite is well modelled by Tapley et al. (2004)

$$\mathbf{F}_{RP} = -P(1+\eta)A\nu\mathbf{u}, \tag{5.8}$$

where P is the momentum flux from the Sun, A is the cross section area of the satellite normal to the Sun, different from the cross section area S used in the drag force formula, η is the reflectivity coefficient, or albaedo, **u** is the unit vector pointing from the satellite to the Sun, and ν is the eclipse factor, that is bounded between 0 (satellite in full shadow) and 1 (satellite in full sunlight). The model can surely be improved by modeling the force acting on the satellite (Gini, 2014) when it passes the penumbra region. However, this is goes beyond our needs and will not be further considered.

5.3 The Equations of Motion and the State Transition Matrix

The equations of motion necessary to propagate the initial state of a spacecraft in a specific acceleration field **a** can be written in general form as

$$\dot{\mathbf{x}}(t) = \mathbf{f}(\mathbf{x}, \mathbf{p}, t), \qquad \mathbf{x}(t_0) = \mathbf{x}_0, \tag{5.9}$$

where as usual **x** is the dynamical state vector and **p** a vector of system parameters, like the Stokes coefficients, or the inertial integrals, or the inertial functions of the present study. These equations are valid in any frame, be it inertial or not, as long as the fictitious accelerations are taken into proper account when the system is not inertial. It is of interest to note that in the synodic system corotating with the central body at constant angular velocity the equations of motion form an autonomous system and this implies the existence of an energy-like first integral like the Jacobi integral in the celebrated Circular Restricted Three-Body Problem (CRTBP).

Alongside the integration of the equations of motion, the sensitivity to initial conditions is a fundamental quantity to propagate as well. Therefore, we need to supplement the six equations of motion of a single particle with the 36 partials of the dynamical state with respect to the initial conditions. This implies that the *state transition matrix,* i.e., the *variational equations* need to be integrated at the same time as the equations of motion are integrated. The variational equations are fundamental for several reasons, mainly for inverse problems like orbit determination and, more specifically in our case, for the search of *periodic orbits.* They are also fundamental for establishing their stability. The sensitivity to initial conditions is the matrix $\partial \mathbf{x}/\partial \mathbf{x}_0$, which is a function of both the initial time t_0 and the current time t. Its value resides in the fact that it allows to propagate any initial error $\delta \mathbf{x}_0 = \delta \mathbf{x}\left(t=0\right)$ to the current time t, that is, it allows to compute

$$\delta \mathbf{x}\left(t\right) = \frac{\partial \mathbf{x}}{\partial \mathbf{x}_0}\left(t, t_0\right)\, \delta \mathbf{x}_0. \tag{5.10}$$

Equation (5.10) can be obtained by Taylor expanding the distance between solutions starting with a small difference $\delta \mathbf{x}_0$ of the initial conditions as

$$\begin{aligned} \delta \mathbf{x}\left(t\right) &= \mathbf{x}\left(t; \mathbf{x}_0 + \delta \mathbf{x}_0\right) - \mathbf{x}\left(t; \mathbf{x}_0\right) && (5.11) \\ &= \frac{\partial \mathbf{x}}{\partial \mathbf{x}_0}\left(t, t_0\right)\, \delta \mathbf{x}_0 + \text{higher-order terms.} && (5.12) \end{aligned}$$

In general, the sensitivity matrix is denoted as the operator $\Phi\left(t, t_0\right)$, i.e.,

$$\Phi\left(t, t_0\right) = \frac{\partial \mathbf{x}}{\partial \mathbf{x}_0}\left(t, t_0\right), \tag{5.13}$$

a square matrix of order six known as the State Transition Matrix (STM).

The STM can be computed by integrating the variational equations, which are themselves derived from partial differentiation of the equations of motion (5.9) leading, after a process of expansion to the first order, to Tapley et al. (2004); Montenbruck and Gill (2001)

$$\dot{\Phi}(t, t_0) = \mathsf{A}(t)\Phi(t, t_0), \qquad \Phi(t_0, t_0) = \mathsf{I}, \tag{5.14}$$

where

$$\mathsf{A}(t) = \left(\frac{\partial \mathbf{f}}{\partial \mathbf{x}}\right)^{*} \tag{5.15}$$

the asterisk being a reminder that the indicated partials are to be computed along the orbit being integrated.

It will be seen that the STM plays a fundamental role in the search for periodic orbits, since it will be used to correct misclosure errors. If computed at the end of one period of a periodic orbit, the STM is also known as the *Monodromy Matrix*, through which the stability or instability of the periodic orbit can be inferred.

5.3.1 The Equations of Motion

The orbits around 67P can be numerically integrated in the corotating, or synodic reference frame. The equations of motion then are

$$\ddot{\boldsymbol{\rho}} = \nabla U_{67P} - \boldsymbol{\omega} \times \left(\boldsymbol{\omega} \times \boldsymbol{\rho}\right) - 2\boldsymbol{\omega} \times \dot{\boldsymbol{\rho}}, \tag{5.16}$$

where $\boldsymbol{\rho}$ is the position vector and $\boldsymbol{\omega}$ is the angular velocity vector of the corotating with respect to an inertial frame, which can be considered fixed in direction, in good agreement with the measurements (Keller et al., 2015). The acceleration taken into account in the integration is only the gravitational acceleration due to 67P, as explained in the first Chapters of this research. Other components of the force field were not considered. We thus effectively treated the comet as an asteroid, since no drag force was implemented. The model is actually more idealized than that, since not even the radiation pressure effects, nor third-body perturbations were taken into consideration. The reason for this choice is multifarious. For gravitational perturbations it can be *safely* assumed that the large distance of the Sun compared to the typical size of the close orbits under study makes them negligible. As for the non-gravitational forces, the typical magnitude of the solar radiation pressure effect is about $5 \cdot 10^{-7}$ m/s^2 at 1 AU from the Sun, and falls to $2 \cdot 10^{-7}$ m/s^2 and $2 \cdot 10^{-8}$ m/s^2 at Mars and Jupiter distance from the Sun respectively, which must be compared to the average gravitational acceleration from the comet nucleus of about 10^{-5} m/s^2. It must be taken into account that the values of the acceleration due to the solar radiation pressure were calculated considering a mass of 1657 kg for Rosetta and the maximum possible area exposed to solar radiation of approximately 70 m^2, making these estimates the maximum of the solar pressure contribution. As far as the drag acceleration is concerned, a model for 67P is still under development and was not available for use in this research. Finally, the third-body effects are totally negligible. We calculated the acceleration contribution of the third-body effects with the spacecraft at 10 km from the center of mass of the comet at conjunction at Earth and Jupiter distances through formula (5.4), yielding $1.6 \cdot 10^{-12}$ m/s^2 and $8.0 \cdot 10^{-13}$ m/s^2 respectively. This is in agreement with the Hill sphere, i.e., the sphere of influence, of 67P being 318 km in radius (Rotundi et al., 2015).

We conclude by pointing out that the largest acceleration that was neglected is radiation pressure, which is nonetheless almost 2 orders of magnitude smaller than the gravitational pull of 67P—which definitely supports our neglect of all forces other than ∇U_{67P}.

5.3.2 The Variational Equations

In the particular case of 67P we need to explicitly write the partials (5.15) in order to integrate the variational equations and obtain the state transition matrix. We can write matrix A separating it in blocks to account for the spatial and velocity components as

$$\mathsf{A} = \frac{\partial \mathbf{f}\,(\boldsymbol{\rho}, \dot{\boldsymbol{\rho}})}{\partial\,(\boldsymbol{\rho}, \dot{\boldsymbol{\rho}})} = \begin{pmatrix} 0 & \mathsf{I} \\ \dfrac{\partial \ddot{\boldsymbol{\rho}}}{\partial \boldsymbol{\rho}} & \dfrac{\partial \ddot{\boldsymbol{\rho}}}{\partial \dot{\boldsymbol{\rho}}} \end{pmatrix}, \tag{5.17}$$

where the four blocks are 3×3 matrices with I the unit matrix. In the corotating reference frame, equation (5.16) holds. This leads to computing $\partial \ddot{\boldsymbol{\rho}} / \partial \boldsymbol{\rho}$ and $\partial \ddot{\boldsymbol{\rho}} / \partial \dot{\boldsymbol{\rho}}$ explicitly as

$$\frac{\partial \ddot{\boldsymbol{\rho}}}{\partial \boldsymbol{\rho}} = \nabla\nabla U_{67P} + \omega^2 \mathsf{I} - \boldsymbol{\omega}\boldsymbol{\omega}^T \tag{5.18}$$

and

$$\frac{\partial \ddot{\boldsymbol{\rho}}}{\partial \dot{\boldsymbol{\rho}}} = -2\Omega_{\boldsymbol{\omega}}, \tag{5.19}$$

where

$$\omega^2 \mathsf{I} - \boldsymbol{\omega}\boldsymbol{\omega}^T = \begin{pmatrix} \omega_y^2 + \omega_z^2 & -\omega_x\omega_y & -\omega_x\omega_z \\ -\omega_x\omega_y & \omega_x^2 + \omega_z^2 & -\omega_y\omega_z \\ -\omega_x\omega_z & -\omega_y\omega_z & \omega_x^2 + \omega_y^2 \end{pmatrix} \tag{5.20}$$

and

$$\Omega_{\boldsymbol{\omega}} = \begin{pmatrix} 0 & -\omega_z & \omega_y \\ \omega_z & 0 & -\omega_x \\ -\omega_y & \omega_x & 0 \end{pmatrix} \tag{5.21}$$

here ω_x, ω_y, and ω_z are the components of the angular velocity vector $\boldsymbol{\omega}$ and $\Omega_{\boldsymbol{\omega}}$ is the skew-symmetric matrix associated with the axial vector $\boldsymbol{\omega}$, sometimes also denoted with the operator symbol $\boldsymbol{\omega}\times\boldsymbol{.}$ In the case under study we have $\omega_x = \omega_y \equiv 0$, which considerably simplifies the two matrices above. In fact, $\boldsymbol{\omega}\boldsymbol{\omega}^T = 0$ so that

$$\omega^2 \mathsf{I} - \boldsymbol{\omega}\boldsymbol{\omega}^T \equiv \omega_z^2 \mathsf{I} \tag{5.22}$$

and

$$\frac{\partial \ddot{\boldsymbol{\rho}}}{\partial \dot{\boldsymbol{\rho}}} = -2\omega_z \begin{pmatrix} 0 & -1 & 0 \\ 1 & 0 & 0 \\ 0 & 0 & 0 \end{pmatrix}. \tag{5.23}$$

Note that equation (5.14), with the block decomposition

$$\Phi = \begin{pmatrix} \Phi_{\boldsymbol{\rho}\boldsymbol{\rho}} & \Phi_{\boldsymbol{\rho}\dot{\boldsymbol{\rho}}} \\ \Phi_{\dot{\boldsymbol{\rho}}\boldsymbol{\rho}} & \Phi_{\dot{\boldsymbol{\rho}}\dot{\boldsymbol{\rho}}} \end{pmatrix}, \tag{5.24}$$

can now be written using the notation introduced in (5.17) as

$$\dot{\Phi}_{\boldsymbol{\rho}\boldsymbol{\rho}} = \Phi_{\dot{\boldsymbol{\rho}}\boldsymbol{\rho}}, \tag{5.25a}$$

$$\dot{\Phi}_{\boldsymbol{\rho}\dot{\boldsymbol{\rho}}} = \Phi_{\dot{\boldsymbol{\rho}}\dot{\boldsymbol{\rho}}}, \tag{5.25b}$$

$$\dot{\Phi}_{\dot{\boldsymbol{\rho}}\boldsymbol{\rho}} = \frac{\partial \ddot{\boldsymbol{\rho}}}{\partial \boldsymbol{\rho}} \Phi_{\boldsymbol{\rho}\boldsymbol{\rho}} + \frac{\partial \ddot{\boldsymbol{\rho}}}{\partial \dot{\boldsymbol{\rho}}} \Phi_{\dot{\boldsymbol{\rho}}\boldsymbol{\rho}}, \tag{5.25c}$$

$$\dot{\Phi}_{\dot{\boldsymbol{\rho}}\dot{\boldsymbol{\rho}}} = \frac{\partial \ddot{\boldsymbol{\rho}}}{\partial \boldsymbol{\rho}} \Phi_{\boldsymbol{\rho}\dot{\boldsymbol{\rho}}} + \frac{\partial \ddot{\boldsymbol{\rho}}}{\partial \dot{\boldsymbol{\rho}}} \Phi_{\dot{\boldsymbol{\rho}}\dot{\boldsymbol{\rho}}}. \tag{5.25d}$$

Since the STM is a fundamental matrix of solutions of the variational equations (5.14), each column of the state transition matrix is independent of the other columns, and can thus be integrated alone.

5.4 Finding periodic orbits in the synodic reference frame

A periodic orbit is a solution $\mathbf{x}(t)$ to the equations of motion (5.9), with initial conditions $\mathbf{x}(0) = \mathbf{x}_0$, for which there exists a minimum $T > 0$, called period, such that

$$\mathbf{x}(t+T) = \mathbf{x}(t) \qquad \forall t. \tag{5.26}$$

Typically, periodic orbits are found by using the symmetries of the body and for point particles systems use can be made of the Roy and Ovenden's Mirror Theorem (Roy, 2004). In our case, however, this theorem is of no help, since the extended body is completely irregular and presents no symmetries whatsoever. We thus have to rely on an iterative algorithm applied to the entire period of the periodic orbit, rather than to the half period at the core of the mirror theorem. This implies some severe numerical problems in connection with the inversion of the monodromy matrix, which, as already noted by Broucke and Boggs (1975), becomes singular as the periodic orbit is approached during the search. The situation can be saved by applying appropriate numerical techniques, mainly by applying singuar value decmposition techniques, as described in (Russell and Lara, 2007).

Let the body rotate around the z axis, parallel to the principal axis of inertia of greatest moment. Let $\mathbf{x}_0$ be the initial state. We impose now that the orbit starts on the x-z plane, so that $y = 0$ for the initial state. We can introduce now the constraint vector

$$\mathsf{K} = \begin{pmatrix} \xi_{\mathbf{T}} - \xi_0 \\ C - C_* \end{pmatrix}, \tag{5.27}$$

where $\xi = (x, z, u, v, w)$, with $u = \dot{x}$, $v = \dot{y}$ and $w = \dot{z}$, and $C = 2U^* - \left(u^2 + v^2 + w^2\right)$ is the Jacobi integral with U^* the effective potential in the synodical reference frame, and C_* is the reference Jacobi integral—usually taken to be the Jacobi integral of the first iteration. We do not consider the y component of the state $\mathbf{x}$ in ξ, since it is set to 0. Assuming an initial guess ξ_0 in the vicinity of a solution will yield a nonzero K. To drive the constraint vector to zero, a $\Delta\xi_0$ is sought satisfying the equation

$$\frac{d\mathsf{K}}{d\xi_0}\Delta\xi_0 = -\mathsf{K}. \tag{5.28}$$

We point out that the system (5.28) has five unknowns in six equations. To ensure a unique solution a least-square approch is adopted, allowing all af the constraints to be enforced. However, there are frequently multiple directions in the phase space where periodic solutions exist. Therefore, despite the fact that the system of equations (5.28) is overcontrained, the dynamics suggest that solutions exist that satisfy all of the constraints. If a solution exists, the least.squaree correction will drive the norm of the constraint down to zero.

The Singular Value Decomposition (SVD) provides a simple solution ot the problem of the degenerate Jacobian associated with the periodic orbit. The dimension of the null space of such Jacobian is non-zero because any direction tangent to the solution leads again to the same periodic solution. An additional degeneracy exist on the case of a bifurcation orbit Russell and Lara (2007), that is an orbit that belongs to two different orbit families. The SVD technique deals efficiently in reducing the system in only the degenerate directions. The 6×5 Jacobian has a singular value decomposition of the form

$$\frac{d\mathsf{K}}{d\xi_0} = \mathsf{UDV}^\mathsf{T} \tag{5.29}$$

where U and V are square orthogonal matrices of dimensions 6 and 5, respectively, and D is a 6×5 matrix with nonnegatives entries along the diagonal, and zeroes etherwise. The pseudoinverse of the Jacobian is thus

$$\left(\frac{d\mathsf{K}}{d\xi_0}\right)^+ = \mathsf{VSU}^\mathsf{T}, \tag{5.30}$$

where the matrix S is diagonal with elements

$$S_{ii} = \begin{cases} 1/D_{ii}, & \text{for } D_{ii} > \varepsilon, \\ 0, & \text{for } D_{ii} < \varepsilon. \end{cases} \tag{5.31}$$

The diagonal elements of D are called *singular values* of the Jacobian. For practical computations, any singular value less than some predefined threshhold ε is considered zero as indicated in equation (5.31). The solution to (5.28) is then

$$\Delta\xi_0 = -(\mathsf{VSU}^\mathsf{T})\mathsf{K}, \tag{5.32}$$

where the problem associated with any degenerate direction is solved through the selection of the paramenter ε.

The Jacobian is calculated as

$$\frac{d\mathsf{K}}{d\xi_0} = \begin{pmatrix} \dfrac{d\xi_T}{d\xi_0} - \mathsf{I}_{5\times5} \\ \dfrac{dC}{d\xi_0} \end{pmatrix}_{6\times5}, \tag{5.33}$$

where

$$\frac{dC}{d\xi_0} = \frac{dC}{d\xi_T}\frac{d\xi_T}{d\xi_0}, \tag{5.34}$$

and

$$\frac{d\xi_T}{d\xi_0} = \frac{\partial\xi_T}{\partial\xi_0} + \frac{\partial\xi_T}{\partial T}\frac{\partial T}{\partial\xi_0}, \tag{5.35}$$

where the partial derivative of the period T with respect to the initial conditions ξ_0 is found from

$$\Delta y_T = \frac{\partial y_T}{\partial\xi_0}\delta\xi_0 + \dot{y}_T\delta T. \tag{5.36}$$

Because the integrator implicitly stops on the x-z plane, equation (5.36) can be solved with $\Delta y_T = 0$, giving

$$\frac{\partial T}{\partial\xi_0} = -\frac{\partial y_T}{\partial\xi_0}\frac{1}{\dot{y}_T}. \tag{5.37}$$

To sum up, equation (5.35) can be now written as

$$\frac{d\xi_T}{d\xi_0} = \boldsymbol{\Phi}\left(T, t_0\right)_{i\neq2, j\neq2} - \frac{1}{\dot{y}_T}\dot{\xi}_T\boldsymbol{\Phi}\left(T, t_0\right)_{i\neq2, j\neq2}, \tag{5.38}$$

where

$$\boldsymbol{\Phi}\left(t, t_0\right) = \frac{\partial\mathbf{x}\left(t\right)}{\partial\mathbf{x}\left(t_0\right)} \tag{5.39}$$

is the state transition matrix that provides the sensitivity to the initial conditions after a time t, as it was shown in the previous Chapter. The state transition matrix is obtained by integrating equations

$$\dot{\boldsymbol{\Phi}}\left(t, t_0\right) = \left.\left(\frac{\partial\mathbf{f}}{\partial\mathbf{x}}\right)\right|_t \boldsymbol{\Phi}\left(t, t_0\right) \tag{5.40}$$

along with

$$\dot{\mathbf{x}}(t) = \mathbf{f}(\mathbf{x}). \tag{5.41}$$

To summarize, given an initial guess ξ_0 in the vicinity of a solution that yields a constraint violation K, the linearized first-order correction is given by equation (5.32). It is useful to scale the correction step in order to not exceed any of the user-defined maximum step sizes. The process is iterated with the corrected guess until convergence as indicated by a constraint violation that is sufficiently small and is no longer reducing in length. The constraints used to check the convergence are based on the values of d_1 and d_2, defined by

$$d_1 = \frac{\left|\mathbf{r}\left(t_f\right) - \mathbf{r}\left(t_0\right)\right|}{\left|\mathbf{r}\left(t_0\right)\right|}, \tag{5.42}$$

$$d_2 = \frac{\left|\mathbf{v}\left(t_f\right) - \mathbf{v}\left(t_0\right)\right|}{\left|\mathbf{v}\left(t_0\right)\right|}. \tag{5.43}$$

Convergence is reached when $d_1 < d_1^*$ and $d_2 < d_2^*$. The constraint associated with the Jacobi integral was not used as a check since the difference between the reference Jacobi integral C_* and the Jacobi integral of the final periodic orbit C_p was unknown and the d_1 and d_2 checks were sufficient to locate a periodic orbit.

After some trials, the parameters ε, d_1, and d_2 were set as $\varepsilon = D_{1,1} \cdot 10^{-10}$, with $D_{1,1}$ the largest singular value, $d_1^* = 10^{-13}$ and $d_2^* = 10^{-8}$. Larger values of ε did not allow the orbit to converge, while lower values of d_1^* and d_2^* were never reached during the selection of the parameters.

To apply this algorithm, one needs to know when to stop the integration of the orbit on the x-z plane. The initial guess of periodic orbit might in fact pass several times through the x-z plane before getting close to the initial conditions, thus enabling the application of the algorithm. During test runs, some checks were tried before choosing the final one. We first counted how many times the orbit passed through the x-z plane, then added the check on the direction of the velocity while passing through the plane, and then also tried to distinguish the number of times that the plane was passed through a point with coordinate $x > 0$ or otherwise. None of these checks were general and useful, since even using a small and controlled grid, no periodic orbits could be found other than the equatorial orbits. Also since there was no check or constraint on the distance to the initial conditions while passing the x-z plane, often the corrections to the initial conditions given by the algorithm described in this Section were outside the linear regime, thus invalidating the theory applied.

The final check used to discriminate when to stop the orbit integration is as follows. Every time the orbit passed through the x-z plane, the state computed just before passing, defined as $\mathbf{x}_b$, was used to calculate the distance from the initial state. The spatial and velocity components were controlled separately through the inequalities

$$|\mathbf{r}_b - \mathbf{r}_0| < a, \tag{5.44}$$

$$|\mathbf{v}_b - \mathbf{v}_0| < b. \tag{5.45}$$

It was not possible to determine the parameters a and b beforehand, so after some trials a was set in the range $[100, 200]$ m and b in the range $[0.4, 0.6]$ m/s. Higher values of a like 800 m were also used when grid search of inclined periodic orbits yielded no results, even though the linearity regime was not satisfied.

5.4.1 Stability Conditions

The stability of a periodic orbit can be derived to first order thanks to the state transition matrix $\Phi(T, 0)$, which takes the name *Monodromy Matrix* in the case of a periodic orbit. We define the monodromy matrix

$$\mathsf{M} = \Phi(T, 0). \tag{5.46}$$

Given a perturbation $\delta\mathbf{x}_0$ to the initial state at time $t = 0$, it is clear that after n periods T of the periodic orbit, the propagation to first order of the perturbation is

$$\delta\mathbf{x}(nT) = \Phi(nT, 0)\,\delta\mathbf{x}_0 \tag{5.47}$$

$$= \mathsf{M}^n \delta\mathbf{x}_0. \tag{5.48}$$

It is clear that for $\delta\mathbf{x}$ not to diverge in time, the eigenvalues of the monodromy matrix must all have absolute valus less than or equal to 1. In particular, for an autonomous system, two eigenvalue are 1, one linked to the existence of the Jacobian integral of motion, the other linked to the fact that the solution is periodic, as explained in Seydel (2010). The remaining four eigenvalues are the ones that determine the stability or instability of the orbit. In particular, since the monodromy matrix is real, the four remaining eigenvalues can be divided into two pairs of conjugate complex numbers.

5.4.2 Potential stationary points stability

There exists stationary solutions to equations (5.9). This solutions are such that

$$\mathbf{x}(t) = \mathbf{s}, \qquad \mathbf{a}(\mathbf{s}, \mathbf{p}, t) = \mathbf{0}. \tag{5.49}$$

In the case of 67P we will see that 4 such points exists in the proximity of the comet surface. Two of them are saddle points, and thus unstable, and the other two are maxima of the effective potential U^* relative to the corotating reference frame. We heuristically show here that all such points are unstable. it is known (Danby, 1976) that in the Restricted Three-Body Problem, the stationary points L_4 and L_5 are linearly stable only if the ratio of the masses of the two main bodies satisfies $\mu_2/\mu_1 < 0.62\ldots$. We hypothesize here that this criterion can be extended to a similar mass ratio, which in the present case could be associated with the masses of the two main lobes, or heads, of the nucleus of 67P, which can be imagined to be concentrated near their respective centers of mass, this way mimicking the CRTBP configuration. The heuristic result seems to point to a failed stability test for the hypothetical triangular homographic solutions.

Chapter 6

Periodic Orbits Around 67P

After introducing the theoretical concepts and the equations of motion and the computaional scheme for finding periodic orbits, we are now ready for their application to the study of the orbital dynamics around comet 67P. Recall that the cometary nucleus will be considered inactive, i.e., we will essentially treat it as it were an asteroid. We start by defining the main orbital and physical characteristics of 67P that are important to our study. Then we will report on the search for periodic orbits close to the nucleus and leave for the following Chapter the assessment of the possibility of designing and characterizing artificial orbits for specific exploration purposes.

One of the main tasks in carrying out the orbital computations is the computation of the gravitational accceleration of the extended central body. We have devoted three Chapters to the study of several different ways of modeling the potential and its gradients in an attempt to find the most computationally efficient method. It is known, in faact, that the Werner algorithm is very computationally intensive, since it must compute several costly mathematical functions for each face and each edge of the polyhedral model of the central body. Time constraint, however, have not allowed us to fully compare the new methods introduced in Chapter 2 and 3, respectively dealing with the inertial integrals and inertial functions representation and with the expansions in Spherical Harmonnics both outside the Brillouin sphere and inside the Hotine sphere for orbits reaching close to the surface. As a result, the method of Werner has been used throughout this investigation. This somewhat limited the extent of the search for periodic orbits in the sense that it was not possible to proceed to a full parallelization of the POLYGRAV code. The search, however, was carried out over significant sections of phase space, as will be reported next.

6.1 Characterization of 67P

67P/Churyumov-Gerasimenko is a short-period comet whose orbital elements at epoch 2457262.5 TDB (2015, Aug. 28.0) are shown in Table 6.1, while Table 6.2 shows other physical parameters of interest, like its mass density.

The main characteristics of the orbit can be summarized by noting that its perihelion distance is $r_p = 1.2432$ AU and its aphelion distance is $r_a = 5.6805$ AU with an associate eccentricity e of approximately 0.64. The radius vector of the comet at quadrature is $p = 2.0400$ AU. The angular velocity at perihelion is 0.908 deg/d and at aphelion 0.0435 deg/day, two rather different values on account of the great eccentricity of the orbit.

The comet rotates around its greatest principal axis with a period $T = 12.4043$ h. However, this value changes over time, mostly due to the sublimation activity during perihelion. The decrease in the rotational period is currently estimated to be 1285 s since the 2009 perihelion passage (Keller et al., 2015).

Element	**Value**
a	3.4619 AU
e	0.64088
i	7.040 deg
Ω	50.1358 deg
ω	12.79600 deg
Perihelion passage τ	2457247.5865 JED
GM	667. $\mathrm{m^3kg^{-1}s^{-2}}$
Period T	6.44 y
Mean motion n	0.153011 deg/d
Parameter p	2.0400 AU
Perihelion distance r_p	1.2432 AU
Aphelion r_a	5.6805 AU
Perihelion speed v_p	34.187 km/s
Aphelion speed v_a	7.479 km/s

Table 6.1. The orbitl elements of comet 67P (JPL/SSD)

Physical parameter	**Value**
Density σ	470 $\mathrm{kg/m^3}$
Mass M	10^{13} kg
Volume V	19 $\mathrm{km^3}$
Rotation period	12.404 h

Table 6.2. Some useful physical parameters of comet 67P from (Sierks et al., 2015)

This body is without a doubt the most irregularly shaped body ever imaged in the Solar System—let alone explored in situ. This poses a new series of problems in terms of modeling its gravitational field, and this is the main reason why we have devoted a large part of this research effort to develop new methods of representing the potential and the gravitationa field of this body, in particular in the region near the surface, where calssicaly no investigation has ever been carried out.

In this work, the shape of the comet nucleus is approximated by a polyhedron model (Jorda et al., 2015) generated from imaging data by the Rosetta/OSIRIS team (Keller et al., 2007). The most recent model available consists of a triangular mesh composed of $1,572,866$ vertices and $3,145,728$ triangular faces. In the interest of computational speed, this mesh was reduced by 95% to a mesh with $7,866$ vertices and $15,728$ triangular faces. This mesh was used to obtain all the results in this and in the following chapter. For the reduction the MeshLab software tool was used (Visual Computing Lab ISTI CNR). The procedure to obtain the reduced meshes was as follows. The original mesh was first centered on its baricenter, which was computed by MeshLab considering the polyhedron as a homogeneous body. Then, an alignment to the principal axes of inertia was performed, using a built-in function of MeshLab. The reduction used the built-in function *Quadratic Edge Collapse Decimation* with the options:

- preserve the normal to the surface,
- preserve the topology of the surface,
- optimal position of simplified vertices,
- post-simplification cleaning,

- percentage reduction of 0.005.

A final rotation to align the body to the principal axes of inertia was performed.

6.2 Search Grid

A FORTRAN90 program was developed to intergate the orbital equations of motion and carry out the search for periodic orbits. The program was not parallellized due to lack of resources, time in particular. The set of initial conditions to start the search was therefore limited to a few linear grids of initial positions and velocities. All initial conditions were set on the $y = 0$ plane and the orbits were integrated using a multi-step, variable-order, variable-step numerical integrator. The time of the $y = 0$ plane crossing was found using locally an RK7(8) algorithm with a precision of 10^{-10} m.

The gravitational acceleration was computed using Werner's method and code POLYGRAV at any point outside polyhedral body. The initial positions were taken very close to 67P's surface, since the objective was the exploration of the dynamical behaviour of test particles very close to the cometary nucleus.

Because of the limited computational power, only small grids were used during the search for periodic orbits. Each grid was composed of a linear spatial component, with a step size in the range $[50, 200]$ m, and a velocity component, in which the direction of the velocity was kept constant and normal to the $y = 0$ plane, while its absolute value was changed by adding or subtracting from the circular velocity v_C an integer multiple of $v_C/20$.

The initial spatial positions were chosen along the x-axis in order to find planar equatorial orbits. The spatial grid was then moved along the z-axis for the search of inclined periodic orbits.

Although direct equatorial periodic orbits were found, the search never converged to any direct inclined periodic orbits. However, the search was successful when it was changed from direct to retrograde orbits (referred to the inertial reference frame).

6.3 Stationary Locations

The potential minima were found by calculating the gravitational potential in a 2-dimensional grid for different values of z. The following image represents a $x - y$ plane of the potential for $z = 0$. Orbits with initial conditions close to the minimum of the potential were integrated, but all orbits resulted to be unstable, some of them crashing in the comet, the others drifting away from the nucleus. Figure 6.1 shows the equipotential lines on the equatorial plane of the comet, from which is clear that the two unstable stationary configurations lie near the x-axis.

6.4 Periodic Orbits

6.4.1 Near-Equatorial Periodic Orbits

We begin by showing the results of the search for planar periodic orbits. Figure 6.4 shows three equatorial *linearly stable* orbits, while Figure 6.5 shows a sample of three *linearly unstable* equatorial periodic orbits. No equatorial orbits closer to the shown ones were found. Planar periodic orbits can only occur near the equatorial plane, due to the rotation and the irregular shape of the central body.

Figure 6.6 shows a view from the negative y-axis of an equatorial orbit. Note that the orbit does not strictly lie on the equatorial plane, caused by the fact that the body is highly irregular.

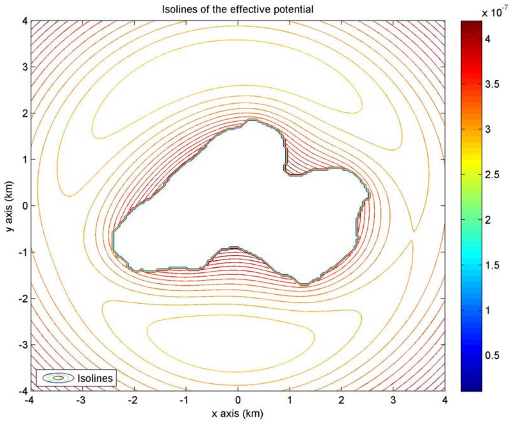

Figure 6.1. Equipotential lines on the equatorial plane of 67P.

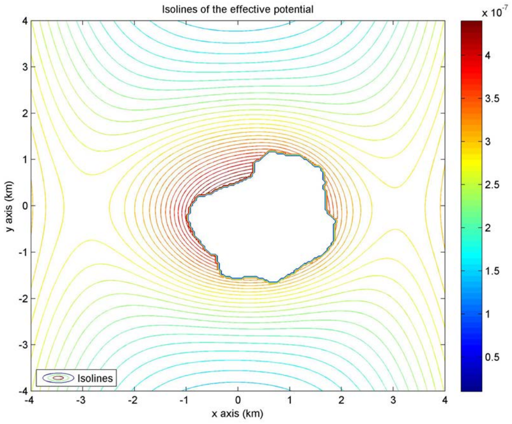

Figure 6.2. Equipotential lines on the y-z plane of 67P.

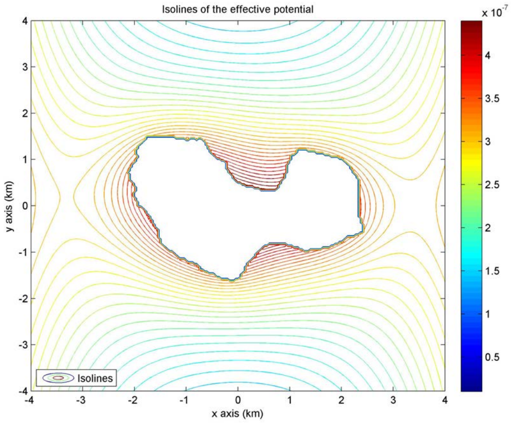

Figure 6.3. Equipotential lines on the x-z plane of 67P.

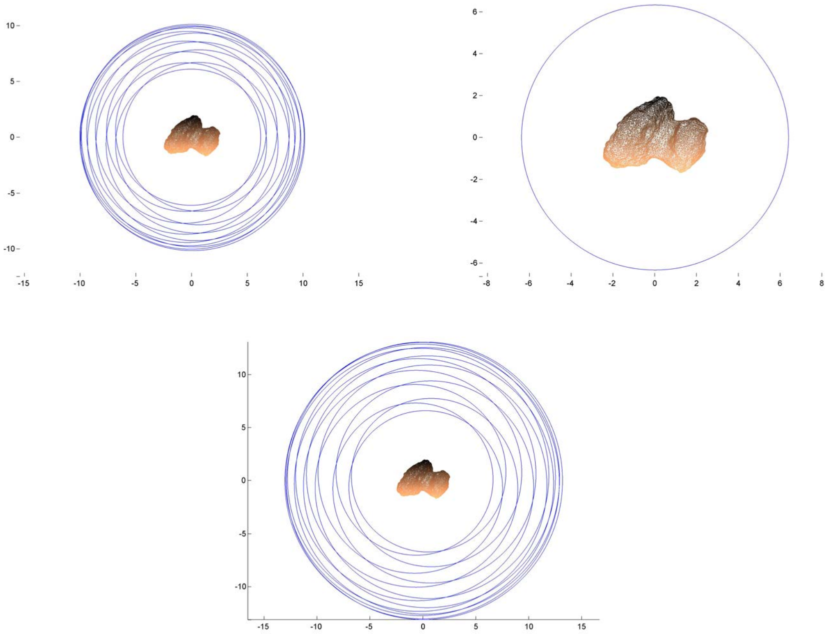

Figure 6.4. Planar and stable periodic orbits 1-2-3 seen from positive z axis.

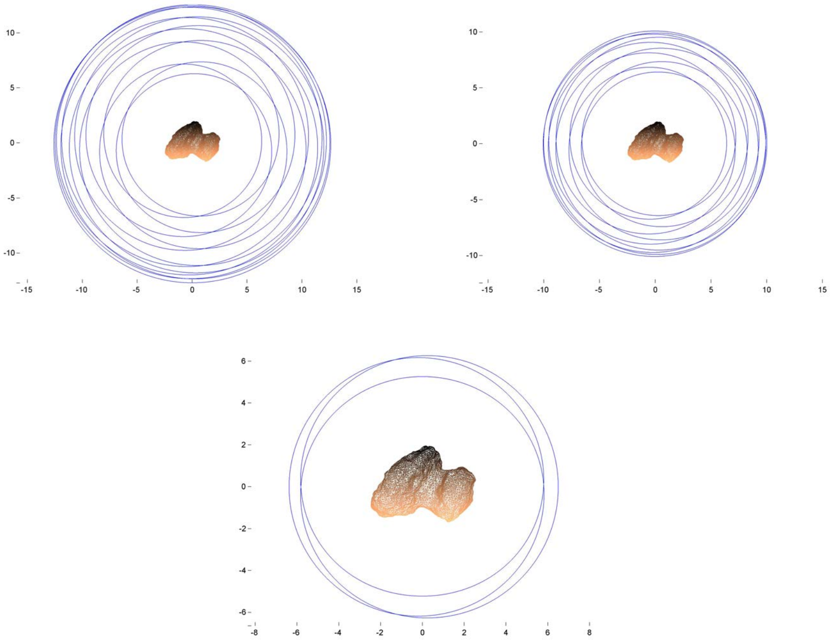

Figure 6.5. Planar and unstable periodic orbit 4-5-6 seen from positive z axis.

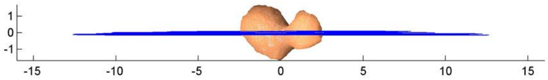

Figure 6.6. Planar and unstable periodic orbit 5 seen from negative x axis.

6.4.2 Inclined Periodic Orbits

Inclined periodic orbits have been a little more difficult to find. However, after some trials and choosing inital conditions for inertially retrograde orbits, the search was successful. We exhibit here just a sample of the set of inclined periodic orbits found. Each Figure from 6.7 to 6.19 display inclined retrograde periodic orbits. Each of them contains four panels with the same periodic orbit viewed from different directions, namely, from left to right and from top to bottom, 1) from the negative y-axis, 2) from the positive x-axis, 3) from the positive z-axis, 4) a view from azimuth 130°and elevation 40°. The units in all Figures are in kilometers. Figures 6.7 to Figure 6.19 display inclined retrograde periodic orbits found from starting paramenters of different grids. The actual number of inclined periodic orbits found was almost three times the number of orbits shown in this Section.

The view of these periodic orbits from inertial frame is also displayed in Figures 6.20 and 6.21,as an example. Figure 6.20 is displayed to show how mush the irregularity of the nucleus perturbs the inertial orbit, while Figure 6.21 is displayed to show the large precession rate to which these orbits are subjected to.

Note that Figure 6.15 displays an orbit that enters the Brillouin sphere of the nucleus. In this case, computing the acceleration with the algorithm described in Chapter 2 is fundamental, since any other method would not converge everywhere outside the body.

6.4.3 Search for Periodic Orbits Deep in the Valley

A search was also carried out for orbits that would fly in the low region of the big valley around the two heads of the nucleus. Since the region where the valley is located is displaced from the center of mass, and the plane of the valley is not parallel to any of the principal planes, and due to the large dimensions of the head region opposite the valley (with respect to the center of mass, which must belong to any osculating orbit plane), any periodic orbit must be highly elliptic on average. The initial conditions used in this search were chosen so that the oribt would start deep inside the valley, and the velocity was chosen so that the trajectory would follow the direction of the valley. A process of trial and error indicated that higher altitude (in the vertical z component) were more suitable. However, even increasing the altitude to about the top of the valley did not yield to convergence. The orbits which yielded the smallest misclosure are nonetheless displayed in Figures 6.22 and 6.23. Clearly a more extensive search on a wider set of

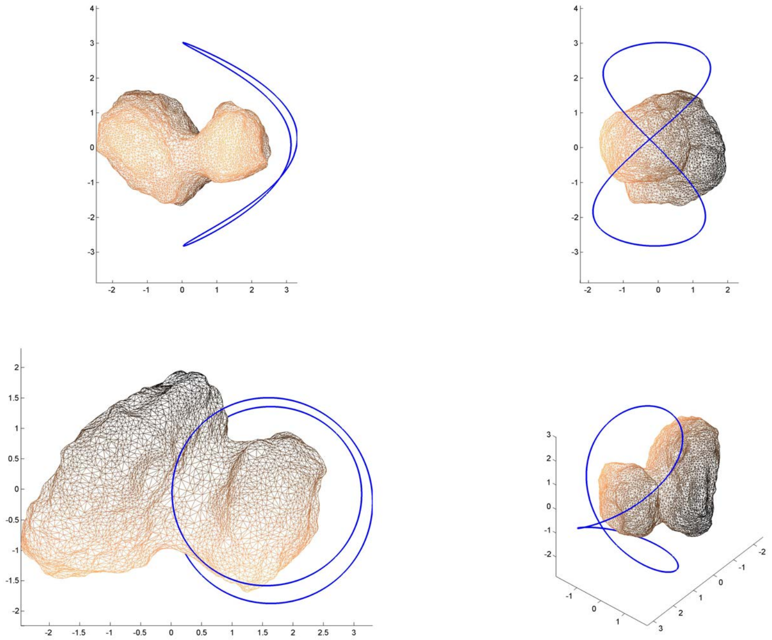

Figure 6.7. Inclined retrograde periodic orbit #1. Unstable

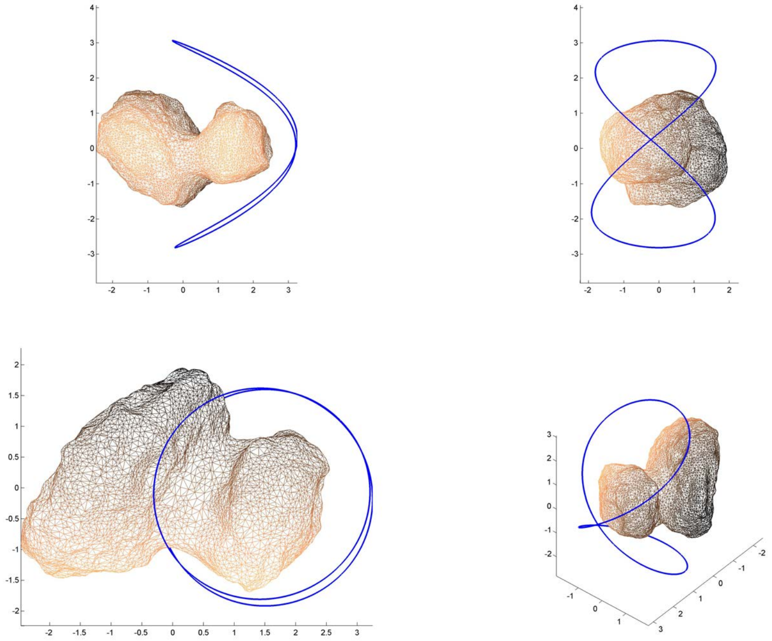

Figure 6.8. Inclined retrograde periodic orbit #2. Unstable.

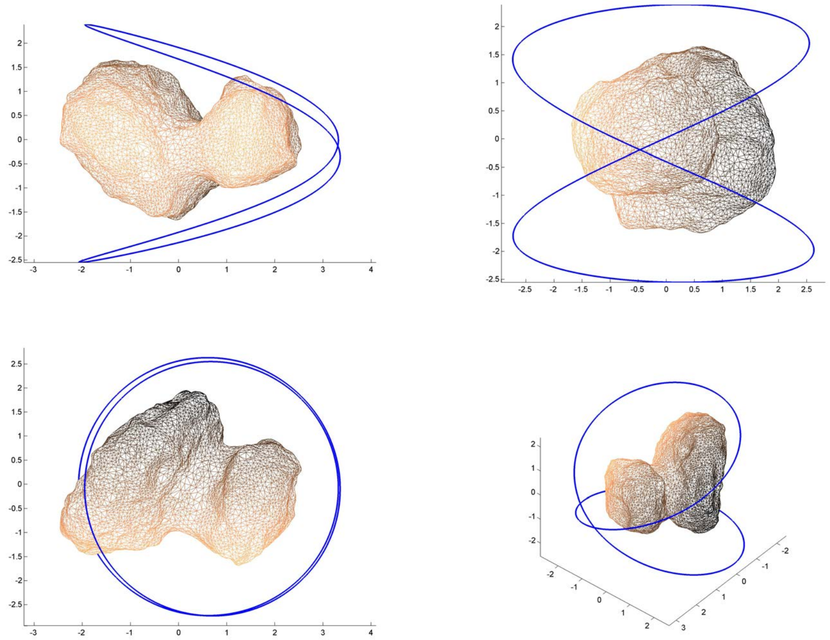

Figure 6.9. Inclined retrograde periodic orbit #3. Unstable.

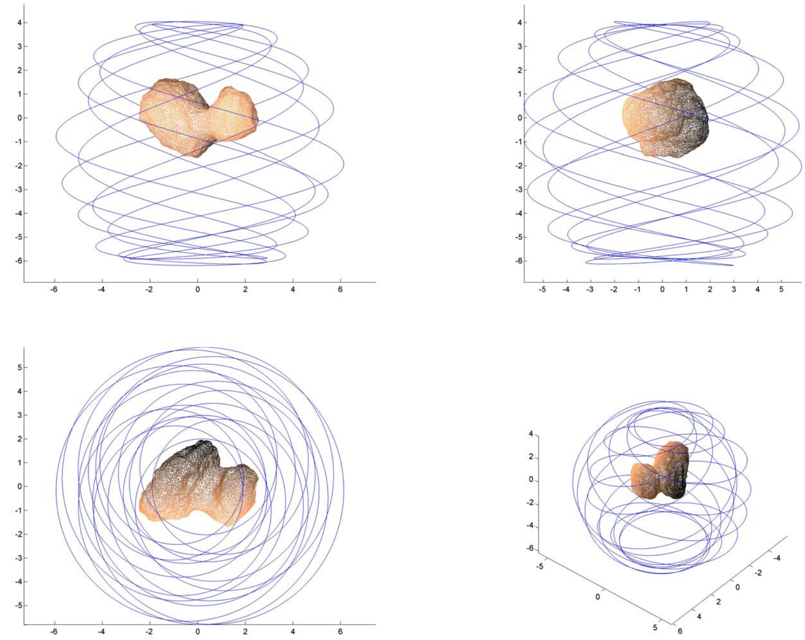

Figure 6.10. Inclined retrograde periodic orbit #4. Unstable

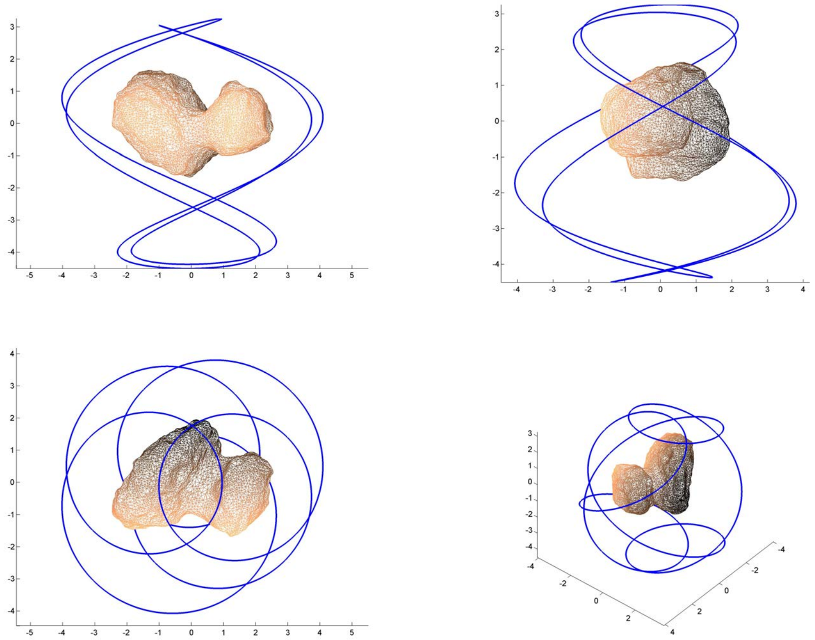

Figure 6.11. Inclined retrograde periodic orbit #5. Unstable

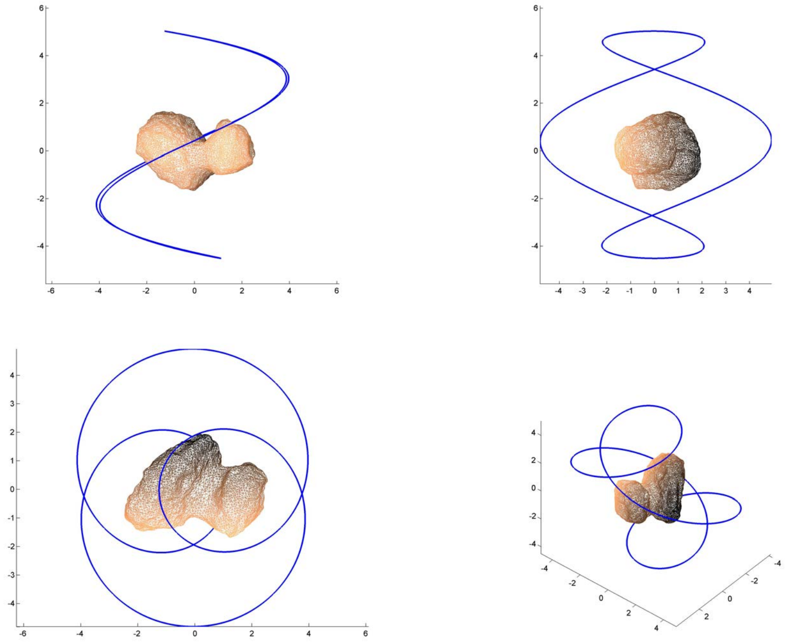

Figure 6.12. Inclined retrograde periodic orbit #6. Unstable

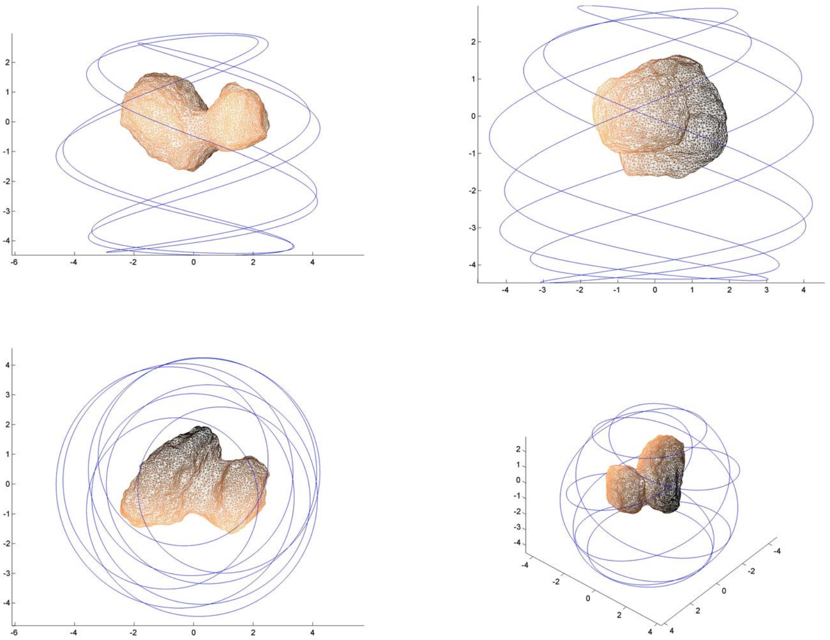

Figure 6.13. Inclined retrograde periodic orbit #7. Unstable

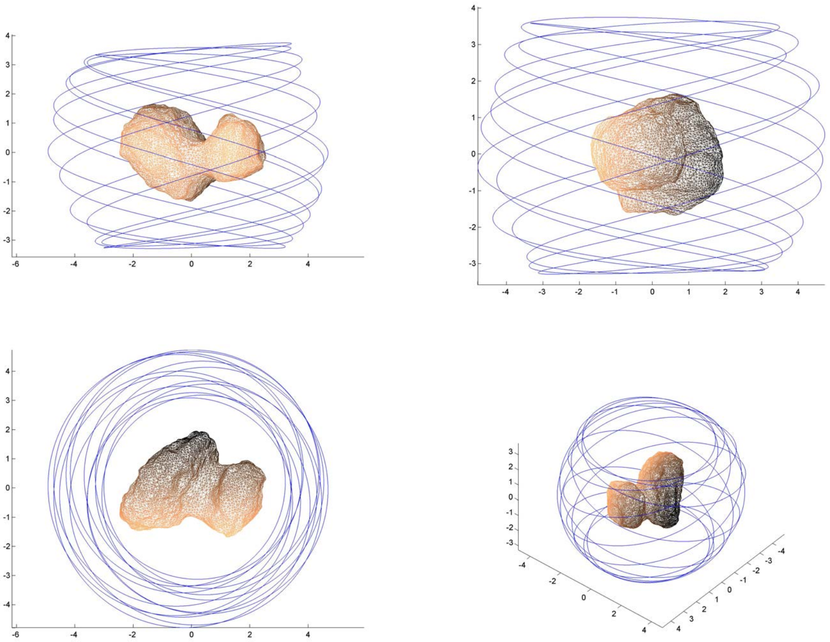

Figure 6.14. Inclined retrograde periodic orbit #8. Unstable

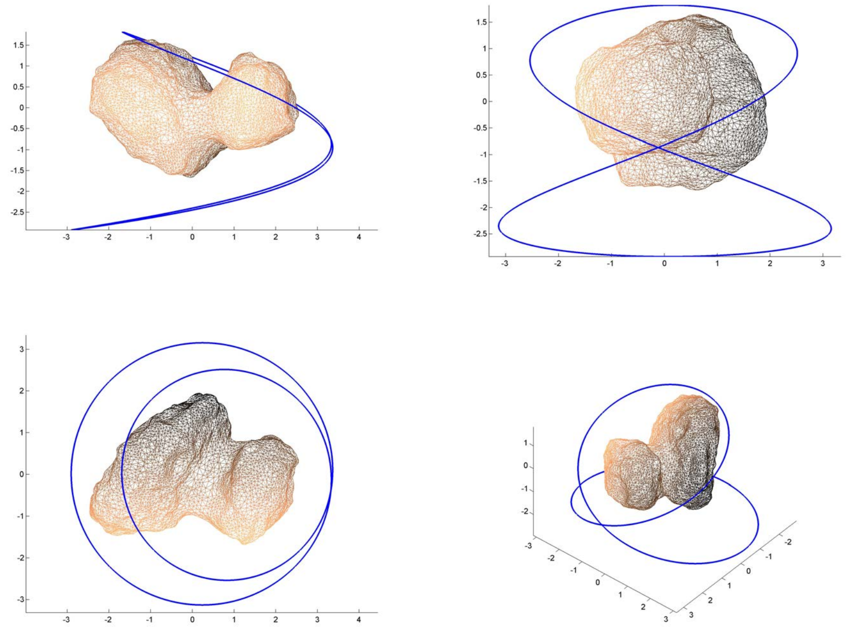

Figure 6.15. Inclined retrograde periodic orbit #9. Unstable

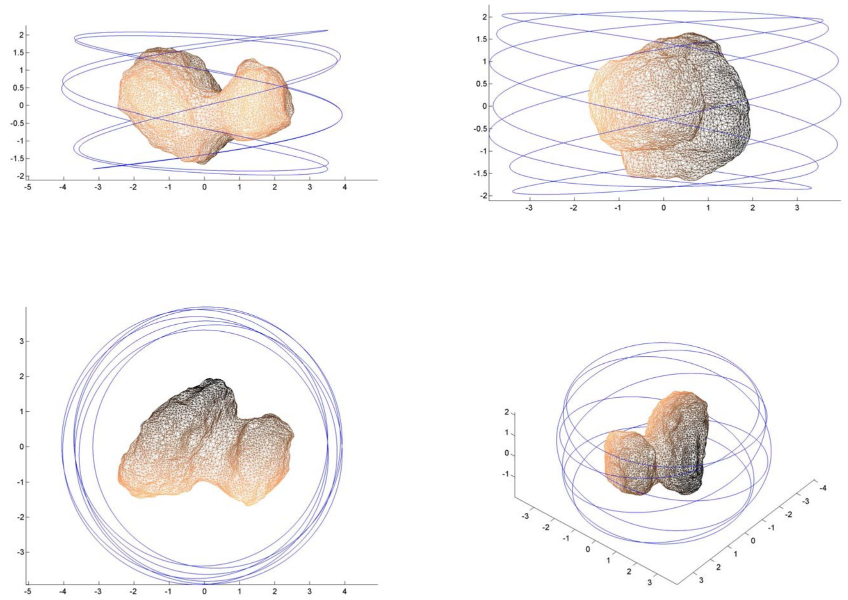

Figure 6.16. Inclined retrograde periodic orbit #10. Stable.

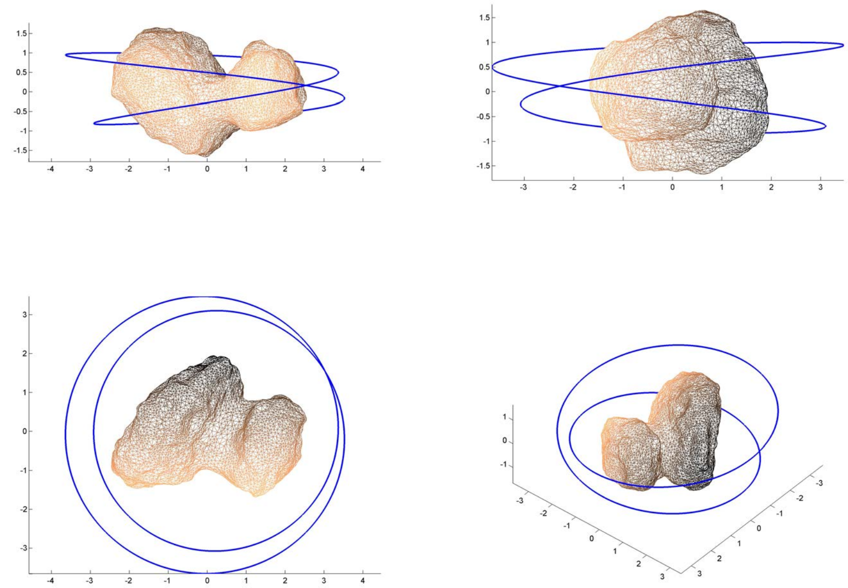

Figure 6.17. Inclined retrograde periodic orbit #11. Unstable.

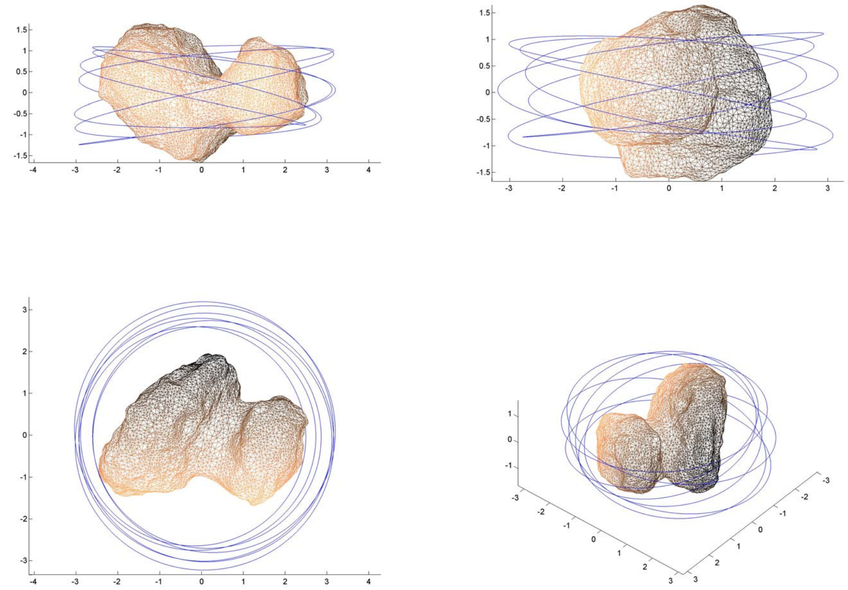

Figure 6.18. Inclined retrograde periodic orbit #12. Unstable

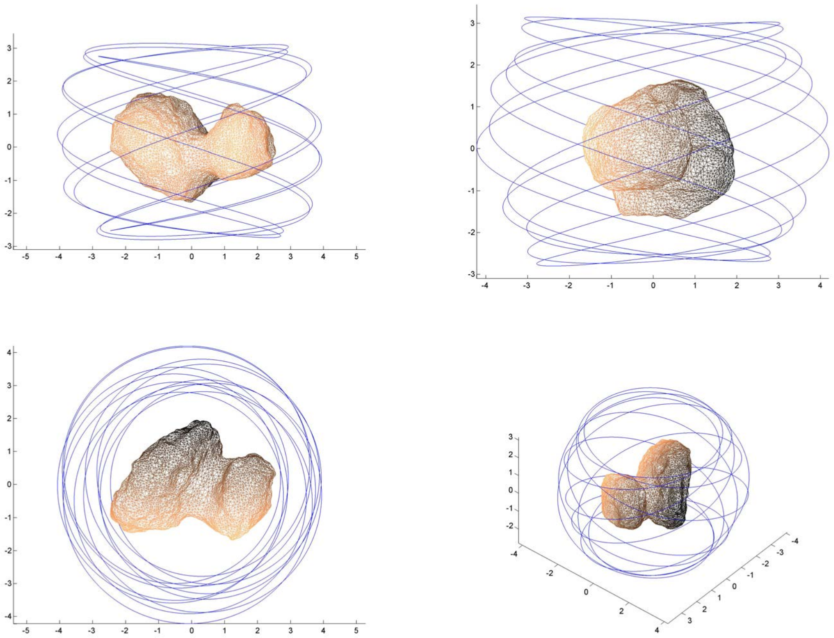

Figure 6.19. Inclined retrograde periodic orbit #13. Unstable

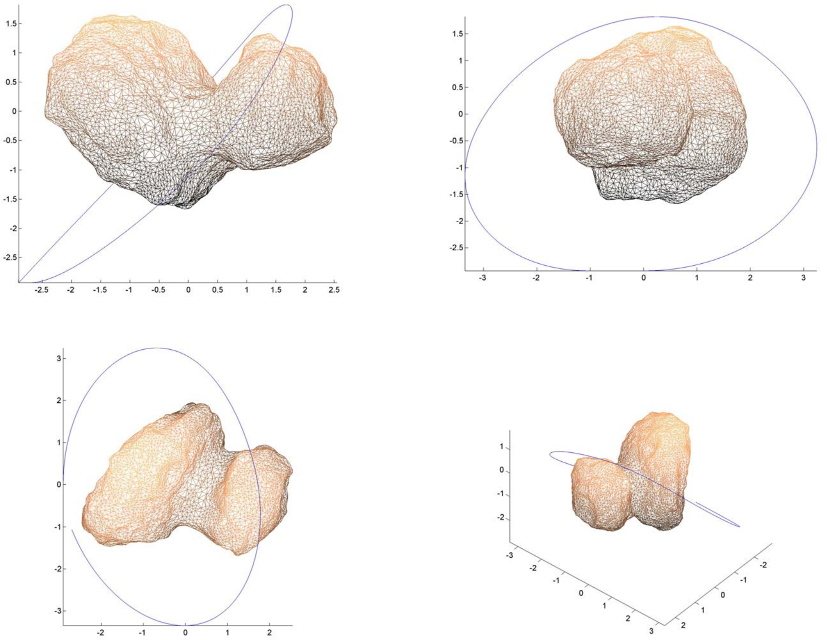

Figure 6.20. Inclined retrograde periodic orbit #9 in the inertial reference frame.

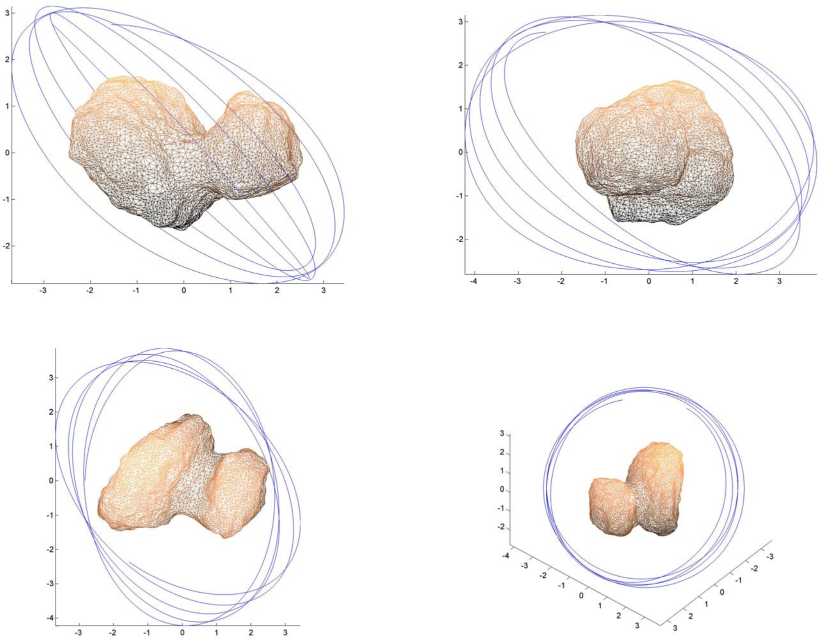

Figure 6.21. Inclined retrograde periodic orbit #13 in the inertial reference frame.

initial conditions is required in order to identily periodic orbits with the desired characteristics. Set forth for this task.

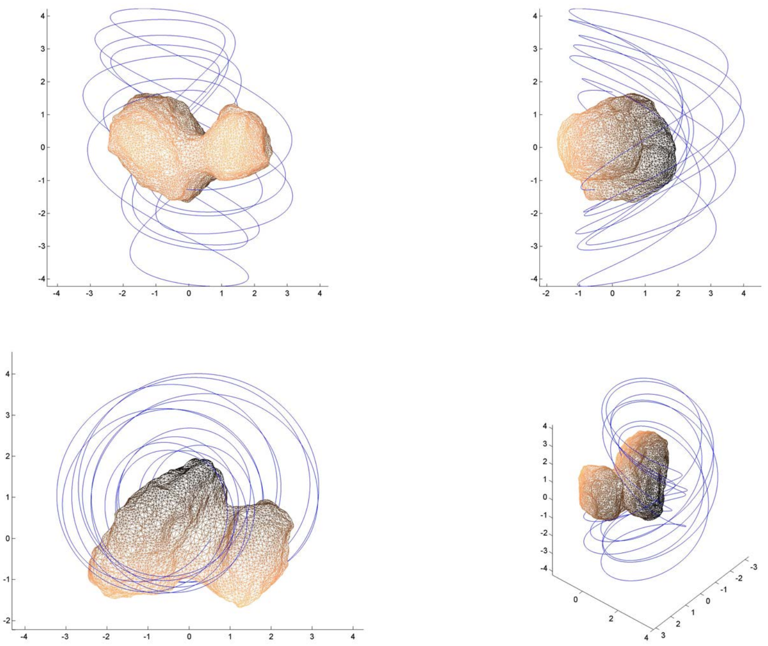

Figure 6.22. Almost periodic orbit 1.

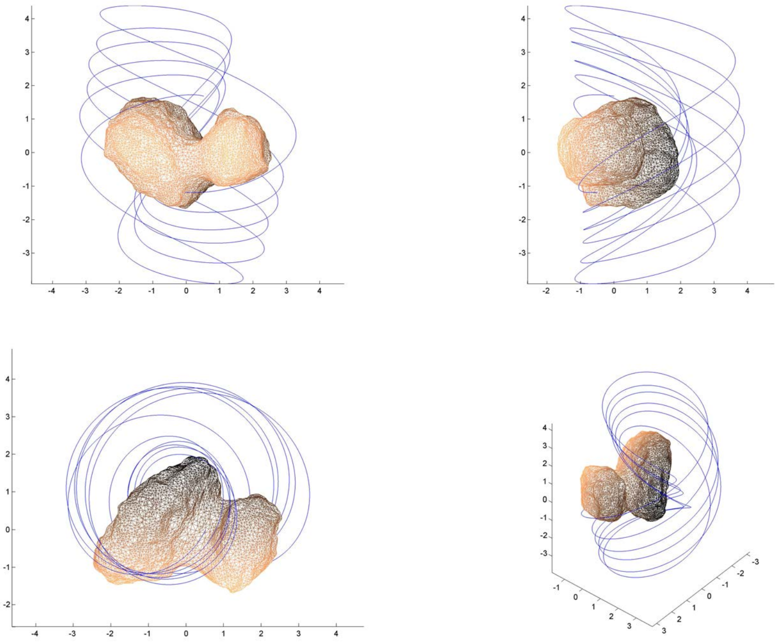

Figure 6.23. Almost periodic orbit 2.

Chapter 7

Orbital Engineering at 67P

The search for periodic orbits close to the comet nucleus has identified several orbits which cover the entire nucleus. However, a specific search for orbits passing extremely close to the surface in the region of the "neck" of the dumbell shape has yielded no results, although some orbits were found that are fairly close to being periodic. It is thought that a more extensive search will yield positive results, i.e., it will lead to finding some periodic orbits that pass through the neck as desired.

In the absence of such results, we can perform an investigation as to whether it might be possible to use the onboard thrusters to guide the Rosetta spacecraft on an artificial, or unnatural orbit which satisfies some criteria as to orbit height, orbital period, and coverage of specific nucleus regions. We will call such an orbit a *design orbit* and this Chapter will be devoted to establish some characteristics of this orbits and evaluate the requirements to implement it during a mission phase, possibly just before the foreseen final impact.

One basic question is to find the thrust profile that will make the design orbit possible. The answer to this is fairly straightforward. Another question is how much fuel is required per orbital period, for instance. Even here the answer is straightforward. As a first step, however, we need to *design* the orbit.

7.1 Artificial Orbit Design

One very basic possibility is to have Rosetta follow a *Keplerian orbit in the synodic system.* The equations of motion of this design orbit are quite simple and can be written as

$$\ddot{\boldsymbol{\rho}} = -\mu \frac{\boldsymbol{\rho}}{\rho^3}, \tag{7.1}$$

where $\boldsymbol{\rho}$ is the position vector of the spacecraft in the synodic reference system and $\mu = GM$ is the gravitational parameter. As a result, the Keplerian orbit will be fixed in this reference system, although it will not be in any inertial reference system. To make things a little more complicated, but satisfying a requirement of orbiting very close around the neck of the nucleus, we can impose that the focus of the Keplerian orbit be displaced from the center of mass of the comet by a vector $\mathbf{c}$. Then the equations of motion read

$$\ddot{\boldsymbol{\rho}} = -\mu \frac{\boldsymbol{\rho} - \boldsymbol{c}}{|\boldsymbol{\rho} - \boldsymbol{c}|^3}. \tag{7.2}$$

The natural acceleration is only the gravitational pull ∇U_{67P} of the cometary nucleus and the non-inertial forces $\mathbf{a}_{NI}$ acting in this reference—here we consider the nucleus as an isolated and inactive body—and in order to have a resultant equal to the Newtonian term on the RHS of equation (7.2) an additional acceleration $\mathbf{f}$ must be applied so that

$$-\mu\frac{\boldsymbol{\rho}-\boldsymbol{c}}{|\boldsymbol{\rho}-\boldsymbol{c}|^3}=\nabla U_{67P}+\mathbf{a}_{NI}+\boldsymbol{f}, \tag{7.3}$$

where the presence of inertial accelerations $\mathbf{a}_{NI}$ has been made explicit. The thrust will be analyzed later. Here we want to define an algorithm to generate the initial conditions for a design orbit of given characteristics, such as the orbital period and type of coverage of the nucleus for a hypothetical close observation mission phase.

The purpose is then to identify a set of free parameters that can be used to design the artificial orbit to satisfy the given requirements. The period of the orbit seems to be a reasonable requirement to be fixed according to the science requirements, or the operational requirements or engineering constraints of the mission. For a Keplerian orbit the orbital period T is in direct relation with the semimajor axis a throught Kepler's third law $\mu = n^2a^3$, where n is the mean motion, $n = 2\pi/T$. It becomes apparent that the gravitational parameter μ plays a fundamental role, since it acts as a scale parameter that defines the size of the orbit—in fact, it is sometimes known as the seventh orbital element. The gravitational parameter μ_{67P} of the nucleus can be used to design the orbit, but its value will hardly meet the design requirements of the artificial orbit. Thus other values can be used for μ and the difference, so to speak, will be payed by the thrust profile that will be necessarily implemented.

We can express the semimajor axis as a function of the orbital period and the gravitational parameter as

$$a=\left(\mu n^{-2}\right)^{1/3}=\left(\mu\frac{T^2}{4\pi^2}\right)^3. \tag{7.4}$$

For ease of treatment, let us stipulate to start the orbit from the pericenter. This fixes one of the orbital parameters, the time of perigee passage. We need to define the remaining initial conditions of position and velocity at this particular point of the Keplerian orbit. The well-known formulae for the radius vector r_p and the speed v_p at pericenter are

$$r_p=a\left(1-e\right), \tag{7.5}$$

$$r_a=a\left(1+e\right), \tag{7.6}$$

$$v_p=\sqrt{\frac{\mu}{a}\left(\frac{1+e}{1-e}\right)}. \tag{7.7}$$

where e is the eccentricity—another parameter to be reckoned with. It seems reasonable a this point to adopt T and r_p as free parameters, so that

$$a=\frac{r_p}{1-e} \tag{7.8}$$

and

$$\mu=\left(\frac{2\pi}{T}\right)^2\left(\frac{r_p}{1-e}\right)^3 \tag{7.9}$$

Therefore the initial conditions of the artificial orbit can be found in terms of the design parameters T, r_p and e. The initial distance from the focus being already set, only the speed is required, and this is given by

$$v_p=\sqrt{\left(1+e\right)\frac{\mu}{r_p}} \tag{7.10}$$

where the gravitational parameter has the expression (7.9).

As an alternative, the eccentricity can be replaced by the radius vector at apocenter r_a so that

$$v_p = \sqrt{\frac{2\mu}{r_a + r_p}\frac{r_a}{r_p}} \tag{7.11}$$

with the gravitational parameter now expressed as

$$\mu = \left(\frac{2\pi}{T}\right)^2 \left(\frac{r_a + r_p}{2}\right)^3 . \tag{7.12}$$

To complete the analysis we now need to find the initial conditions in $\mathbb{R}^3$ to find the oriantation of the orbit in space. In particular, we need expressions for the components of the velocity, given that we already know its absolute value given by the speed (7.10) or (7.11). This can be accomplished by consdering the expression for the specific angular momementum $\mathbf{h}$ given by

$$\mathbf{h} = h \sin i \sin \Omega \, \mathbf{i} - h \sin i \cos \Omega \, \mathbf{j} + h \cos i \, \mathbf{k}, \tag{7.13}$$

with the usual notation for the inclination i and the longitude of the ascending node Ω. The longitude of the node can be considered as free perameter, since they can be set by the designers on the basis of geometric considerations. Since i and the initial position vector $\mathbf{r}_p$ are not independent anymore, we can choose one of them as free parameter. Both parameters have been used as free parameters while searhcing for the sought designed orbits. The relation between these two parameters is

$$i = \cos^{-1}\left(\mathbf{k} \cdot \hat{\mathbf{r}}_p\right). \tag{7.14}$$

At this point, we set that the starting position satisfies

$$y = 0 \tag{7.15}$$

$$v_z = 0. \tag{7.16}$$

We thus know that $h = v_p r_p$. We conclude by finding the cartesian components of the starting velocity. Writing the definition $\mathbf{h} = \mathbf{r} \times \mathbf{v}$ of the specific angular momentum componentwise, we have

$$y v_z - z v_y = h \sin i \sin \Omega, \tag{7.17}$$

$$z v_x - x v_z = -h \sin i \cos \Omega, \tag{7.18}$$

$$x v_y - y v_x = h \cos i. \tag{7.19}$$

From the first and the second of these equations, given that at the initial position $y = 0$ and $v_z = 0$, we find the components along $\mathbf{i}$ and $\mathbf{j}$ of the initial velocity to be

$$v_y = -\frac{v_p r_p}{z} \sin i \sin \Omega, \tag{7.20}$$

$$v_x = -\frac{v_p r_p}{z} \sin i \cos \Omega. \tag{7.21}$$

where we have used the fact that the specific angular momentum h is already known to be $h = v_p r_p$. Note that the initial velocity components of the design orbit have thus been found in terms of the free parameters r_p, r_a, T, Ω, with possibly radial distance at apocenter r_a exchanged with the eccentricity e, or the direction of vector $\mathbf{r}_p$ exchanged with i. The sixth free parameter has actually been used in setting the initial conditions at pericenter.

Another set of parameters may also be used in case the location of the pericenter is defined by the coordinates x_p and y_p, rather than by r_p and the inclination i. The set of free parameters is x_p, y_p, r_a, T, Ω, where now the velocity components at pericenter are given by

$$v_y = -\frac{v_p y_p}{z} \sin\Omega, \tag{7.22}$$

$$v_x = -\frac{v_p y_p}{z} \cos\Omega. \tag{7.23}$$

The sixth free parameter has actually been used in setting the initial conditions at pericenter. Also note that the focus of the Keplerian orbit is at $\mathbf{c}$, which may differ from the nucleus's center of mass.

We conclude this Section by recalling that the preceding analysis has been done in the synodic reference system and the Two-Body formulae have been used as required by simple geometric considerations in order to have the Keplerian orbit fit the constraints dictated by the shape of the nucleus of 67P and in particular to satisfy the goal of orbiting low in the neck region of the body. No reference has been made or implied as to the actual dynamics of the orbit, which will be investigated in the next Section.

7.2 Equations of Motion of the Artificial Orbit and Thrust Profile

The equations of motion (7.2) have been written in the synodic system since the orbit design was carried out in that reference system. To find the actual thrust to be applied in order to meet the requirements, the equations of motion must be written in an inertial reference system. The inertial equations of motion are then

$$\ddot{\mathbf{r}} = \nabla U_{67P} + \mathbf{f} \tag{7.24}$$

where $\ddot{\mathbf{r}}$ is the vector indicating inertial acceleration and $\mathbf{f}$ the inertial thrust acceleration.

Rewrite then the equations of motion in the synodic reference frame as

$$\ddot{\boldsymbol{\rho}} = \nabla U_{67P} - \boldsymbol{\omega} \times (\boldsymbol{\omega} \times \boldsymbol{\rho}) - 2\boldsymbol{\omega} \times \dot{\boldsymbol{\rho}} + \mathbf{f}, \tag{7.25}$$

where the form of the non-inertial accelrations has been made explicit (the Euler acceleration is not present on account of the assumed uniformity of the rotational motion). Since (7.2) holds, we find that the active force $\boldsymbol{f}$, or thrust, in the synodic system needed to realize such orbit is

$$\boldsymbol{f} = -\mu \frac{\boldsymbol{\rho} - \mathbf{c}}{|\boldsymbol{\rho} - \mathbf{c}|^3} - \nabla U_{67P} + \boldsymbol{\omega} \times (\boldsymbol{\omega} \times \boldsymbol{\rho}) + 2\boldsymbol{\omega} \times \dot{\boldsymbol{\rho}}. \tag{7.26}$$

To find the components of the thrust $\boldsymbol{f}$ in the inertial system we apply the rotation operator R_z about the z-axis

$$\mathsf{R}_z(\omega t) = \begin{pmatrix} \cos\omega t & -\sin\omega t & 0 \\ \sin\omega t & \cos\omega t & 0 \\ 0 & 0 & 1 \end{pmatrix}, \tag{7.27}$$

where t is the time passed from the beginning of the integration and ω is the absolute value of the angular velocity of the cometary nucleus.

Thrust components are conventionally expressed in the orbital refrence system, also known as the radial-transverse-normal (RTN) reference system. This is defined, as the name implies, by axes along the three unit vectors $\hat{\mathbf{r}}, \hat{\mathbf{t}}, \hat{\mathbf{n}}$ which are defined in terms of the dynamical state components as

$$\hat{\mathbf{r}} = \frac{\mathbf{r}}{r}, \tag{7.28}$$

$$\hat{\mathbf{t}} = \hat{\mathbf{n}} \times \hat{\mathbf{r}}, \tag{7.29}$$

$$\hat{\mathbf{n}} = \frac{\mathbf{r} \times \mathbf{v}}{|\mathbf{r} \times \mathbf{v}|}. \tag{7.30}$$

The RTN reference system can be taken with the origin at the spacecraft, or coincident with the origin of the inertial frame. The RTN frame is most useful for Earth-, or in this case, comet-observing missions, since its first axis is in the radial direction to the center of mass. As far as the thrust implementation is concerned, the RTM frame acts as an intermediary reference frame to the satellite-fixed axes, where the thrusters are fixed.

7.3 Fuel Consumption

Once the thrust profile for a circular Keplerian orbit around the neck of the comet has been designed in the synodical reference frame, we naturally come to ask if, considered as a function of the orbital period T, a minimum exists, i.e., if we can find a period T_{opt} that minimizes the "orbit maintenance" ΔV required over a period of the orbit (in the synodical frame), where

$$\Delta V = \int_0^T |\mathbf{f}(t)| \, dt. \tag{7.31}$$

In a sense, this is equivalent to asking what the associated fictitious mass M is in equation (7.9) that generates the Newtonian field closest to the actual field ∇U_{67P} generated by 67P in the corotating frame along the artificial, or engineered, orbit.

For very large T, the thrust profile will lead to huge ΔV, since the spacecraft will barely be moving in the corotating frame, and will thus have to oppose the full gravitational attraction of the body to "almost" a stand still. Furthermore, appropriately large inertial forces will need to be generated as part of the thrust.

At the opposite end, when the period T becomes very short, then what is needed is the equivalent of a large gravitational parameter to make the period as short as needed, in contrast to the much longer period that would naturally be associated with the mass of the nucleus. The actual fictitious accelerations will not need to be very large, since the inertial angle over which the orbital plane precesses is very small.

These considerations seem to provide a physical basis for expecting that a minimum ΔV actually exists, which can be verified by computing the fuel consumption over an appropriate range of values of the design orbital period. Several periods were thus assumed and orbits integrated without changing any other design parameters.

By numerically integrating the equation of motion we obtain the thrust profile needed to maintain the spacecraft in the design orbit. In order to get the fuel mass consumption as well, we can at the same time integrate the variable mass equation Prussing and Conway (2013)

$$\frac{dm}{dt} = -\frac{m}{I_{sp} g_0} |\mathbf{f}(t)| \tag{7.32}$$

over the required time period, starting with the initial wet mass $m = m_0$ of the spacecraft. In this equation I_{sp} is the specific impulse of the thruster and g_0 is a normalizing factor equal to the gravitational acceleration at the Earth's surface. The product $I_{sp} g_0$ is equal to the exhaust velocity from the thruster, which is here assumed to be of the constant specific impulse type.

The variable mass equation can easily be solved and yields (Prussing and Conway, 2013) the fuel mass consumption Δm_f over a period T equal to

$$\frac{\Delta m_f}{m_0} = 1 - \exp\left(-\frac{1}{I_{sp} g_0} \int_0^T |\mathbf{f}(t)|\, dt\right). \tag{7.33}$$

From (Stramaccioni, 2004) we know that the specific impulse of the Rosetta thrusters is $I_{sp} = 292$ s. The Rosetta dry mass is $m_0 = 1335$ kg, which includes the mass $m_{Phil} = 108$ kg of the Philae lander. Originally the stored fuel mass was $m_{fuel} = 1719$ kg, capable of producing a total $\Delta V = 2300$ m/s, with an implementation capability precision of the order of 1 mm/s. Due to our lack of information about the real current mass of the Rosetta spacecraft, since a large fraction of the fuel has probably been used, we assume that the remaining propellant is about one fourth of its initial mass, or $m_{fuel} = 430$ kg, equivalent to assuming a current total wet mass $m_0 = 1657$ kg.

We note that this is not sufficient to actually perform an artificial orbit around the celestial body. Optimal control and the Ricci formula should be implemented to obtain that result. However, this is sufficient to estimate the order of magnitude of fuel necessary for the spacecraft to perform an artificial orbit.

7.4 Results

The first artificial orbits found were integrated while keeping the force center $\mathbf{c}$ at the center of mass of 67P. An example is shown in Figure 7.1. This specific orbit was obtained for a design period T of $70,000$ s. The computed total ΔV needed for the manouver is 2.482 m/s per orbital period. The thrust profile in the RTN reference system required to maintain this orbit is shown in figure 7.2. It can be seen that the thrust amplitude excursion differes for the three components. It can also be appreciated that the thrust profile is not periodic. This is a consequence of the fact that the thrust is an inertial acceleration and the fact that the orbit in the synodic system has been forced to be Keplerian does not imply that the thrust is inertially periodic. Since the RTN decomposition shows the same inertial components resolved along different axes, this character is also seen in the plots of Figure 7.1. This is in line with the fact that the trajectory is periodic in the synodic frame, but not in the inertial frame.

The center of the Keplerian force field was then moved from the center of mass of 67P, i.e., the origin of the corotating reference system, to a point $\mathbf{c}$ in the middle of the neck of the comet with coordinates $\mathbf{c} = (0.6, 0.0, -0.2)$ km. Figure 7.3 represents an eccentric periodic orbit resulting from an integration characterized by a period $T = 90,000$ s. To accomplish this manoeuver, $\Delta V = 4.18$ m/s per period is required. Figure 7.4 shows the thrust profile needed to realize such orbit.

To investigate the existence of a minimum ΔV as a function of the design orbital period, different values of T in the rangee from $10,000$ s to $100,000$ s were used to integrate the same geometric orbit. An example is shown in Figure 7.5 and Table 7.1. We see that a minimum ΔV does exist corresponding to a period T of approximately $34,000$ s.

Artificial orbits hovering in the deep valley of the comet were also computed. With the center of attraction $\mathbf{c}$ of the Keplerian orbit moved outside the body, orbits such as the one shown in Figure 7.6 were obtained, for which $\mathbf{c} = (0.5, 0.0, 0.5)$ km. Figure 7.7 shows the acceleration required to realize this artificial orbit, expressed as previously in RTN reference frame components. The period of this specific orbit is $T = 70,000$ s, with an associated ΔV of 0.6m/s needed per orbit.

We point out that the choice of the period of the artificial orbit is a fundamental parameter, and must be chosen wisely. Given a Keplerian orbit, it is the only remaining free parameter.

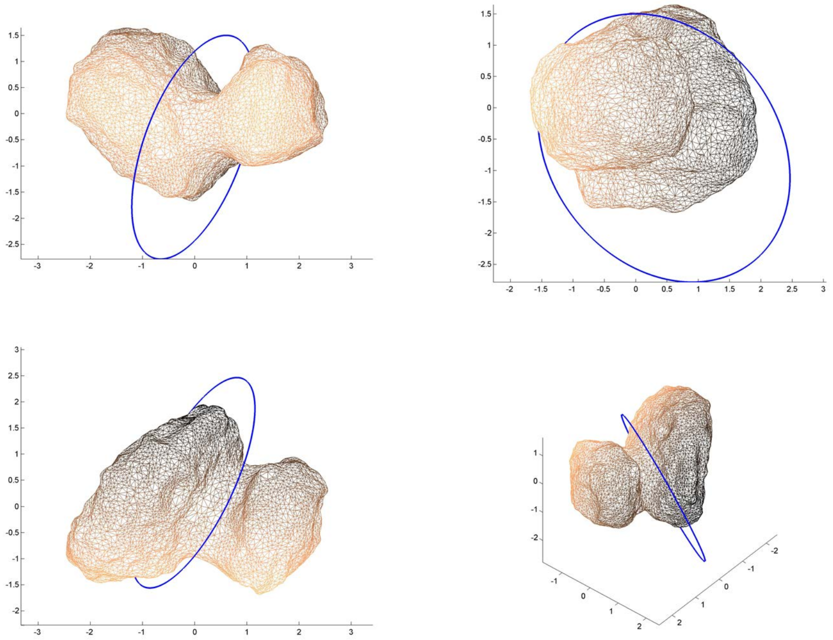

Figure 7.1. Example of an artificial Keplerian orbit in the corotating reference frame. From left to right and top to bottom they are seen from 1) the negative y axis, 2) the positive x axis, 3) the positive z axis, 4) azimuth 130°and elevation 40°.

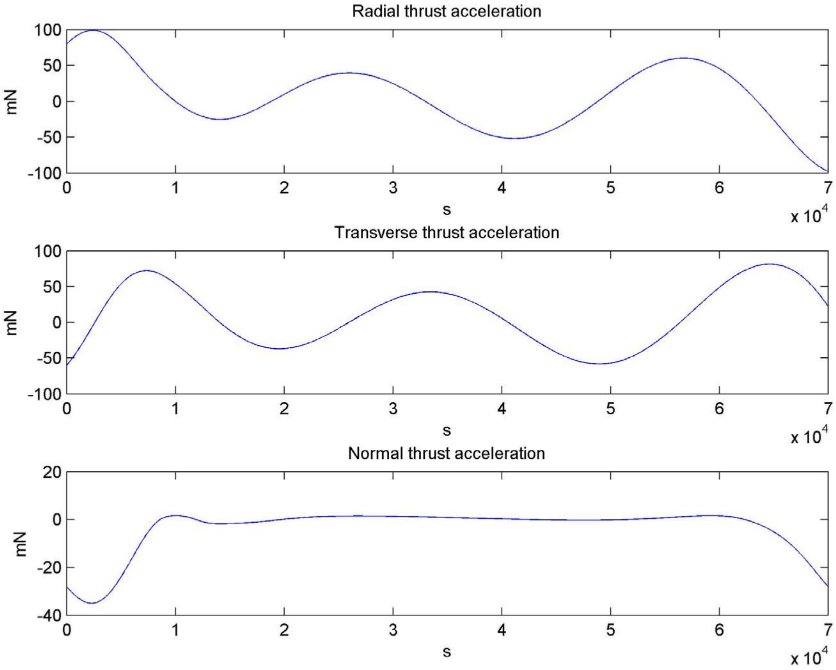

Figure 7.2. Thrust profile in the RTN reference frame for orbit in Figure 7.1

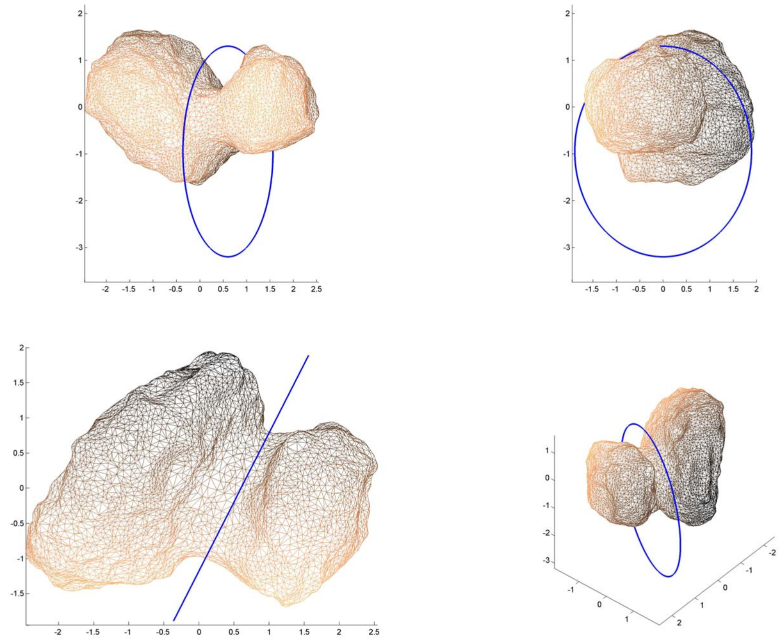

Figure 7.3. Example of an artificial Keplerian orbit in the corotating reference frame, with center of mass **c** inside the cometary neck. From left to right and top to bottom they are seen from 1) the negative y axis, 2) the positive x axis, 3) the positive z axis, 4) azimuth 130°and elevation 40°.

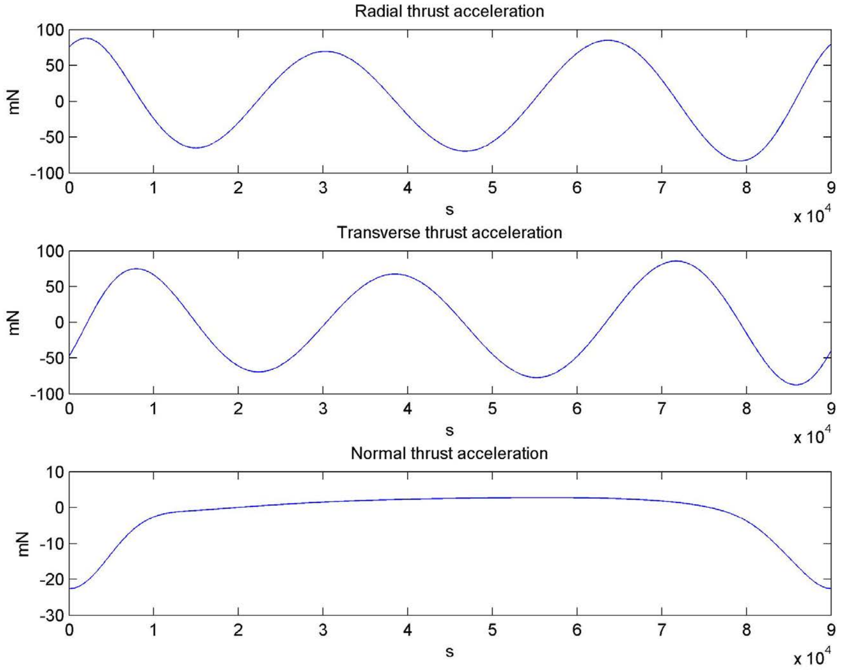

Figure 7.4. Thrust profile needed to follow artificial orbit centered at the comet neck depicted in Figure 7.3

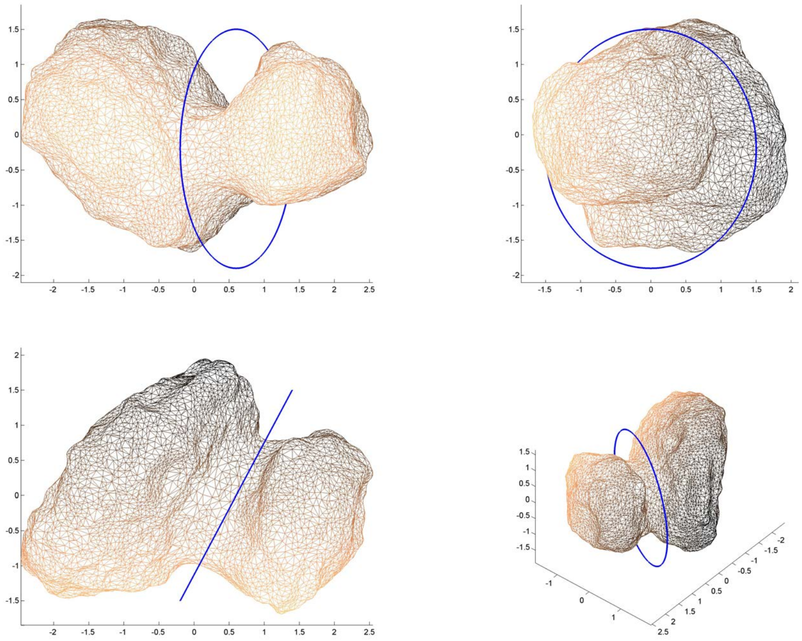

Figure 7.5. Example of artificial circular Keplerian orbit in the corotating reference frame, with center of mass $\mathbf{c} = (0.6, 0.0, -0.2)$ km inside the cometary neck. Semimajor axis $a = 1.7$ km. From left to right and top to bottom they are seen from 1) the negative y axis, 2) the positive x axis, 3) the positive z axis, 4) azimuth 130°and elevation 40°.

Period T (s)	Fictitious GM ($\mathrm{m}^3\mathrm{s}^{-2}$)	ΔV (m/s)
25000	1241.32	2.651
26000	1147.67	2.636
27000	1064.23	2.623
28000	989.57	2.613
29000	922.50	2.605
30000	862.03	2.599
31000	807.31	2.595
32000	757.64	2.592
33000	712.42	2.590
34000	671.13	2.590
35000	633.33	2.590
36000	598.63	2.592
37000	566.71	2.595
38000	537.27	2.598
39000	510.07	2.603
40000	484.89	2.608

Table 7.1. ΔV per orbit required to maintain the Keplerian circular orbit shown in Figure 7.5 for different design orbital periods T. Also shown are the correspong values of the fictitious gravitational parameter.

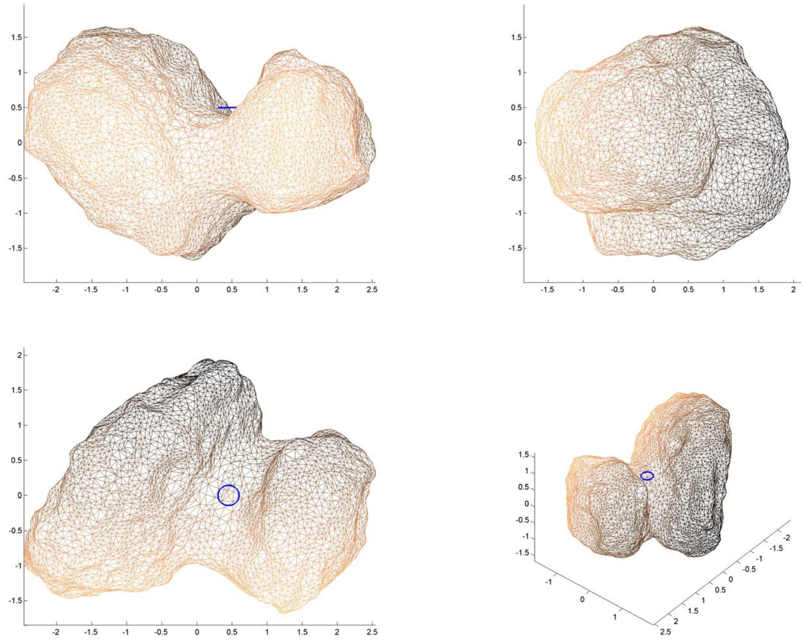

Figure 7.6. Example of an artificial Keplerian orbit in the corotating reference frame hovering the neck of the comet. From left to right and top to bottom they are seen from 1) the negative y axis, 2) the positive x axis, 3) the positive z axis, 4) azimuth 130°and elevation 40°.

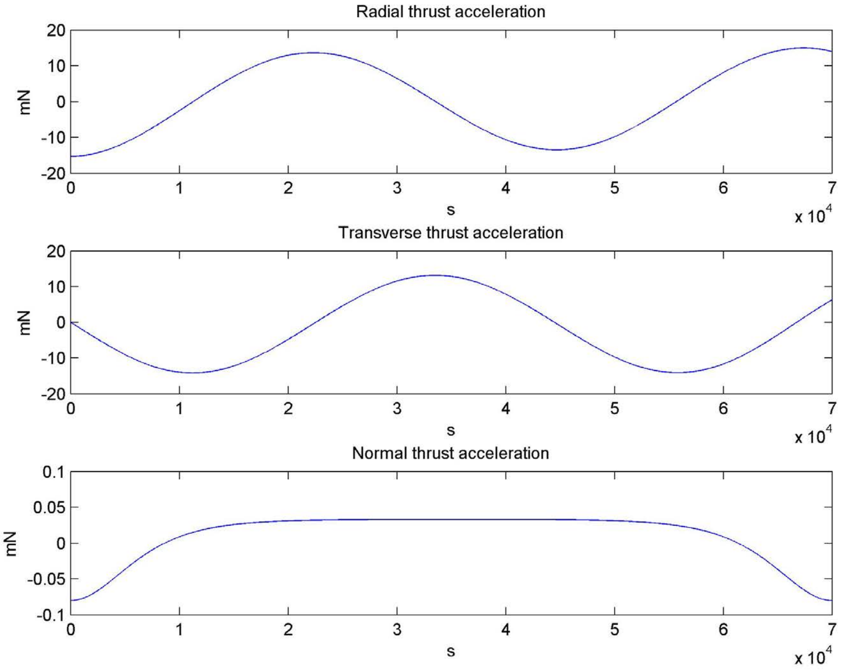

Figure 7.7. Thrust profile needed to follow artificial orbit hovering over the neck of the comet's nucleus depicted in Figure 7.6

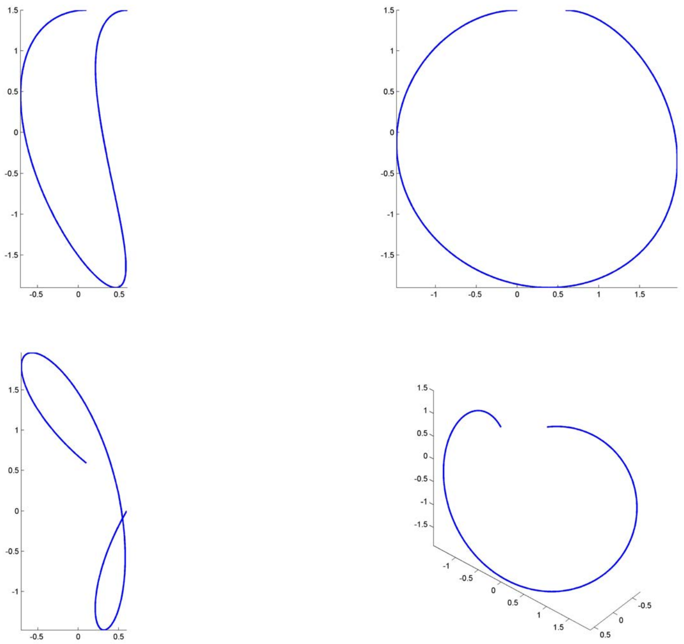

Figure 7.8. Example of an artificial Keplerian orbit in the inertial reference frame of period $T = 10^4$ s. From left to right and top to bottom they are seen from 1) the negative y axis, 2) the positive x axis, 3) the positive z axis, 4) azimuth 130°and elevation 40°.

The total ΔV and, more importantly, the maximum acceleration the thrusters need to supply depend entirely on it. In fact, if we wanted to orbit around the comet at a much faster rate, the thrusters would have to supply an enormous amount of acceleration, which could not reach by design.

Representations of the inertial trajectories of the same design orbits that are travelled with different periods are shown in Figures 7.8 and 7.9, both of which refer to the same corotating trajectory, shown in Figure 7.5. The greater number of loops the spacecraft must perform in the inertial frame for the orbit with larger period, pictured in Figure 7.9, are an indication of the inertial accelerations the spacecraft has to supply with its thrusters to maintain the design orbit. The total ΔV per orbit needed was computed as 3.438 m/s for a period of $T = 10^5$ s. When the period is small, however, as in Figure 7.8 where $T = 10^4$ s, $\Delta V = 3.901$ m/s per orbit, which is comparable to the one computed for the long period orbit, since the spacecraft will have to supply the thrust needed for the centripetal acceleration.

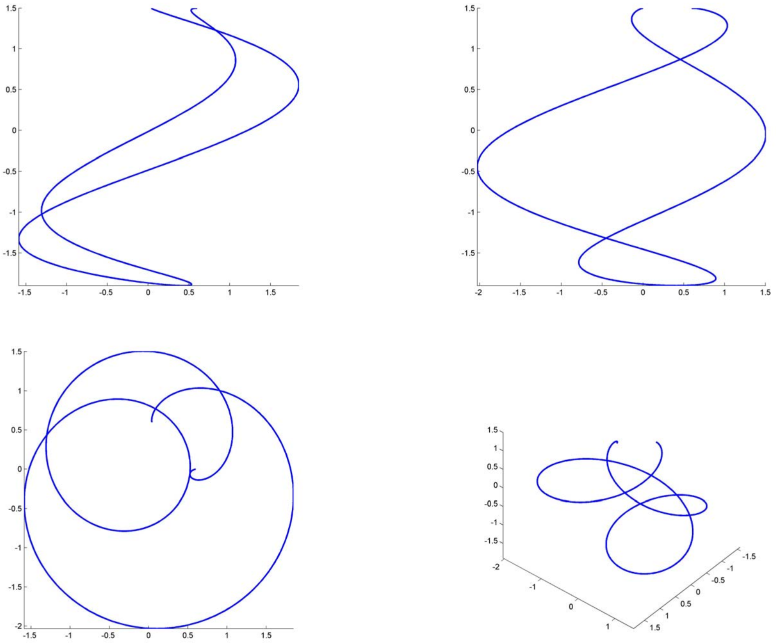

Figure 7.9. Example of an artificial Keplerian orbit in the inertial reference frame of period $T = 10^5$ s. From left to right and top to bottom they are seen from 1) the negative y axis, 2) the positive x axis, 3) the positive z axis, 4) azimuth 130°and elevation 40°.

Chapter 8

Conclusions and Future Work

The reasearch carried out in this thesis work has focused on the modeling of orbits in the near space of comet 67P/Churyumov-Gerasimenko. Due to the extremely unusual shape of the nucleus of this comet, as revealed by the images collected during the ongoing ESA mission Rosetta, the task of simulating the dynamics of a spacecraft orbiting close to the comet presents unusual problems in terms of the computational of its gravitational field. The first step of this work thererefore addressed the problem of modeling the gravitational potential of an irregular body in the near regionds in a numerically efficient manner. This was done under the strict assumption of constant mass density of the body. After a review of the only available method to carry out the computation of the gravitational accelerations and the gravity gradient necessary for arbital analysis,—a method originally due to Robert Werner as far as applications to orbital dynamics are concerned— two alternative methods of series expansions were investigated. The first one is an expansion in Cartesian coordinates based on the use of inertial integrals, the second is the very well-known method of expansion in Spherical Harmonics. The novelty of the present analysis is that both methods were extended to the regions near the surface, or within what is usually known as the Brillouin sphere, within which the known series expansions do not converge. A new terminology has been introduced in this regard—the Hotine sphere—so named to honor a researcher among the pioneers of the analysis of the convergence of series expansions of the potential near the surface of extended bodies. Keeping for simplicity the Hotine sphere devoid of matter and thus completely outside the body, to which it may only be tangent, we have developed a series expansion which does converge within such sphere. The expansion introduced a generalization to *inertial functions* of MacMillan's inertial integrals. This was possible only after a careful analysis of the 24 subregions into which the body must be sectioned in order to ensure convergence of the series. The method appears to be new and is presented here for the first time. The advantage of the formulation in inertial functions or inertial integrals is twofold. In the first place the coefficients of the series need only be computed once, and secondly the formulation is entirely in Cartesian coordinates and thus is intrinsically regular and presents no singularities. A new method has also been introduced to compute these coefficients, be they inertial intergals or inertial functions, based on the application of knwon theorems of vector analysis through which the computations are reduced to simple functions of the coordinates of the vertices of the polyhedron model of the extended body and the associated connectivity matrix.

The expansion of the gravitational potential has also been carried out in terms of Spherical Harmonics, the novelty in this case being that a method has been found which allows to express the harmonic coefficients for both the external and the internal field, respectively related to the Brillouin and the Hotine spheres, as linear combinations of the inertial integrals or the inertial functions. This result is actually known in the case of the external potential, but appears here for the first time for the internal potential inside the Hotine sphere.

The new methods, although completely developed from the analytical point of view, were not fully tested for numerical applications—something which will be reserved for a future phase of research. Rather, the well-tested Werner's method was used in the interest of completing the research within a reasonable time frame.

The core of the research consisted, in fact, in exploring the orbital space near comet 67P. A methodology has been described and implemented in a software code to find periodic orbits using standard techniques, except for the fact that in the case of an extended irregular body no appeal can be made to the Mirror Theorem, which usually simplifies the search by limiting the the temporal extent to half the period. The disadvantage of having to use the monodromy matrix in the search strategy implies that the inversion of near-singular matrices has to be carried out. The device used is the algorithm of singular value decomposition, which is extremely powerful but must be handled with much care in terms of the threshhold to neglect singular values in order for the search to be successful. This was done by trial and error until convergence of the search algorithm was reached.

Periodic orbits were identified for initial conditions related to both near-equatorial and inclined orbits up to near polar. The force field adopted was a simplified one, which only consisted of the gravitational attaction of the nucleus. Although admittedly incomplete, this force field is adequate for the study of orbits of natural or artificial bodies in the near regions around the nucleus, where other gravitational disturbing forces, as well as solar radiation pressure, are negligible, at least for relatively high-mass test particles like a spacecraft or large ejecta from the nucleus. The search for periodic orbits was carried out by using initial conditions from various small grids of approximately 500 starting dynamical states each, with position vectors in several locations of the xz-plane. The grids were chosen manually after a brief evaluation of test integrations.

A few hundred periodic orbits were found, many of which very similar to each other. Just a handful of them were found to be stable, the majority of them being near equatorial. Some of these periodic orbits seem well suited to exploration of the nucleus from close distance. Periodic orbits passing throught the low neck region, or valley, of 67P were not found, even though the search was conducted as best allowed by manual trial and error. The best results in this context were a few orbits in the high neck region, which however did not reach convergence, although they were apparently close to being periodic.

Equatorial periodic orbits were far more easy to find than inclined periodic orbits. Due to the rotational motion of the comet, in fact, finding suitable initial conditions leading to periodic inclined orbits was found to be difficult, especially in close proximity of the surface, where crashing on the nucleus is the norm.

Finally, although periodic orbits were not found, a different strategy was pursued and orbits were engineered to satify the requirement of orbiting low in the comet's valley. This was accomplished by a very straightforward planning of Keplerian orbits in the corotating system of the nucleus. These artifical orbits can only be realized with the use of continuous thrusting.

The thrust profile of these orbits was computed in the RTN reference frame and an estimate of the required ΔV per orbit was computed. Since the period T of the Keplerian orbit was set as a free parameter, we were also able to find a period T that minimized the required ΔV to continuously follow the same geometric artificial orbit.

The research carried out has touched several different aspects of the dynamical modeling and behavior of test particles orbiting in close proximity of a very irregular, homogeneous body. Much, however, remains to be investigated. In particular, the new algorithm introduced in this work need to be implemented numerically, and fully tested. Their efficiency must then be compared to that of the Werner method. It is expected that, although several Hotine sphere expansions will be needed to cover the region inside the smallest Brillouin sphere of the body, the fact that the greatest comoputational effort is relegated to the preprocessing stage, in which the inertial functions are computed, this algorithm will be faster than the Werner method.

As for the search for periodic orbit, a parallelization of the code will be necessary in order to extend the search to a wider set of initial conditions. The parallelization will also make it possible to use finer meshes to describe the body. Further research is also needed to correctly reduce (Werner) the extremely detailed meshes that are generated by image analysis, maintaining important physical characteristics such as the center of mass and the direction of the principal axes of inertia, but not limited to these. This has important implications as to the capabilities to represents the actual fields using a minimum set of paramenters.

The research for the artificial orbits, that was motivated by the idea that a much closer inspection of the surface might be a desirable science objective in the final phases of the mission, can be extended in order to find implementation strategies for sequentially hopping from one orbit type to another. Optimal control theory will be useful in achieving this result. Minimization of the ΔV per orbit required to maintain the design orbit, and optimizing the geometry of the design orbit is another further research goal reserved for the future.

We may conclude with the wild idea that the currently planned final impact of Rosetta on the surface of the comet might be preceded by a close exploration phase—if the risk of flying deep inside the valley of 67P would be deemed tolerable—in which the novel and challenging orbital acrobatics just proposed could be implemented.

Bibliography

M Abramowitz and I. A. Stegun. *Handbook of Mathematical Functions.* Dover, 1965.

R. H. Battin. *An introduction to the mathematics and methods of Astrodynamics.* AIAA Education Series, 1989.

E. Betti. *Teorica delle Forze Newtoniane.* Nistri, Pisa, 1879.

R. Broucke and D. Boggs. Periodic orbits in the planar general three-body problem. *Celestial Mechanics*, 11:13–38, 1975.

A. Colombi, A. N. Hirani, and B. F. Villac. Adaptive geopotential force representation for fast trajectory propagation near small bodies. *Journal of Guidance, Control, and Dynamics*, 31: 1041–1051, 2008.

J.M.A. Danby. *Fundamentals of Celestial Mechanics, 2nd Rev. & Enl. Ed.* Willmann-Bell, 1976.

H. B. Dwight. *Tables of Integrals and Other Mathematical Data.* MacMillan, 1989.

E. Fantino and S. Casotto. Methods of harmonic synthesis for global geopotential models and their first-, second- and third-order gradients. *Journal of Geodesy*, 83(7):595–619, 2009.

G. Farin. *Curves and Surfaces for Computer-Aided Geometric Design.* Academic Press, 1997.

T. Fukushima. Numerical computation of spherical harmonics of arbitrary degree and order by extending exponent of floating point numbers: II first-, second-, and third-order derivatives. *Journal of Geodesy*, 86(11):1019–1028, 2012.

F. Gini. *Goce Precise Non-Gravitational Force Modeling For Pod Applications.* PhD thesis, University of Padua, 2014.

W. A. Heiskanen and H. Moritz. *Physical Geodesy.* Freeman, San Francisco, 1967.

E. W. Hobson. *The Theory of Spherical and Ellipsoidal Harmonics.* Cambridge, 1931.

M. Hotine. *Mathematical Geodesy.* Washington, U.S. Environmental Science Services Administration, 1969.

O. Jamet, J. Verdun, D. Tsoulis, and N. Gonindard. Assessment of a numerical method for computing the spherical harmonic coefficients of the gravitational potential of a constant density polyhedron. In S. P. Mertikas, editor, *Gravity, Geoid and Earth Observation*, volume 135 of *International Association of Geodesy Symposia*, pages 437–443. Springer, 2010.

L. Jorda, R. Gaskell, C. Capanna, S. Hviid, P. Lamy, J. Durech, G. Faury, O. Groussin, P. Gutierrez, C. Jackman, H. U. Keller, J. Knollenberg, E. Kürt, S. Mottola, E. Palmer, H. Sierks, and J.-B. Vincent. The Global Shape, Density and Rotation of Comet 67P/Churyumov-Gerasimenko from Pre-Perihelion Rosetta/OSIRIS Observations, 28 September 2015. Submitted to *Icarus*.

M. Jutzi and E. Asphaug. The shape and structure of cometary nuclei as a result of low-velocity accretion. *Science*, 348(6241):1355–1358, 2015.

H. U. Keller, S. Mottola, Y. Skorov, and L. Jorda. The changing rotation period of comet 67P/Churyumov-Gerasimenko controlled by its activity. *A&A*, 579:L5, 2015.

H.U. Keller, C. Barbieri, P. Lamy, H. Rickman, R. Rodrigo, K.-P. Wenzel, H. Sierks, M.F. A'Hearn, F. Angrilli, M. Angulo, M.E. Bailey, P. Barthol, M.A. Barucci, J.-L. Bertaux, G. Bianchini, J.-L. Boit, V. Brown, J.A. Burns, I. Büttner, J.M. Castro, G. Cremonese, W. Curdt, V. Dadeppo, S. Debei, M.De Cecco, K. Dohlen, S. Fornasier, M. Fulle, D. Germerott, F. Gliem, G.P. Guizzo, S.F. Hviid, W.-H. Ip, L. Jorda, D. Koschny, J.R. Kramm, E. Kührt, M. Küppers, L.M. Lara, A. Llebaria, A. López, A. López-Jimenez, J. López-Moreno, R. Meller, H. Michalik, M.D. Michelena, R. Müller, G. Naletto, A. Origné, G. Parzianello, M. Pertile, C. Quintana, R. Ragazzoni, P. Ramous, K.-U. Reiche, M. Reina, J. Rodríguez, G. Rousset, L. Sabau, A. Sanz, J.-P. Sivan, K. Stöckner, J. Tabero, U. Telljohann, N. Thomas, V. Timon, G. Tomasch, T. Wittrock, and M. Zaccariotto. OSIRIS - The Scientific Camera System Onboard Rosetta. *Space Science Reviews*, 128(1-4):433–506, 2007.

O. D. Kellogg. *Foundations of Potential Theory.* Ungar, New York, 1929.

W. Kofman, A. Herique, Y. Barbin, J.-P. Barriot, V. Ciarletti, S. Clifford, P. Edenhofer, C. Elachi, C. Eyraud, J.-P. Goutail, E. Heggy, L. Jorda, J. Lasue, A. C. Levasseur-Regourd, E. Nielsen, P. Pasquero, F. Preusker, P. Puget, D. Plettemeier, Y. Rogez, H. Sierks, C. Statz, H. Svedhem, I. Williams, S. Zine, and J. Van Zyl. Properties of the 67P/Churyumov-Gerasimenko interior revealed by CONSERT radar. *Science*, 349(6247), 2015.

S. G. Krantz and H. R. Parks. *A Primer of Real Analytic Functions.* Birkhäuser, 2002.

S. Lien and J. T. Kajiya. Symbolic method for calculating the integral properties of arbitrary nonconvex polyhedra. *IEEE Computer Graphics and Applications*, 4(10):35–41, 1984.

W. D. MacMillan. *The Theory of the Potential.* McGraw-Hill, 1930.

O. Montenbruck and E. Gill. *Satellite Orbits.* Springer, 2001.

J. Murdock. A unified treatment of some expansion procedures in perturbation theory: Lie series, Faá di Bruno operators, and Arbogast's rule. *Celestial Mechanics*, 30:283–295, 1983.

S. Petrovic. Determination of the potential of homogeneous polyhedral bodies using line integrals. *Journal of Geodesy*, 71(1):44–52, 1996.

S. Petrovic and D. Tsoulis. On the singularities of the gravity field of a homogeneous polyhedral body. *Geophysics*, 66:535–539, 2001.

J. E. Prussing and B. A. Conway. *Orbital Mechanics.* Oxford UP, 2013.

A. Rotundi, H. Sierks, V. Della Corte, M. Fulle, P. J. Gutierrez, L. Lara, C. Barbieri, P. L. Lamy, R. Rodrigo, D. Koschny, H. Rickman, H. U. Keller, J. J. López-Moreno, M. Accolla, J. Agarwal,

M. F. A'Hearn, N. Altobelli, F. Angrilli, M. A. Barucci, J.-L. Bertaux, I. Bertini, D. Bodewits, E. Bussoletti, L. Colangeli, M. Cosi, G. Cremonese, J.-F. Crifo, V. Da Deppo, B. Davidsson, S. Debei, M. De Cecco, F. Esposito, M. Ferrari, S. Fornasier, F. Giovane, B. Gustafson, S. F. Green, O. Groussin, E. Grün, C. Güttler, M. L. Herranz, S. F. Hviid, W. Ip, S. Ivanovski, J. M. Jerónimo, L. Jorda, J. Knollenberg, R. Kramm, E. Kührt, M. Küppers, M. Lazzarin, M. R. Leese, A. C. López-Jiménez, F. Lucarelli, S. C. Lowry, F. Marzari, E. M. Epifani, J. A. M. McDonnell, V. Mennella, H. Michalik, A. Molina, R. Morales, F. Moreno, S. Mottola, G. Naletto, N. Oklay, J. L. Ortiz, E. Palomba, P. Palumbo, J.-M. Perrin, J. Rodríguez, L. Sabau, C. Snodgrass, R. Sordini, N. Thomas, C. Tubiana, J.-B. Vincent, P. Weissman, K.-P. Wenzel, V. Zakharov, and J. C. Zarnecki. Dust measurements in the coma of comet 67p/churyumov-gerasimenko inbound to the sun. *Science*, 347, 2015.

A.E. Roy. *Orbital Motion, 4th Ed.* Cambridge, 2004.

R. P. Russell and N. Arora. Global point mascon models for simple, acurate, and prallel geopotential computation. *Journal of Guidance, Control, and Dynamics*, 35:1568–1581, 2012.

R. P. Russell and M. Lara. Long-lifetime lunar repeat ground track orbits. *Journal of Guidance, Control, and Dynamics*, 30:982–993, 2007.

D. J. Scheeres, F. Marzari, L. Tomasella, and V. Vanzani. Rosetta mission: satellite orbits around a cometary nucleus. *Planetary and Space Science*, 46:649–671, 1998.

R. Seydel. *Practical Bifurcation and Stability Analysis.* Springer, 2010.

H. Sierks, C. Barbieri, P. L. Lamy, R. Rodrigo, D. Koschny, H. Rickman, H. U. Keller, J. Agarwal, M. F. A'Hearn, F. Angrilli, A.-T. Auger, M. A. Barucci, J.-L. Bertaux, I. Bertini, S. Besse, D. Bodewits, C. Capanna, G. Cremonese, V. Da Deppo, B. Davidsson, S. Debei, M. De Cecco, F. Ferri, S. Fornasier, M. Fulle, R. Gaskell, L. Giacomini, O. Groussin, P. Gutierrez-Marques, P. J. Gutiŕrez, C. Güttler, N. Hoekzema, S. F. Hviid, W.-. Ip, L. Jorda, J. Knollenberg, G. Kovacs, J. R. Kramm, K. Kührt, M. Küppers, F. La Forgia, Luisa M. Lara, M. Lazzarin, C. Leyrat, J. J. Lopez Moreno, S. Magrin, S. Marchi, F. Marzari, M. Massironi, H. Michalik, R. Moissl, S. Mottola, G. Naletto, N. Oklay, M. Pajola, M. Pertile, F. Preusker, L. Sabau, F. Scholten, C. Snodgrass, N. Thomas, C. Tubiana, J.-B. Vincent, K.-P. Wenzel, M. Zaccariotto, and M. Pätzold. On the nucleus structure and activity of comet 67P/Churyumov-Gerasimenko. *Science*, 347(6220), 2015.

R. Sigl. *Introduction to Potential Theory.* Abacus Press, 1985.

W. D. Sternberg and T. L. Smith. *The Theory of Potential and Spherical Harmonics.* University of Toronto Press, 1946.

D. Stramaccioni. The Rosetta Propulsion System. In *4th International Spacecraft Propulsion Conference*, volume 555 of *ESA Special Publication*, page 3, 2004.

Y. Takahashi and D.J. Scheeres. Small body surface gravity fields via spherical harmonic expansions. *Celestial Mechanics and Dynamical Astronomy*, 119(2):169–206, 2014.

Y. Takahashi and Werner R. A. Scheeres, D. J. Surface gravity fields for asteroids and comets. *Journal of Guidance, Control, and Dynamics*, 36:362–374, 2013.

B.D. Tapley, B.E. Schutz, and G. H. Born. *Statistical Orbit Determination.* Elsevier, 2004.

D. Tsoulis. Analytical computation of the full gravity tensor of a homogeneous arbitrarily shaped polyhedral source using line integrals. *Geophysics*, 77:F1, 2012.

D. Tsoulis, O. Jamet, J. Verdun, and N. Gonindard. Recursive algorithms for the computation of the potential harmonic coefficients of a constant density polyhedron. *Journal of Geodesy*, 83(10):925–942, 2009.

D.A. Vallado. *Fundamentals of Astrodynamics and Applications.* Kluwer, 2001.

J.-B. Vincent, D. Bodewits, S. Besse, H. Sierks, C. Barbieri, P. Lamy, R. Rodrigo, D. Koschny, H. Rickman, H. U. Keller, J. Agarwal, M. F. A'Hearn, A.-T. Auger, M. A. Barucci, J.-L. Bertaux, I. Bertini, C. Capanna, G. Cremonese, V. da Deppo, B. Davidsson, S. Debei, M. de Cecco, M. R. El-Maarry, F. Ferri, S. Fornasier, M. Fulle, R. Gaskell, L. Giacomini, O. Groussin, A. Guilbert-Lepoutre, P. Gutierrez-Marques, P. J. Gutiérrez, C. Güttler, N. Hoekzema, S. Höfner, S. F. Hviid, W.-H. Ip, L. Jorda, J. Knollenberg, G. Kovacs, R. Kramm, E. Kührt, M. Küppers, F. La Forgia, L. M. Lara, M. Lazzarin, V. Lee, C. Leyrat, Z.-Y. Lin, J. J. Lopez Moreno, S. Lowry, S. Magrin, L. Maquet, S. Marchi, F. Marzari, M. Massironi, H. Michalik, R. Moissl, S. Mottola, G. Naletto, N. Oklay, M. Pajola, F. Preusker, F. Scholten, N. Thomas, I. Toth, and C. Tubiana. Large heterogeneities in Comet 67p as revealed by active pits from sinkhole collapse. *Nature*, 523:63–66, July 2015.

Visual Computing Lab ISTI CNR. MeshLab. http://meshlab.sourceforge.net/.

R. A. Werner. Simplifying polyhedra for gravitational evaluation. Unpublished note, November 2010.

R. A. Werner. The gravitational potential of a homogeneous polyhedron or don't cut corners. *Celestial Mechanics and Dynamical Astronomy*, 59(3):253–278, 1994.

R. A. Werner. Spherical harmonic coefficients for the potential of a constant-density polyhedron. *Computers & Geosciences*, 23(10):1071 – 1077, 1997.

R. A. Werner and D. J. Scheeres. Exterior gravitation of a polyhedron derived and compared with harmonic and mascon gravitation representations of asteroid 4769 castalia. *Celestial Mechanics and Dynamical Astronomy*, 65:313–344, 1997.

Appendix A

Point in Polyhedron Algorithm

To check if the orbit intersects with the nucleus, an algorithm was implemented to check wheather each successive point of the orbit lied inside the polyhedron. Two were the main algorithms taken into consideration to achive this goal.

The first is to calculate the number of steradians covered by the nucleus at the test-mass point. If the number of steradians is 4π then the point lies inside the polyhedron, while if the number is 0, the polyhedron lies outside of it. The case in which the test-mass lies on the surface of the polyhedron is not considered since it is very unlikely that an orbit-point is contained in a face of the mesh given at least a 15 digit precision. However, this algorithm is not the most efficient way to obtain the result needed. Given a number N of faces, this calculation needs a computational effort of $O(N)$, slowing down the program.

The second and more efficient way is to take a ray starting from the test-point and calculate how many times the ray intersects with the surface of the polyhedron, which is closed and oriented. If the number of intersections is odd, the point will lie inside the polyhedron, while if it is even, it will lie outside. This does not take into consideration singular cases, for example if the ray is tangent to the surface in a face or in an edge. However, if not considering those cases, this calculation can take much less calculation time if a preprocessing is carried out. The preprocessing should be done as follows. First create the Bounding Box (BB) of each face projection onto the x-y plane. Next find the biggest x-edge and y-edge among the BBs separately, $Lx_{\max}$ and $Ly_{\min}$. Rearrange the order of the faces with respect to the x coordinate of the center of each BB. With this preprocessing, the computation time to find the intersections of the ray with the mesh is lowered to $O(N^{1/2})$ approximately. This is because assuming a homogeneous distribution of the faces on the mesh and making the approximation that ... To find the number of intersections of a ray starting at $\vec{r_0} = (x_0, y_0, z_0)$, we first find through bisection method the two faces in the re-ordered sequence that have the x-coordinate of the BB closer to $x_0 - Lx_{\max}/2$ and $x_0 + Lx_{\max}/2$, and consider from now on only the faces that are included between these two faces plus their exterior next neighbors. This algorithm has the known computational cost of $O(\log N)$. The next step is to exclude all faces whose BB projection onto the y-axis does not include y_0. This has a computational cost of order $O(\sqrt{N})$. A number of faces of order $O(1)$ remains now to be checked for intersection with the ray. The greatest computational effort in this algorithm is represented by the step in which all faces whose BB projection onto the y-axis does not include y_0 are excluded. Thus the computational effort of this algorithm is of order $O(\sqrt{N})$, depending thus substantially on the number of faces the polyhedron is composed of.

Appendix **B**

Binomial Coefficients

Many of the developments of the potential in Chapter 2 are based on the use of the binomial expansion, both for positive powers, as well as for negative rational powers. We here present some properties of binomial coefficients that are of use in such developments, and some which are especially useful in connection with numerical evaluations.

The binomial coefficients $\binom{n}{m}$ arise in the expansion of the power of a binomial,

$$(x+y)^n = \sum_{m=0}^{n} \binom{n}{m} x^{n-m} y^m. \tag{B.1}$$

The definition of the binomial coefficient is

$$\binom{n}{m} = \frac{n\,(n-1)\,(n-2)\,...\,(n-m+1)}{m!}, \tag{B.2}$$

which is easily seen to be symmetric to the eschange $m \leftrightarrow (n-m)$ so that

$$\binom{n}{m} = \binom{n}{n-m}. \tag{B.3}$$

In turn, implies that the binomial expansion may be written in several different ways as

$$(x+y)^n = \sum_{m=0}^{n} \binom{n}{m} x^m y^{n-m} = \sum_{m=0}^{n} \binom{n}{n-m} x^m y^{n-m} = \sum_{m=0}^{n} \binom{n}{n-m} x^{n-m} y^m, \tag{B.4}$$

which may be exploited depending on the circumstances.

The fact that the numerator of (B.2) consists of m factors can be exploited for computational purposes. In fact, the evaluation of a binomial coefficient $c = \binom{n}{k}$ can be done recursively, as implied by

$$\binom{n}{m} = \frac{(n)}{(m)} \frac{(n-1)}{(m-1)} \frac{(n-2)}{(m-2)} ... \frac{(n-m+2)}{(2)} \frac{(n-m+1)}{(1)}. \tag{B.5}$$

which can be rephrased algorithmically into the loop

$$\begin{aligned} c_0 &= \frac{n}{k}, \\ c_i &= \frac{n-i}{k-i}\, c_{i-1}, \qquad i = 1, 2, ..., k-1. \end{aligned}$$

Note that the commonly used definition

$$\binom{n}{m} = \frac{n!}{n!\,(n-m)!} \tag{B.6}$$

can be useful for analytical developments, but is inefficient for computing the coefficient.

When n is a negative number, even rational, the numerical algorithm implied by equation (B.5) is certainly valid. From an analytical point of view, however, we have from the definition (B.2) that

$$\binom{-n}{m} = \frac{(-n)\,(-n-1)\,(-n-2)\ldots(-n-m+1)}{m!}, \tag{B.7}$$

which can manipulated as

$$\begin{aligned}\binom{-n}{m} &= \frac{\overbrace{(-n)\,(-n-1)\,(-n-2)\ldots(-n-m+1)}^{m\,factors}}{m!}\\ &= (-1)^m\,\frac{(n)\,(n+1)\,(n+2)\ldots(n+m-1)}{m!}\\ &= (-1)^m\,\frac{\overbrace{(n+m-1)\,(n+m-2)\ldots n}^{m\,factors}}{m!}\end{aligned}$$

from which

$$\binom{-n}{m} = (-1)^m\binom{n+m-1}{m}, \tag{B.8}$$

or

$$\binom{-n}{m} = (-1)^m\,\frac{(n+m-1)!}{m!\,(n-1)!}, \tag{B.9}$$

both forms being useful in analytical manipulations.

Note that by definition, with $m > 0$,

$$\binom{n}{-m} = 0, \qquad \binom{n}{0} = 1.$$

The case of negative upper entry in the binomial coefficients is related to the expansion of negative powers. In that case the expansion is non-terminating, as can be seen by rewriting (B.8) using (**??**) as

$$\binom{-n}{m} = (-1)^m\binom{n+m-1}{n-1}. \tag{B.10}$$

In fact, the expansion of the binomial function $f(x) = (1+x)^{-n}$ can be written as

$$(1+x)^{-n} = \sum_{m=0}^{\infty}\binom{-n}{m}x^m, \tag{B.11}$$

where the upper limit of the summation index is infinity, in line with the fact that this is the Taylor series of $f(x)$ subject to the restriction $|x| < 1$.

It may also be useful to have some explicit formulae related to negative half-integer powers. In that case the binomial coefficient has the form $\binom{-\frac{n+1}{2}}{n}$ and can be manipulated as follows

$$
\begin{aligned}
\binom{-\frac{n+1}{2}}{m} &= \frac{\left[\left(-\frac{n+1}{2}\right)\left(-\frac{n+1}{2}-1\right)\left(-\frac{n+1}{2}-2\right)\cdots\left(-\frac{n+1}{2}-m+1\right)\right]}{m!} \\
&= \frac{\left[\left(-\frac{n+1}{2}\right)\left(-\frac{n+1+2}{2}\right)\left(-\frac{n+1+4}{2}\right)\cdots\left(-\frac{n+1+2(m-1)}{2}\right)\right]}{m!} \\
&= (-1)^m \frac{\left[(n+1)(n+1+2)(n+1+4)\cdots(n+1+2(m-1))\right]}{2^m m!} \\
&= (-1)^m \frac{\left[(n+1)(n+3)(n+5)\cdots(n+1+2m-2)\right]}{2^m m!} \\
&= (-1)^m \frac{\left[(n+1)(n+3)(n+5)\cdots(n+2m-1)\right]}{2^m m!} \\
&= (-1)^m \frac{\left[(n+2m-1)(n+2m-3)\cdots(n+5)(n+3)(n+1)\right]}{2^m m!}
\end{aligned}
$$

to finally yield the expression

$$
\binom{-\dfrac{n+1}{2}}{m} = (-1)^m \frac{(n+2m-1)!!}{(2m)!!(n-1)!!} \tag{B.12}
$$

in terms of the double factorial, or Schuster notation

$$
(n)!! = n\,(n-2)\,(n-4)\ldots(n_0)\,, \tag{B.13}
$$

where n_0 can be either 2 or 1, depending on the parity of n. With this notation we can write the identities

$$
\begin{aligned}
(2n)!! &= 2^n n! && \text{(B.14)} \\
(2n+1)!! &= \frac{(2n+1)!}{2^n n!} && \text{(B.15)} \\
(2n-1)!! &= \frac{(2n)!}{2^n n!} && \text{(B.16)} \\
n! &= n!!\,(n-1)!! && \text{(B.17)}
\end{aligned}
$$

which were used in deriving (B.12). As useful examples of the application of this equation we may write

$$
\binom{-\frac{1}{2}}{n} = (-1)^n \frac{(2n-1)!!}{(2n)!!} \tag{B.18}
$$

and

$$
\binom{-\frac{3}{2}}{n} = (-1)^n \frac{(2n+1)!!}{2^n n!}. \tag{B.19}
$$

Appendix C

Bernstein Polynomials

We provide a brief introduction to Bernstein polynomials, referring to (Farin, 1997) for further details. Bernstein polynomials are defined as

$$B_k^n(\lambda) = \binom{n}{k} \lambda^k (1-\lambda)^{n-k}, \qquad 0 \le k \le n, \tag{C.1}$$

which clearly shows that they are associated with the binomial expansion

$$[\lambda + (1-\lambda)]^n = \sum_{k=0}^{n} \binom{n}{k} \lambda^k (1-\lambda)^{n-k} = \sum_{k=0}^{n} B_k^n(\lambda), \tag{C.2}$$

of the constant function 1. These polynomials form a basis over $[0,1]$.

Bernstein polynomials enjoy many properties, like the integral formula

$$\int_0^1 B_k^n(\lambda)\, d\lambda = \frac{1}{n+1}, \tag{C.3}$$

the differentiation formula

$$\frac{d}{d\lambda} B_k^n(\lambda) = n\left[B_{k-1}^{n-1}(\lambda) - B_k^{n-1}(\lambda)\right] \tag{C.4}$$

and the subdivision formula

$$B_k^n(\lambda\mu) = \sum_{s=0}^{n} B_k^s(\lambda)\, B_s^n(\mu). \tag{C.5}$$

More important for our purposes is the product formula of two Bernstein polynomials,

$$B_i^p(\lambda)\, B_k^q(\lambda) = \frac{\binom{p}{i}\binom{q}{k}}{\binom{p+q}{i+k}} B_{i+k}^{p+q}(\lambda). \tag{C.6}$$

This is easily proved by noting that

$$\begin{aligned} B_i^p(\lambda)\, B_k^q(\lambda) &= \binom{p}{i}\binom{q}{k} \lambda^{i+k} (1-\lambda)^{p+q-i-k} \\ &= \binom{p}{i}\binom{q}{k} \frac{B_{i+k}^{p+q}(\lambda)}{B_{i+k}^{p+q}(\lambda)} \lambda^{i+k} (1-\lambda)^{p+q-i-k} \\ &= \binom{p}{i}\binom{q}{k} \frac{B_{i+k}^{p+q}(\lambda)}{\binom{p+q}{i+k} \lambda^{i+k} (1-\lambda)^{p+q-i-k}} \lambda^{i+k} (1-\lambda)^{p+q-i-k} \end{aligned}$$

which after simplification leads to (C.5). Repeated application of the product formula provides the formula for the product of three Bernstein polnomials used in the main text,

$$B_i^p(\lambda)\, B_k^q(\lambda)\, B_l^r(\lambda) = \frac{\binom{p}{i}\binom{q}{k}\binom{r}{l}}{\binom{p+q}{i+k}\binom{p+q+r}{i+k+l}} B_{i+k+l}^{p+q+r}(\lambda)\,. \tag{C.7}$$

This can be generalized to the product of any number n of Bernstein polynomials to yieldor

$$\prod_{k=1}^{n} B_{i_k}^{p_k}(\lambda) = \frac{\prod\limits_{k=1}^{n}\binom{p_k}{i_k}}{\prod\limits_{m=2}^{n}\binom{P_m}{I_m}}, \tag{C.8}$$

where

$$P_m = \sum_{k=1}^{m} p_k, \qquad I_m = \sum_{k=1}^{m} i_k. \tag{C.9}$$

Bernstein polynomials also satisfy some useful recurrence relations. Using the known identity

$$\binom{n}{k} + \binom{n}{k+1} = \binom{n+1}{k+1}$$

we can write

$$\begin{aligned}
B_k^n(\lambda) &= \binom{n}{k}\lambda^k(1-\lambda)^{n-k} \\
&= \left[\binom{n+1}{k+1} - \binom{n}{k+1}\right]\lambda^k(1-\lambda)^{n-k} \\
&= \binom{n+1}{k+1}\lambda^k(1-\lambda)^{n-k} - \binom{n}{k+1}\lambda^k(1-\lambda)^{n-k} \\
&= \lambda^{-1}\binom{n+1}{k+1}\lambda^{k+1}(1-\lambda)^{n-k} - \lambda^{-1}(1-\lambda)\binom{n}{k+1}\lambda^{k+1}(1-\lambda)^{n-k-1} \\
&= \lambda^{-1}B_{k+1}^{n+1}(\lambda) - \lambda^{-1}(1-\lambda)\,B_{k+1}^{n}(\lambda)
\end{aligned}$$

which leads to

$$B_{k+1}^{n+1}(\lambda) = \lambda B_k^n(\lambda) + (1-\lambda)\,B_{k+1}^n(\lambda) \tag{C.10}$$

Other properties, known under the name of degree elevation, are

$$(1-\lambda)\,B_k^n(\lambda) = \frac{n+1-k}{n+1}B_k^{n+1}(\lambda)\,, \tag{C.11}$$

$$\lambda B_k^n(\lambda) = \frac{k+1}{n+1}B_{k+1}^{n+1}(\lambda)\,, \tag{C.12}$$

the combination of which provides another recurrence formula as

$$B_k^n(\lambda) = \frac{n+1-k}{n+1}B_k^{n+1}(\lambda) + \frac{k+1}{n+1}B_{k+1}^{n+1}(\lambda)\,. \tag{C.13}$$